MACQUARIE
University
Faculty of Science and Engineering
Department of Molecular Sciences

# Development of an immunoluminescence assay to detect Glypican 1 in urine cells, as a candidate biomarker for diagnosis of prostate cancer.

By Irene Ofelia Justiniano Fuenmayor, BSc.

Supervised by: Prof. Robert Willows.

Co-Supervised by: Prof. Nicolle Packer.

Sponsored by Minomic International Ltd and the Australian Research Council through the linkage project “Rapid detection of rare event cells by SUPER Dots: finding a needle in a haystack”

Sydney, 6th of December 2018

# TABLE OF CONTENTS

# ABSTRACT

Among the cancers of the urinary tract in men, prostate cancer is the most common and with the second highest mortality rate if not detected on time. The current protocol for prostate cancer diagnosis includes a screening blood test for prostate specific antigen (PSA), which is problematic due to its low specificity. Patients who present high levels of PSA undergo invasive procedures that are often unnecessary. Voided urine is the biological source of choice for the investigation of biomarkers for cancers of the urinary tract. GPC1, also known as Glypican 1, is a cell surface glycoprotein involved in cell division and growth regulation. It has been linked to some types of cancers, such as pancreas, breast and prostate. The main goal of this work was to develop an assay platform in order to determine whether GPC1 has potential as a biomarker for detection of prostate cancer in voided urine sediments samples. MIL38 is a mouse monoclonal antibody, originally raised against a bladder cancer cell line, that binds to GPC1; it is used as the core tool for this work. A fluorescence immunoassay for urine sediments was developed using MIL38 to detect GPC1 positive cells. Autofluorescence and low cells numbers generated bias in the study, which was otherwise promising. To overcome these problems, optimisation in the sample processing was done and upconversion nanoparticles (UCNP) and luminescent europium chelates tools were explored to develop an immunoassay to eliminate autofluorescence interference.

# STATEMENT OF ORIGINALITY

This work has not previously been submitted for a degree or diploma in any university. To the best of my knowledge, the material contained in it has not been published or written by another person before, except where it is referenced in this written manuscript. The use of human urine specimens analysed in this work was approved by the Human Research Ethics Committee of University of New South Wales for the project "Use of a Monoclonal Antibody toward a cell surface biomarker to detect Prostate Cancer" (HREC 10174), by the Macquarie University Human Research Ethics Committee, Ref# 5201500707 and by the Biohazard and Biosafety Committee, Ref# ROW190614.

Irene O. Justiniano Fuenmayor

6th of December 2018

# ACKNOWLEDGEMENTS


- Professor Robert Willows, for his advice and professional support, essential for the completion of this work.
- Macquarie University and the Department of Molecular Sciences, for the space, resources and academic support, essential for the development of this work.
- Minomic International Ltd, Professor Bradley Walsh and Dr. Douglas Campbell, for the always generous material and intellectual support that I received during the development of this work.
- Australian Research Council, for the funding of this project, through the linkage project "Rapid detection of rare event cells by SUPER Dots: finding a needle in a haystack".
- Professor David Gillatt at Macquarie University Hospital; Dr. Paul Cozzi, from Hurstville Community Private Hospital; Prof. Paul D'Souza from St George Private Hospital; Prof. Mark Frydenberg from the Australian Urologist Associates Clinic; Prof Mark Willcox, School of Optometry and Vision Science, UNSW; for their invaluable collaboration providing patient samples for this research.
- Dr. Russell Connally and Dr. Nima Sayyadi, for their unconditional support and collaboration during the development of the immunoluminescence assay.
- Dr. Jie Lu and Dr. Ante Jerkovic, for their valuable advice and collaboration with the development of the upconversion nanoparticles conjugates.
- Professor Dayong Jin, for introducing me to this opportunity and giving me the initial tools to start this journey.

# ABBREVIATURES

**ABS**: acetate buffered saline

**AMACR**: alpha-methyl-acyl-CoA racemase

**BCA**: bicinchoninic acid

**BHHBCB**: 1,2 bis[4'-(1",1",1",2",2",3",3"-heptafluoro-4",6"-hexanedion-6"-yl)-benzyl]-4-chlorosulfobenzene

**BHHBTEGBS**: 1,2-bis[4'-(1",1",1",2",2",3",3"-heptafluoro-4",6"-hexanedion-6"-yl)-benzyl]-4-sulfonylamino-tetraethyleneglycol-succinimidyl carbonate-benzene

**BHMT**: bis(hexamethylene)triamine

**BPH**: benign prostate hyperplasia

**CaP**: cancer of the prostate

**CT**: computed tomography

**CTC**: circulating tumour cells

**CV**: column volume

**DAPI**: 4',6-diamidino-2-phenylindole

**DMF**: dimethyl formamide

**DMSO**: dimethyl sulfoxide

**DNA**: deoxyribonucleic acid

**DPBS**: Dulbecco phosphate buffered saline

**DRE**: digital rectal examination

**DTT**: dithiothreitol

**EDC**: 1-Ethyl-3-(3-dimethylaminopropyl)-carbodiimide

**EDTA**: ethylenediaminetetraacetic acid

**EGF**: epidermal-like growth factor)

**ELISA**: enzyme linked immunosorbent assay

**ERG**: ETS-related gene

**ETU**: energy transfer upconversion

**FAD:** flavin adenine dinucleotide

**FBS**: foetal bovine serum

**FEB**: fluorescence enhancement buffer

**FGF-2**: fibroblast growth factor 2

**FISH**: fluorescence in situ hybridisation

**FITC**: fluorescein isothiocyanate

**FN**: false negative

**FP**: false positive

**FPLC**: fast protein liquid chromatography

**GALD**: gated autosynchronous luminescence detector

**GPC1**: glypican 1

**GPI**: glycosylphosphatidylinositol

**HREC**: human research ethics committee

**ICC**: immunocytochemistry

**IFA**: immunofluorescence assay

**IgG**: immunoglobulin G

**IHC**: immunohistochemistry

**ITC**: isothermal titration calorimetry

**MES**: 2-(N-morpholino)ethane-sulfonic acid

**MRI**: magnetic resonance imaging

**NADH**: reduced form of nicotinamide adenine dinucleotide

**NADPH**: reduced form of nicotinamide adenine dinucleotide phosphate

**NHS**: N-hydroxysuccinimide

**NIR**: near infrared

**NMP22**: nuclear matrix protein 22

**NSW**: New South Wales

**OSAM**: orthogonal scanning automated microscopy

**PAA**: polyacrylic acid

**PHI**: prostate health index

**PIN**: prostatic intraepithelial neoplasia

**PSA**: prostate specific antigen

**PSGR**: prostate specific G coupled protein receptor

**PSMA**: prostate specific membrane antigen

**PVP**: polivynyl pyrrolidone

**RNA**: ribonucleic acid

**RP**: radical prostatectomy

**RP-HPLC**: reverse phase high performance liquid chromatography

**ssDNA**: single strand deoxyribonucleic acid

**TBS**: tris buffered saline

**TBS-T**: tris buffered saline Tween-20

**TEAA**: triethylammonium acetate

**TEG**: tetraethylene glycol

**TEM**: transmission electron microscopy

**TFA**: trifluoroacetic acid

**TGF-β**: tumour growth factor beta

**TGL**: time gated luminescence

**THPTA:** tris(3-hydroxypropyltriazolylmethyl)amine

**TN**: true negative

**TNM**: tumour, node and metastasis

**TOPO**: trioctylphosphine oxide

**TP**: true positive

**TRF**: time resolved fluorescence

**UCNP**: upconversion nanoparticle

**UNSW**: University of New South Wales

**UV**: ultraviolet

# 1. INTRODUCTION

## 1.1. CANCER OF THE PROSTATE

The prostate is an exocrine gland located between the bladder and the penis, in front of the rectum, and is crossed by the urethra. It is composed of approximately 70% glandular tissue, where cancer is more likely to be found, and 30% muscle tissue, which is rarely invaded by carcinoma. The glandular region is divided in three parts: the transition zone, where benign prostatic hyperplasia (BPH) and 20% of cancers are located; the central zone, only accounting 1-5% of prostatic cancers; and the peripheral zone, which is the biggest part of the glandular region, accounting for around 70% of carcinoma development[1].

Different forms of prostate cancer are classified according to the tissue of origin as prostatic intraepithelial neoplasia (PIN), adenocarcinoma (which comprise the majority of the prostate cancers), and more aggressive and rarer such as mucinous adenocarcinoma, prostatic duct adenocarcinoma, small cell carcinoma, lymphoma and sarcoma[1]. It is also classified according to its grade (Gleason score), which describes the loss of prostate tissue structure, and gives a scale of malignancy of the tumour based on the 2 most prevalent patterns observed in the tissue[2]; and stage, which describes the degree of invasion or spread of malignant cells (tumour, node and metastasis or TNM)[1, 3].

According to the Australian Institute of Health and Welfare, the estimated incidence of prostate cancer for 2017 in Australia was over 16,600 newly diagnosed cases, accounting for 23% of all cancer diagnosis in men, being the second cause of death for cancer, after lung carcinomas [4]. In NSW alone, there is an estimate of 66,000 men living with the disease in 2017[5]. It is an age-related disease, rarely appearing in men younger than 40 years[1], and

with an increased risk within older men, with 1 in 7 men 85 years old and over at risk of developing the disease[4]. As the life expectancy in Australia is increasing over the years, the incidence of prostate cancer is likely to keep increasing as well. However, early diagnosis and adequate treatments have increased the chances of survival[4].

## 1.2. CURRENT DIAGNOSTICS: CAPACITY AND LIMITATIONS

The diagnosis of prostate cancer can be done through screening tests of asymptomatic men at risk (with direct family history of prostate cancer, aged between 55-69)[6], or when presenting some symptoms, such as urine haematuria, difficulty to urinate, and pelvic pain [3]. The initial tests are blood levels of prostate specific antigen (PSA), which is an androgen regulated serine protease which functions to digest proteins from the semen and it is secreted almost exclusively by the prostate epithelium[1, 7]; and digital rectal examination (DRE)[1, 3]. When abnormalities are found in these tests, a transrectal ultrasound-guided needle biopsy of the prostate is performed[1, 3]. The tissue is then analysed by pathologists and graded according to the Gleason Score[2]. For high degree tumours, and PSA levels above 10ng/mL, imaging techniques such as Magnetic Resonance Imaging (MRI)[8], and Computed Tomography (CT) scanning are used to search for metastasis[1].

The use of blood PSA levels as a screening tool for early diagnosis of prostate cancer has remained controversial for many years. There is not a clear cutoff level above which it can be undoubtedly concluded that a malignancy is present. The standard cutoff of PSA to undergo a biopsy is of 4 ng/mL, but only about 30% of men tested would be positive for prostate cancer[7] at these levels, which means that the remaining 70% would have unnecessarily been through a risky and uncomfortable procedure that can bring

consequences such as pain, haemorrhages and infections[9]. From those diagnosed with prostate cancer, most men will chose radical treatments even in those cases of low grade tumours that would be indolent over the life time of the patients, in the hope of avoiding progression to more serious forms of the disease, despite the secondary effects such treatments can have, such as incontinence and impotence[6]. In addition, most of the more aggressive types of prostate cancer are present in men with normal levels of PSA[1, 6]. The health care system therefore faces a dilemma: whether to run screening tests in men within the range of age of risk (55-69 years old) and over-diagnose and over-treat patients, or modify the policies to reduce the over-diagnosis, risking missing patients with aggressive pathologies. To address this problem, there are significant research efforts to identify novel biomarkers and find new technologies to increase the specificity of the standard screening tests, in order to better discern between indolent and clinically significant cancers and provide a reliable prognosis that help to make adequate decisions for the care of the patient.

## 1.3. OTHER BIOMARKERS FOR PROSTATE CANCER DIAGNOSIS AND PROGNOSIS

A lot of effort has been invested in the improvement of the performance of PSA tests in order to increase specificity and to be able to build a risk stratification scale to provide the most adequate treatment to the patients. As more information has been discovered about the biology of PSA, several attempts have been made to use this information to generate confirmation tests for PSA screening. Table 1.3.1 summarises the most important variants of PSA test.

**Table 1.3.1**. Variants of PSA test in detecting cancer of the prostate (CaP)

| Test | Principle | Application | Sensitivity/ Specificity | Ref |
|---|---|---|---|---|
| Total PSA | All immunologically detected PSA. High levels are associated with CaP. | Diagnosis | High/Low | [10-12] |
| PSA density | PSA/prostate volume ratio. Elevated values associated with CaP. | Diagnosis and Prognosis | High/Moderate | [13] |
| PSA velocity | Rate of change of PSA: increase of 2 ng/L/year associated with CaP lethality | Prognosis | High/Moderate | [14] |
| Free PSA | Unbound from alpha-1-antichymotrypsin. Free to total PSA ratio lower than cutoff level is associated with CaP. | Diagnosis | High/Low | [15-17] |
| ProPSA | Uncleaved precursor of PSA. High levels are associated with CaP | Diagnosis | High/Low | [18, 19] |
| PHI | Prostate Health Index, a relationship between proPSA, free-PSA and Total-PSA(elevated in BPH) levels in blood. | Diagnosis | Better than PSA | [20] |
| hK2 | PSA (hK3) like peptidase. High levels are associated with CaP | Prognosis | Better than PSA | [21, 22] |
| hK2/fPSA | Detection of CaP in PSA in “grey area” (2-10ng/mL) | Diagnosis | Better than PSA | [23, 24] |
| 4K | Relationship of Total-PSA, free-PSA, proPSA, and hK2 | Prognosis | Better than PSA | [25, 26] |

Total PSA and the PSA/freePSA ratio are currently run in Australia pathology labs (according to brochures of Douglass Hanly Moir Pathology and Laverty Pathology labs, two important pathology services providers) to monitor prostate health. In general, the performance of any of these models improved the specificity of total PSA and the sensitivity in what is known as “grey area”, which is a PSA concentration range in which the power of the test reaches a minimum. However, they do not address the problem of prognosis or risk stratification.

Research in novel biomarkers, not only for prostate cancer detection, but for prognosis, has been very prolific in the last 20 years. Urinary biomarkers are of particular

interest, given that urine is a complex body fluid easy to obtain in a non-invasive manner. As described in a previous section, the urethra crosses the prostate and merges with ejaculatory ducts through which prostate fluid passes into the urethra. This way, biological material from the prostate (proteins, nucleic acids, cells, etc.) is found in urine. In Table 1.3.2 some of the most studied urine biomarkers are summarised.

**Table 1.3.2** Other biomarkers in urine for diagnosis and prognosis of prostate cancer (CaP).

| Biomarker | Principle | Application | Sensitivity/ Specificity | Ref |
|---|---|---|---|---|
| PCA3 | Post-DRE urinary non-encoding RNA, highly over expressed in CaP. | Diagnosis | Low/High | [27, 28] |
| TMPRSS2:ERG | Post-DRE urinary androgen-regulated gene (measured as RNA) fused to an oncogene, present in ~50% of CaP. | Diagnosis | Higher than PSA in combination with PCA3 | [29] |
| DLX1 and HOXC6 | Post-DRE urinary genes (measured as RNA) up-regulated in mid to high grade tumours, evaluated in complex multifactorial models. | Diagnosis and Prognosis | Low/High | [30] |
| AMACR or P504S | Enzyme involved in metabolism of fatty acids, found to be overexpressed in CaP. Detected by Immunocytochemistry. | Diagnosis | Moderate/High | [31, 32] |
| hTERT | Telomerase activity | Diagnosis | Moderate/High | [33, 34] |

Nucleic acid biomarkers are the most abundant among those studied in relation to prostate cancer diagnosis and prognosis and have been reviewed extensively[35-37]. Some work has been developed in detecting the expression of certain proteins associated with cancer on the surface of the cells from urine sediments by immunocytochemistry[38, 39]. This

is the approach taken in the present work to study the relevance of a novel biomarker, Glypican 1 (or GPC1), for the detection of prostate cancer in urine sediments.

## 1.4. MIL38 AND GLYPICAN 1

### 1.4.1. MIL38 History

MIL-38, formerly known as BLCA-38, is a mouse monoclonal antibody (IgG1) raised against the bladder cancer cell line UCRU-BL-17 [40]. It has been shown that it is able to detect bladder cancer cells in voided urine [40], and it specifically stains cancer cells in prostate tissue[41]. It has been tested in subcutaneous xenografts for imaging and therapy with high tumour binding specificity[42-44]. Minomic International Limited acquired the rights over the antibody and changed its name to MIL-38.

For just over 10 years, the antigen of this antibody was unknown, and it was reported as very difficult to determine[41]. Its identification by mass spectrometry was elusive, it was found to be a highly glycosylated protein and the epitope was sensitive to reduction. All these factors made it very difficult to identify. However, the antigen was eventually found belong to Glypican 1[45].

There are other anti-GPC1 antibodies commercially available. However, the immunogen for these antibodies are in their majority peptides or truncated recombinant proteins produced in bacteria, and their ability to detect the native form is poor (data not shown). The advantage of MIL38 antibody to study expression of GPC1 in human samples (tissues and cells) is that the antibody binds strongly to the native form of the protein, which has a very compact tertiary structure (See Figure 1.4.2.1 below). This ability and the observed

robustness of the antibody itself, make it ideal to develop a diagnostic platform that could potentially be incorporated into pathology laboratories.

### 1.4.2. GPC1 structure and function

Glypican 1 (GPC1) is a GPI-anchored membrane glycoprotein. It belongs to a family of 6 proteins (Glypicans 1 to 6) which share signals for translocation, a hydrophobic GPI anchor site, 14 Cysteines and a domain for heparan sulphate binding near the C terminus[46, 47]. They also present two N-glycosylation sites that are not conserved. In GPC1 it has been shown that the N-glycans affect the protein expression and the heparan sulphate substitution[46]. The protein forms a very tight $\alpha$-helical globular structure[47], (Figure 1.4.2.1-A). The correct folding is independent of N-glycans, but heparan sulphates seems to play a role in the folding of the protein [46]. It also has been shown that GPC1 is able to form dimers[47].

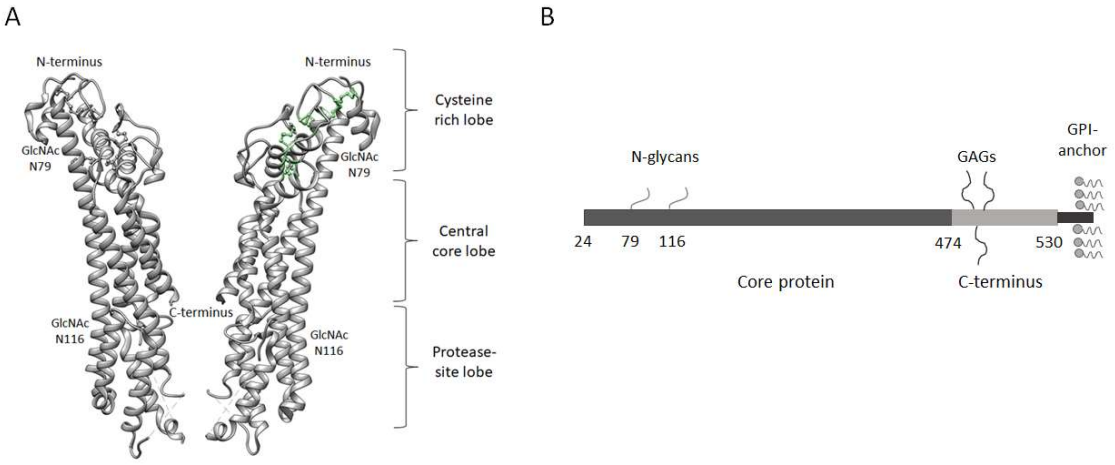


**Figure 1.4.2.1**.- **A**. Model of GPC1 protein core, showing different domains and positions of N-glycosylations. Figure prepared with Chimera[48], using data from the Protein Data Base (PDB), accession 4YWT, based on [49] **B**. Schematic representation of GPC1, showing major domains and glycosylation sites[49].

The molecular weight of the mature protein with glucosaminoglycans (GAGs or heparan sulphates) and N-linked glycans can reach over 220 kDa. On removal of the heparan-sulphates and N-linked glycans the molecular weight of the protein is ~55 kDa. This is smaller than the precursor, which is 60 kDa, due to cleavage of residues at the N-terminal during processing through the endoplasmic reticulum and Golgi.

GPC1 is expressed in developing and adult brain and has been linked to neuronal differentiation [50]. GPC1 is involved in Fibroblast Growth Factor (FGF-2), Transforming Growth Factor-β (TGF- β) and Epidermal-like Growth Factor (EGF) mediated signalling[51-54]. These growth factors are thus known as Heparin Binding Growth Factors (HBGF). It has been shown that GPC1 stimulates S-phase of the cell cycle and can promote DNA mutation[55], but if it is either over expressed or knocked down, it interferes with cell growth by arresting the cell cycle in metaphase [56].

The involvement of GPC1 in cell growth processes and cell differentiation suggests this protein may be important in cancer related studies.

### 1.4.3. GPC1 and cancer

Over the last 20 years, interest in GPC1's involvement in cancer has been increasing. However, there are conflicting results about the role of GPC1 in cell proliferation. There are only a few reports of overexpression of GPC1 in cancerous tissue: GPC1 is reported to be overexpressed in glioma vessels, and that it stimulates FGF-2 signalling mediated growth of cultured brain [54]. Although not over expressed, GPC1 has been suggested to participate in angiogenesis and cell proliferation in pancreatic cancer [57, 58], breast cancer [52], prostate cancer [59], and ameloblastomas [60]. Moreover, expression of GPC1 in neuroendocrine

tumours decreases as malignancy increases [61]. All these studies suggest that GPC1 has potential as a cancer biomarker, and therefore, it is of interest to investigate how the expression of GPC1 in urine sediments is related to cancers of the urinary tract.

### 1.4.4. Biomarker discovery and validation

A biomarker is an indicator that can be measured (a cellular, biochemical, and/or molecular characteristic), that describes a biological state in association with disease [62-64]. It can be classified as "predictive biomarker" (predicts response to specific treatments); "prognostic biomarker" (informs about risks and progression of a condition) and "diagnostic biomarker" (identifies a condition present in a patient)[62, 64]. The first step in the development of biomarkers research is the "discovery" of the biomarker. Candidates can be sourced from a well-defined biological process or from high throughput techniques, such as proteomics and genomics[64]. The development of assays to monitor a new biomarker is usually contrasted with a gold standard, which is the best diagnostic or prognosis test available at the time. For example, for prostate cancer, typical gold standard for diagnosis are blood PSA and biopsy.

The validation process as described by the National Cancer Institute's Early Detection Research Network (EDRN) consists of 5 different phases: 1) preclinical exploratory studies, in which a case for a specific marker is made through the collection of evidence for suitability; 2) clinical assay development, which consist of 3 steps: analytical validity (development and validation of a test or assay, from patient selection criteria, sample collection and processing, assay platform and data analysis), clinical validity (biomarker power of discriminating two or more populations, e.g. healthy and cancer patients), and clinical utility (whether the knowledge of the biomarker state helps to improve patients outcome); 3) retrospective

longitudinal repository studies, in which, through a large number of samples, it is confirmed the ability of the biomarker test in detecting the disease and a cut-off is defined; 4) prospective screening studies, aiming to determine the ability of the biomarker test in detecting early stages of the disease; and 5) cancer control studies, which is similar to clinical utility, but with a large population[62, 63]. The work presented here fits under steps 1 and 2 of phase 2, clinical development.

### 1.4.5. Goals of this study

The main goal of the present study was to determine whether GPC1 expressed on the surface of the prostate cells found in urine sediments has potential to be used for the detection of prostate cancer. In order to achieve that, an immunofluorescence assay using MIL38 antibody was developed and a small patient trial was run. Several problems related to different interferents with the assay reduced the value of the trial, but results seemed to be promising. Therefore, different approaches to overcome these problems were taken. A final improved test platform was developed and is ready to be used to run a second patient trial.

# 2. DEVELOPMENT OF AN IMMUNOFLUORESCENCE ASSAY TO DETECT GLYPICAN 1 ON URINE CELLS FOR PROSTATE CANCER DIAGNOSIS

## 2.1. SUMMARY

An immunofluorescence assay using MIL38 antibody to detect GPC1 in urine cells has been developed, in order to assess the suitability of GPC1 as a biomarker for diagnosis of prostate cancer. A small pilot trial was done with patient samples, but low yield of cells, complex sample matrixes and autofluorescence interfered with the assay, introducing bias in the results. Despite the difficulties, a sensitivity of 55.6% and a specificity of 73.4% were achieved, therefor an improvement of the assay platform was pursued.

## 2.2. INTRODUCTION: URINE CYTOLOGY AND IMMUNOASSAYS

### 2.2.1. Cytology for diagnosis of cancers of the urinary tract

Urine cytology is the microscopic examination of sediments obtained from urinary specimens, which can be voided urine (collected directly in an appropriate container), catheterised urine (collected directly from the bladder using a catheter), bladder and urinary tract washes (obtained with a cystoscope) and ileal conduit (for patients that have undergone radical cystectomy)[65]. Normal urine sediments are composed mainly of urothelial cells and some non-cellular elements such as crystals and casts, but it also contains glandular cells from the prostate (men), endometrium (women), renal tubular cells, peripheral blood cells and sperm [65].

Urine cytology is used mainly for screening or surveillance of people with risk factors associated with, or history of, urothelial cancer, and for diagnosis in patients presenting symptoms, in joint with cystoscopy and tissue biopsy[65]. However, studies have shown that cytology has high specificity but very poor sensitivity when challenged with low grade bladder cancer, due to a lack of characteristics that would make these cells recognizable as malignant by the examiner[66, 67]. Moreover, it has been reported that agreement among multiple pathologists examining the same samples is limited [68], despite some efforts made to establish structural features to recognise these pathologies[66, 69]. Additionally, urinary sample preparation also affects accuracy of cytological tests, as shown by some studies[67, 70-73], given the different methods used to prepare urine sediment specimens. First, sample preservation varies depending on the time between collection and analysis: fresh specimens up to 24h might not need fixation and can be preserved refrigerated; above this time, preservation with an equal volume of 50% - 70% ethanol and 2% carbowax (Saccomanno fluid) is recommended to avoid degeneration[74]. Second, slides can be prepared using different techniques, depending on the laboratory. These include sedimentation and smearing, membrane filtration, cytocentrifugation (cytospin), and thin layer methods (ThinPrep)[75]. In order to alleviate these problems, efforts are being made to unify and systematise the classification protocol for urinary cytology[66], including the use of biomarkers linked to cancer and its progression [66, 76]

### 2.2.2. Approaches using detection of cancer biomarkers on urine cells

Several studies have been done to improve current urine tests performance by the use of molecular and protein biomarkers. Some of these have been tested to detect malignant

cells in urine sediments using DNA probes in fluorescence in situ hybridisation (FISH)[77], or antibodies in immunocytochemistry (ICC)[78], and immunofluorescence assays (IFA)[38, 39]. Some of these studies done for bladder cancer have made their way through clinical trials to commercial products: UroVysion, which detects aneuploidy for chromosomes 3, 7, 17, and loss of the 9p21 locus; and ImmunoCyt (or uCyt), detects a high molecular-weight form of glycosylated carcinoembryonic antigen and two sub-glycosylated mucins. Comparative studies between these assays and standard cytology suggest that the use of them together increase the sensitivity and specificity when compared with the individual tests [79-81].

Other biomarkers are currently being investigated for the detection of prostate cancer cells in urine sediments by fluorescence microscopy, such as alpha-methylacyl CoA racemase (AMACR) and erythroblast transformation-specific related gene (ERG) [38, 39, 82]; receptors for the vasoactive intestinal peptide (VPAC1 and VPAC2)[83]; and accumulation of protoporphyrin IX in the presence of an excess of 5-aminolevulinic acid [84], this last also tested successfully on bladder cancer specimens[85].

Efforts are aimed not only to assist current non-invasive tests in early detection of the diseases, but also for prognosis and progression surveillance. For example, a combination of cytology, UroVysion, UCyt and soluble marker NMP22 have proven useful to monitor recurrence of non-muscular invasive bladder cancer [86].

### 2.2.3. MIL38, urine cells and prostate cancer

As described previously, MIL-38 antibody (originally BLCA-38) was raised against a bladder cancer cell line[40]. It had been tested before in urine cells from patients presenting transitional cell carcinoma of the bladder (stages T2-T4) in an immunofluorescence assay

successfully [40], and it had been proven to detect cancer cells in frozen sections of prostate cancer tissue[41]. In this work it was intended to optimise a urine cells IFA for the detection of prostate cancer cells in voided urine samples using MIL-38 antibody as a probe.

## 2.3. MATERIALS AND METHODS

### 2.3.1. Equipment and supplies

**i.** Centrifuges:

**a**. Fixed angle, to fit 1.5 mL microcentrifuge tubes and able to reach speeds of 500-2000 g

**b**. Fixed angle, to fit 50 mL centrifuge tubes and able to reach speeds of 200-500 g

**ii.** Inverted microscope (Zeiss Observer 5) with 10X and 20X objectives.

**iii.** Fluorescent microscope (Zeiss) with a mercury lamp, objectives of 40X and 100X magnification and filters for 490 nm and 350 nm.

**iv.** Cell culture incubator with $CO_2$ feed.

**v.** Laminar flow safety cabinet class II.

**vi.** Incubator 37$^{o}$ C.

**vii.** Fume hood.

**viii.** Automatic pipettes ranging from 0.5 to 1000 µL.

**ix.** Epoxy-coated slides for immunohistochemistry (IHC) or immunofluorescence assay (IFA), one or two 8 mm wells (Medical Packaging Corporation # CPS-0108 (1 well per slide) or # CPS-0208 (2 wells per slide).

**x.** Cover slips (22x22 mm$^2$, thickness per the objectives used)

**xi.** Coplin Staining Jars

**xii.** General plastic ware: microcentrifuge tubes (1.5 mL), conical centrifuge tubes (15 mL and 50 mL), pipette tips, tissue culture flasks, sterile transfer pipettes.

### 2.3.2. Reagents

All chemicals used were analytical grade. Ultra-pure water (Milli-Q); sodium phosphate monobasic; sodium phosphate dibasic; potassium phosphate monobasic; sodium chloride; potassium chloride; Ammonium chloride; potassium bicarbonate; Ethylenediaminetetraacetic acid (EDTA); 4',6-diamidino-2-phenylindole (DAPI, Sigma# D9542, powder, stock of 5mg/mL in DMSO) or Hoechst dye (Thermo-Fisher# H1399, powder, stock of 10mg/mL in water); Glycerol. Skim Milk powder used was purchased in the supermarket. MIL-38 antibody was kindly provided by Minomic International Inc. Goat anti-mouse IgG, conjugated with FITC (Jackson Immuno-Research# 115-095-062) or Alexa Fluor 488 (Highly cross-adsorbed, Life Technologies# A11029). Goat anti-rabbit IgG conjugated with FITC (Cayman# 10006588). Fluoroshield mounting medium (SIGMA# F6182). For cell culture, RPMI-1640 culture medium supplemented with L-glutamine (Gibco# 61870127) and Foetal Bovine Serum.

### 2.3.3. Solutions

All solutions were prepared in MQ water, unless specified otherwise.

**i. Neutralising Phosphate Buffer:** $NaH_2PO_4$ - $Na_2HPO_4$ 100 mM, pH 7.

**ii. Dulbecco's Phosphate buffered saline (DPBS)**: 0.137 M NaCl, 3 mM KCl, 10 mM $Na_2HPO_4$, 2 mM $KH_2PO_4$ pH 7.2-7.4

**iii. Red blood cells lysis solution:** 1.5 M $NH_4Cl$, 70 mM $KHCO_3$, 1.3 mM EDTA

**iv. Blocking solution:** 5% skim milk in DPBS.

**v. Counterstaining solution:** DAPI or Hoechst 1-10 µg/mL in DPBS

**vi. Primary antibody solution**: 10 µg/mL of MIL38 antibody in blocking solution.

**vii. Secondary antibody solution:** 10 µg/mL goat anti-mouse-FITC, 4 µg/mL goat anti-mouse-Alexa488, in blocking solution (Protect from light).

### 2.3.4. Cells

**i. Cultured cells**

Two cell lines were used as controls for the assay using MIL38 antibody: Prostate Cancer cell line (DU145, derived from a brain metastasis, ATCC-HTB-81) was used as positive control[41]; non-invasive bladder cancer (C3, derived from Bladder Cancer cell line UCRU-BL-17CL[87, 88], kindly provided by Dr Pamela Russell), was used as a negative control, as it historically had been used in the laboratory. Breast cancer cell line MDA MB 231 (ATCC-HTB-26) was used in some specificity experiments. DU145 and MDA MB 231 cells were cultured as recommended by ATCC with some modifications. Briefly, cells were grown in T75 culture flasks (Greiner) in RPMI-1640 medium containing Glutamax and supplemented with 10% Foetal Bovine Serum (FBS). Passages were done when reaching 75% confluence, detaching the cells with 10 mM EDTA in PBS and subculturing in a 1/5 ratio. Procedure to culture and subculture the C3 cell line was the same used for DU145. Culture medium used was RPMI-1640 supplemented with 20% FBS.

**ii. Urine Cells**

Patient samples analysed in this part of the work correspond to those approved by the Human Research Ethics Committee of University of New South Wales for the project “Use of

a Monoclonal Antibody toward a cell surface biomarker to detect Prostate Cancer" (HREC 10174, see Appendix A-1) run by Minomic International Ltd. Mid-stream void urine was collected by the patient into 100 mL urine containers with 50 mL neutralisation buffer (200 mM sodium phosphate pH 7.0). Upon arrival to the lab, samples were transferred to 50 mL centrifuge tubes and spun down at 300 g for 5 min to collect the cells. Supernatant was discarded, and cells were resuspended in 1 mL DPBS and transferred to 1.5 mL centrifuge tubes. Cells were washed twice with DPBS and resuspended in this buffer for further processing. The volume of DPBS used to resuspend the cells depended on the size of the cell pellet, although using a subjective criterion.

### 2.3.5. Basic slide assay

**i. Slides:**

The slides used for this assay were coated with epoxy groups, in order to stabilise the cells onto the slide. The epoxy groups bind the primary amino groups present on the surface of the cells, which minimises the loss of cells during the processing. Slides had either one or two 8 mm wells, where the cells were spotted.

**ii. Cells fixation:**

The general procedure consisted of spotting a drop of cells suspended in DPBS (either urine or cultured cells) onto a well and air-dry the slides either at room temperature or at 37°C. Slides were then immersed into ice-cold acetone at -20°C during 3 min for fixation, followed by another air-dry step. At this point, slides were either wrapped into tissue paper and stored into a plastic bag with desiccant in the fridge or were immunostained directly.

**iii. Immunostaining:**

All the incubations were performed in a humid chamber at room temperature, for 30 min. Fixed slides were rinsed with DPBS and blocked (30 μL/well; blocking agent optimisation below). Slides were washed once with DPBS and carefully dried around the wells with a tissue. Cells were incubated with the primary antibody diluted into blocking solution (mainly MIL38 at 10 μg/mL, 30 μL/well). A secondary antibody alone control was always prepared to monitor non-specific binding of this antibody. For that control, blocking solution was used instead of the primary antibody solution in this step. Slides were washed once with DPBS and incubated with the secondary antibody diluted in blocking solution (mainly goat-anti mouse-FITC at 10 μg/mL, 30 μL/well). Slides were washed twice with DPBS and incubated in DPBS containing 1 μg/mL of DAPI (for nuclear counterstaining). Slides were air-dry for 5 min and mounted with 8 μL/well of Fluoroshield mounting medium before putting on the coverslip. Slides were then manually scanned, using eyepieces, in a fluorescence microscope, under the blue filter ("FITC" filter) to inspect for antibody staining and under the ultraviolet filter ("DAPI" filter) to confirm the presence of a nucleus.

## 2.4. ASSAY OPTIMISATION

**i. Staining intensity scale**

For most of this assay development, an arbitrary and subjective scale was used to assign a staining degree, from "negative" to "very strong", based on the brightness perceived in the microscope and with no quantitative measurement of the background. Figure 2.4.1 shows an example of the intensities associated with the different degrees of staining used in the following sections, for reference.

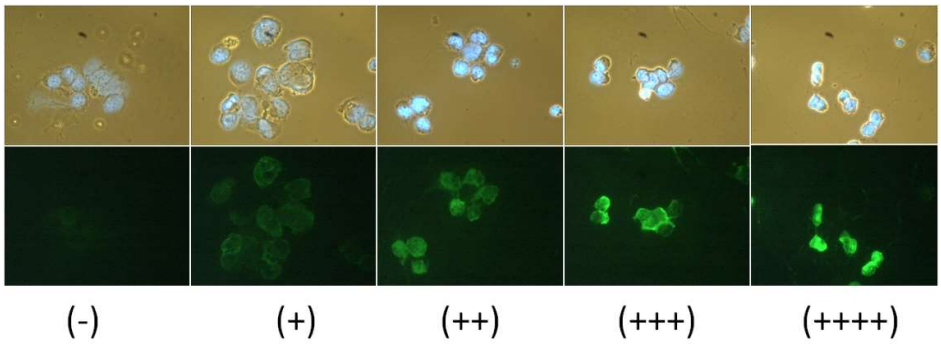


**Figure 2.4.1.** Example of fluorescence intensities associated with different staining degrees, from "negative" (-) to "very strong" (++++). **Top**: bright field. **Bottom**: fluorescence under blue filter, 20 ms.

**ii. Blocking**

Originally, the assay did not have a blocking step, and sometimes results were not clear: normally, cultured cells wouldn't show a strong autofluorescence. However, the secondary alone controls, which test non-specific binding to the cells without primary antibody, gave inconsistent results, i.e. often negative, but sometimes positive. Therefore, a screening of blocking agents was performed. Bovine serum albumin (BSA, 1%), goat and sheep sera (1% and 10%) and skim milk (5%) in DPBS were tested. Protocol described above was followed, using MIL38 as a primary antibody and goat-anti mouse-FITC as secondary antibody. Results are summarised in Table 2.4.1

**Table 2.4.1.** Summary of results of blocking screening. Samples were run in duplicates. 2 Ab alone: secondary antibody alone control. Intensity of the fluorescence observed in the microscope is described with an arbitrary scale: from very strong (++++), strong (+++), weak (++), very weak (+) and negative (–).

| Blocking Agent | Antibody | Reaction* |
|---|---|---|
| **5% skim milk** | MIL38 | ++++ |
| | 2 Ab alone | - |
| **1% BSA** | MIL38 | ++++ |
| | 2 Ab alone | - |
| **1% sheep serum** | MIL38 | ++++ |
| | 2 Ab alone | ++ |
| **10% sheep serum** | MIL38 | +++ |
| | 2 Ab alone | + |
| **1% goat serum** | MIL38 | +++ |
| | 2 Ab alone | + |
| **10% goat serum** | MIL38 | ++ |
| | 2 Ab alone | + |

*The reaction grading was done arbitrarily, based on the overall brightness of the staining observed under the microscope. As staining is not uniform in all the cells, a qualitative approach was preferred.

Traditionally, serum from the species in which the secondary antibody is raised into is used as blocking agent in the different immunoassay formats. Also, skim milk and BSA are popular for this application. Both skim milk and BSA worked well as blocking agents in this assay. However, neither goat of sheep sera in any of the concentrations used was effective, and rather increased the non-specific binding, observed as a positive signal in the secondary antibody alone (2 Ab alone) control.

Based on these results, it is observed that both 1% BSA and 5% skim milk in DPBS were good blockers. For this work, due to its lower price, 5% skim milk in DPBS was selected as a blocking agent for the immunofluorescent assay (IFA).

**iii. Search for a prostate specific marker:**

MIL38 antibody was raised against the bladder cancer cell line UCRU-BL-17-CL[40]. Given that urine sediments include cells from the whole urinary tract (from the bladder, all the way to the urethra), it is likely that the assay will detect bladder cancer cells in urine sediment specimens. Both prostate and bladder cancers are among the 10 more commonly diagnosed cancers in Australia, being the incidence of prostate cancer higher than that for bladder cancer (23% and 3% of cases reported respectively)[4]. Despite the higher probability of prostate cancer, cells from the prostate in urine sediments are scarce, predominating the cells from the bladder. The cross-reactivity of MIL38 with both prostate and bladder cancer cells makes it desirable to have a multiplex system that confirms that every positive cell for the biomarker under scrutiny for prostate cancer is indeed from the prostate, and also to confirm the presence of prostate cells in both test and control samples. At this point of the development, the Prostate Specific G-protein coupled Receptor (PSGR) was tested, using 3 different cell lines (DU145, prostate cancer; MDA MB 231, breast cancer; and C3, bladder cancer) and healthy urine sediments (male and female). As a preliminary assay to test the suitability of this reported prostate specific marker, the same IFA protocol described above was followed; using either MIL38 detected with a goat anti-mouse-FITC secondary antibody or with rabbit polyclonal anti PSGR antibody (Sapphire Bioscience) detected with a goat anti-rabbit-FITC secondary antibody. The IFA was also performed with secondary antibody alone controls to monitor non-specific binding of these conjugates. Results are shown in Table 2.4.2

**Table 2.4.2.** Summary of results of preliminary test of PSGR as a prostate biomarker. Cultured DU145, C3 and MDA-MB-231 cell lines were prepared as described in 2.3.4-i. Normal male and female urine cells were prepared as described in 2.3.4-ii. Intensity of the fluorescence observed in the microscope is described with an arbitrary scale: from very strong (++++), strong (+++), weak (++), very weak (+) and negative (–).

| Sample | Antibody | Reaction |
|---|---|---|
| DU145 | MIL38 | ++++ |
| | Anti-mouse alone | - |
| | PSGR | ++++ |
| | Anti-rabbit alone | - |
| C3 | MIL38 | - |
| | Anti-mouse alone | - |
| | PSGR | ++++ |
| | Anti-rabbit alone | - |
| MDA MB 231 | MIL38 | ++ |
| | Anti-mouse alone | - |
| | PSGR | ++++ |
| | Anti-rabbit alone | - |
| Male urine | MIL38 | - |
| | Anti-mouse alone | - |
| | PSGR | +++ |
| | Anti-rabbit alone | + |
| Female Urine | MIL38 | - |
| | Anti-mouse alone | - |
| | PSGR | +++ |
| | Anti-rabbit alone | + |

Results show that with the method used and the particular antibody chosen for the experiment, PSGR is not a suitable marker to identify prostate cells, as it binds to all of the cells tested. Moreover, it has been demonstrated that its expression varies among prostate cancer cells, depending on the malignancy [89, 90], which would make interpretation of results difficult. Other proteins have been reported as prostate specific markers in IFA of urine sediments, such as Prostein [39] and Nkx3.1 [38]. However, these markers have been linked to cancer of the prostate too [91, 92]. These and other markers, such as Prostate Specific Membrane Antigen (PSMA) and ETS-related Gene (ERG) are used to identify prostatic origin of metastatic lesions [93]. However, Nkx3.1 has been reported in liver cells[94].

Despite the lack of success in the optimisation of a multiplex system to detect prostate specific GPC1 positive cells, a small pilot study was done to test the suitability of GPC1 on urine sediments for prostate cancer diagnosis, using MIL38 antibody.

## 2.5. PILOT STUDY WITH PATIENT SAMPLES

### 2.5.1. Study design

With the optimised assay, a pilot study with patient samples was run. All the patients were male between 40 and 80 years of age. The samples collected were classified according to the following groups:

- Normal (N): normal healthy men.
- Benign Prostate Hyperplasia (BPH).
- Prostate Cancer (CaP), with or without metastasis.
- Radical Prostatectomy (RP), with low PSA levels.

N, BPH and RP (for which low levels of PSA are an indication of absence of metastasis) are used as negative controls. Patients with prostate cancer were all treated the same, without discriminating the severity of the condition, i.e. without sub-classifications based on the aggressiveness of the tumour or the presence or absence of metastasis. Given that this was a preliminary study, the main focus was on the performance of the assay and a gross examination of GPC1 as a cell surface cancer biomarker, using MIL38 antibody.

Patients were approached by the collaborator clinicians (Dr. Paul Cozzi, from Hurstville Community Private Hospital, Hurstville NSW-for BPH and RP samples; Prof. Paul D'Souza from St George Private Hospital, Kogarah, NSW-for CaP samples; A-Prof. Mark Frydenberg from the Australian Urologist Associates Clinic, Malvern, Victoria-negative controls; Prof Mark Willcox, School of Optometry and Vision Science, UNSW, Kensington NSW-for normal healthy controls). Patients were all informed about the study and informed consent was received from each patient to get, process and analyse their samples.

Samples were collected as described above and transported to the lab on ice (an express courier service was used for samples collected in Melbourne), where they were processed within 3 days of collection as described above. Samples were randomly numbered by a colleague and processed in a single blind fashion, in duplicates, as per optimised assay. A single negative control assay (secondary antibody alone control) was done per sample. A minimum of 10 cells per well were required to accept a sample for analysis. A full screening of the whole well was done in each case, and a single positive cell was sufficient to declare the sample positive. Positive fragments were not considered. After obtaining results, these were matched with the original sample type (CaP, RP, BPH or N) to quantify specificity and sensitivity of the assay. A summary of the analysed samples can be found in Appendix A-2.

### 2.5.2. Results

A total of 122 samples were analysed: 26 N, 33 BPH, 38 RP and 25 CaP. However, only 60% of the total samples met the criteria of 10 cells per well for further analysis. To determine the performance of the assay as a diagnosis tool for prostate cancer, two parameters were calculated:

-Sensitivity (false negative results):

$$Sensitivity = \frac{True\ Positives}{True\ Positives + False\ Negatives} * 100$$

-Specificity (or false positive results):

$$Specificity = \frac{True\ Negatives}{True\ Negative + False\ Positives} * 100$$

These values are typically arranged in a table like this:

| | ***Problem samples*** | ***Control samples*** | ***Total*** |
|---|---|---|---|
| ***Positive*** | True positive | False positive | TP + FP |
| ***Negative*** | False negative | True negative | FN + TN |
| ***Total*** | TP + FN | FP + TN | Total samples |

Using this criterion, both parameters were calculated to evaluate the performance of the assay to detect prostate cancer. Table 2.5.2.1 shows the results when combining all the negative controls.

**Table 2.5.2.1.** Determination of sensitivity and specificity of the immunofluorescence assay.

| | ***CaP*** | ***N+BPH+RP*** | ***Total*** |
|---|---|---|---|
| ***Positive*** | 5 | 17 | 22 |
| ***Negative*** | 4 | 47 | 51 |
| ***Total*** | 9 | 64 | 73 |
| ***Sensitivity*** | 55.6 | | |
| ***Specificity*** | 73.4 | | |

Although the sensitivity of the assay was only 55.6%, the specificity was relatively high. The identity of the cells as prostate cells was not monitored, as no suitable prostate marker was available at the time of this study, and there is no certainty of the efficiency of the sample collection method used in recovering cells from the prostate. It has been extensively reported that digital rectal examination (DRE) or prostate massage previous to sample collection, is preferred to ensure the release of prostatic fluids and thus prostate cells into the urinary ducts for urine tests associated with the prostate [95-97]. This requisite remains controversial, as it makes both clinicians and patients uncomfortable. Some have reported that "first catch urine" samples are enriched in prostate fluids, when compared with mid-stream urine samples [98, 99]. The results observed may be influenced by the collection method as it is possible the collected samples might have not been appropriate (mid-stream, collected after releasing the first few millilitres) and therefore the low sensitivity might be partially due to a low level of prostate cells in the samples.

Both parameters were calculated discriminating by group sample, results shown in Table 2.5.2.2:

**Table 2.5.2.2.** MIL38 antibody test performance parameters, discriminated by group sample.

| | *CaP* | *N* | *BPH* | *RP* | *Total* |
|---|---|---|---|---|---|
| ***Positive*** | 5 | 6 | 4 | 7 | 22 |
| ***Negative*** | 4 | 8 | 19 | 20 | 51 |
| ***Total*** | 9 | 14 | 23 | 27 | 73 |
| ***Specificity*** | - | 57.1 | 82.6 | 74.1 | |
| ***Sensitivity*** | 55.6 | - | - | - | |

Specificity was calculated with results for CaP samples and each of the negative controls separately. This way, information about the discrimination power between CaP and each of the separate negative controls is obtained. Performance on normal samples was not optimal but is interesting that the discrimination between CaP and BPH is good, given the low discrimination power of PSA screening between these two conditions. Also, specificity on RP samples was good. The high percentage of samples rejected (~40%) is problematic. Table 2.5.2.3 summarises the samples that were rejected and those from which useful results were obtained:

**Table 2.5.2.3.** Summary of accepted and rejected samples, discriminated by sample group

| **Samples** | **Result** | | **Discarded** | | **Total** | |
|---|---|---|---|---|---|---|
| | n | % | n | % | n | % |
| **N** | 14 | 53.8 | 12 | 46.2 | 26 | 100 |
| **BPH** | 23 | 69.7 | 10 | 30.3 | 33 | 100 |
| **RP** | 27 | 71.1 | 11 | 28.9 | 38 | 100 |
| **CaP** | 9 | 36.0 | 16 | 64.0 | 25 | 100 |
| **Total** | 73 | 59.8 | 49 | 40.2 | 122 | 100 |

n = number of samples; % = percentage from the total number of the group; N = normal; BPH = benign prostate hyperplasia; RP = radical prostatectomy; CaP = prostate cancer.

A total of 49 samples out of 122 were rejected, constituting about 40% of the total of the samples collected. Even though a similar amount of patient samples were collected for each group, failed assays completely imbalanced the numbers, reducing the confidence in the results. The most common cause of sample rejection was low cell yield, followed by autofluorescence. Only 5 samples were rejected due to any other interferents, such as bacteria, crystals and precipitates. It is worth noting that 10/16 of the CaP samples were rejected due to autofluorescence, and 7/12 of the N samples failed the acceptance criteria due to low cell yield. This suggests a sample type related limitation in the assay and, therefore, bias.

## 2.6. DIFFICULTIES TO BE OVERCOME – SAMPLE PREPARATION AND AUTOFLUORESCENCE INTERFERENCE

Despite the problems with the performance of the assay, results in terms of improved specificity compared with the gold standard PSA were encouraging to pursue the improvement of the method. Although the sensitivity of the assay was not very good, the capacity to discriminate between CaP and BPH is an important goal for the current prostate cancer screening programs. Two major problems needed to be solved to overcome the bias of the method: low cell yield and high levels of autofluorescence, in particular that observed in cancer samples.

**i Urine sample preparation:**

Urine samples are very heterogeneous, and to have a unique method of preparation has been challenging. Urine from patients can be very difficult to work with, including interferents such as blood, yeast and bacterial infections, presence of crystals and mucus. Red blood cells were lysed successfully simply incubating the cell pellets with the ammonium carbonate buffer (red blood cell lysis solution), which is a popular method (Dagur and McCoy, 2015). Unfortunately, bacteria and yeast, as well as crystals, were not possible to eliminate from the samples. Samples with mucus presented a strong autofluorescent background, as shown in figure 2.6.1.

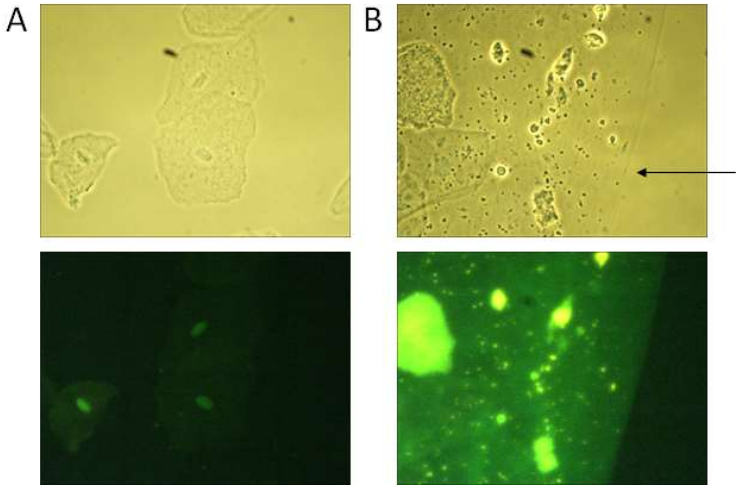


**Figure 2.6.1** Example of fluorescence background generated by the presence of mucus in the urine sample. **Top**: bright field. **Bottom**: fluorescence under blue filter, 20 ms. **A**. Clean urine sample, with very low background. **B**. Urine sample with mucus, showing strong background. Arrow shows in the bright field the edge of a layer of material where cells and other elements are embedded into.

Mucus is a colloidal mixture of different proteins and other molecules. Among the most abundant proteins in mucus are mucins, which form gels by polymerising through disulphide bonds. In order to break the mucin nets and release the urine cells from the mucus, a test using dithiothreitol (DTT), a known reducing agent, was conducted. Briefly, after spinning down the urine samples, the pellet was washed for 10 minutes with a commercial solution called Cytolyt (a methanol based buffered preservative solution for slide preparation, by ThinPrep®) or DPBS with or without 5mM DTT, followed by two rinses with DPBS and fixation on the slides. A representative result is shown in figure 2.6.2.

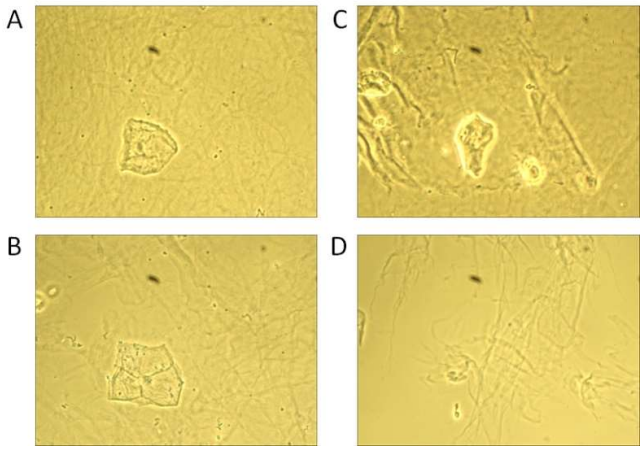


**Figure 2.6.2.** A urine sample presenting mucus treated with **A.** DPBS **B**. DPBS + 5 mM DTT **C.** CytoLyt or **D.** CytoLy + 5 mM DTT.

The sample used for this image is an example of samples presenting abundant mucus that interferes with the assay. The results show that the most efficient treatment to disaggregate the mucins that supports the layer of material in which the cells are trapped is the combination of CytoLyt and DTT (picture D).

Because MIL38 epitope is sensitive to reduction of disulphide bonds, an immunofluorescence assay was performed to test whether cells treated with CytoLyt and DTT would preserve the antigen integrity for it to be detected by the antibody. An indirect IFA was performed on DU145 cells treated as described above. For this assay, detection was done using a goat-anti-mouse Alexa 594 (red). Results are shown in Figure 2.6.3.

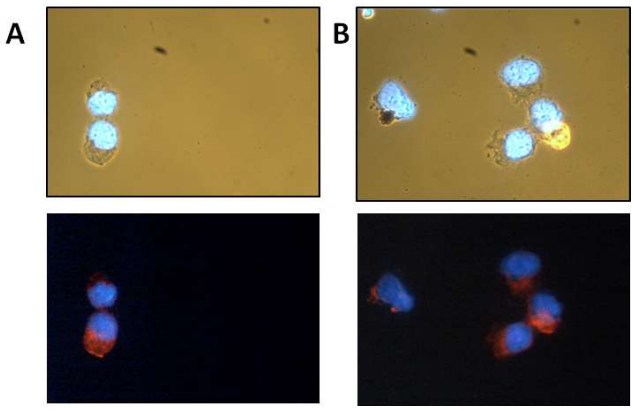


**Figure 2.6.3.** Effect of CytoLyt-DTT treatment on DU145 cells, on the integrity of MIL38 epitope on GPC1. **A.** CytoLyt. **B**. CytoLyt+DTT. **Top**: bright field. **Bottom**: fluorescence under green filter, 50 ms

The experiment showed that the treatment is harsh enough to disrupt a mucus rich matrix, but gentle enough to keep the integrity of the antibody epitope for it to be detected in IFA.

It was also noticed that the number of cells recovered from the samples treated with CytoLyt solution was higher than the simple wash with DPBS. Figure 2.6.4 shows a representative image of the same sample treated with DPBS or CytoLyt:

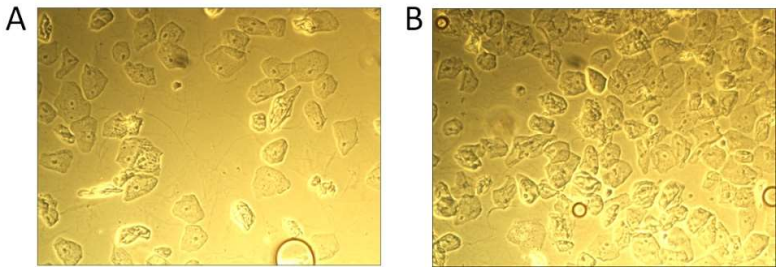


**Figure 2.6.4.** Cell recovery in the same sample treated with **A.** DPBS or **B.** CytoLyt solution.

From these experiments some tools were obtained to overcome some of the obstacles that led to the rejection of some of the samples in the pilot study. Two different cell washes were optimised to eliminate red blood cells and mucus interferents, and the recovery of cells was also improved by the use of the CytoLyt solution.

**ii Use of more photo-stable fluorophores**

Autofluorescence is a property of the cells in which endogenous fluorophores emit light when excited with UV-visible radiation, without any exogenous tag. Among the most important contributors to autofluorescence in cells are NADH, NADPH, FAD, and structures such as mitochondria and lysosomes, and collagen and elastin in the extracellular matrix[100]. Metabolic changes in cells can be monitored using analytical methods, such as flow cytometry[101], spectroscopy[102] and fluorescence microscopy[100], based in autofluorescence of these molecules, in order to understand their relationship with certain conditions, such as cancer[101, 102].

Despite being a useful characteristic for certain analytical approaches, autofluorescence is a burden when the objective is the detection of other biomarkers using

fluorescence, which was the case in the attempt to detect GPC1 in urine cells using MIL38 antibody and a secondary antibody labelled with FITC. The use of a more stable fluorophore, Alexa Fluor 488, conjugated to a goat-anti-mouse antibody, was used in an attempt to obtain a stronger signal that would be discernible over the autofluorescence background. It is reported that the emission of Alexa Fluor 488 is between 1.5 to 2 times more intense than FITC, and it is also more resistant to photobleaching. In figure 2.6.5 it can be seen an example of how difficult it is to discern a positive cell from the autofluorescence background, even using Alexa Fluor for detection. The sample is from catheterised urine from a patient with bladder cancer, and it was processed as per optimised assay, but using an Alexa Fluor 488 labelled secondary antibody.

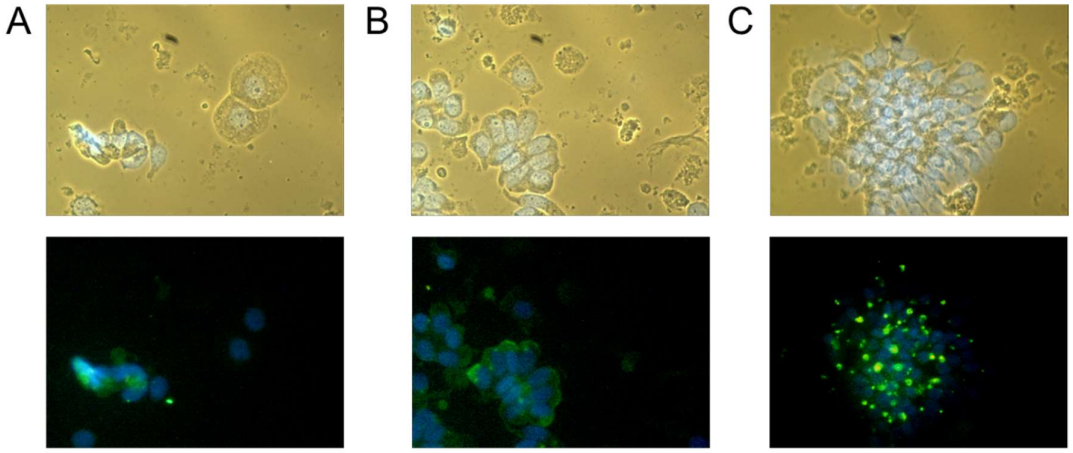


**Figure 2.6.5.** Example of a typical result using the immunofluorescence assay with Alexa Fluor 488 for detection. The sample is from a catheterised urine sample from a bladder cancer patient. **Top**: bright field showing nuclear counterstaining (DAPI). **Bottom**: AF488 and DAPI emissions merged. **A** An example of a field with positive and negative cells. **B**. An example of a field with positive cells. **C**. An example of a field with strongly autofluorescent cells. This belongs to a secondary antibody alone control.

Although the study was originally done on prostate cancer patients, the use of the MIL38 antibody to test bladder cancer samples was being considered at this point of the project, as it was originally raised from a bladder cancer cell line [40]. For this reason, some bladder cancer patient samples were used in the optimisation of this method. However, as observed in figure 2.6.5, the autofluorescence was still a major challenge.

**iii Possible tags for antibody labelling.**

The ideal label used for antibody conjugation must overcome the high autofluorescence of urine cells and be bright enough to be able to detect few cells expressing GPC1. Autofluorescence can be overcome using molecules of long decay times (µs-ms). That way, given an excitation pulse of light, the emission of autofluorescent molecules present in the samples would be exhausted by the time signals from the labelled antibody are collected by the detector. Brightness is then a secondary factor, because removing most of the background signal increases the sensitivity of the system used. Two different types of labels were tested in this work, lanthanide doped upconverting nanoparticles and lanthanide chelates. Results of the research exploring these two options are presented in the following chapters.

## 2.7. CONCLUSION

A slide assay for urine cells was developed using MIL38 antibody to detect GPC1 in prostate cells. A blocking step was established, but an attempt to run a multiplex assay to confirm positive cells were from the prostate failed, as the biomarker chosen reacted with breast and bladder cancer cells. A pilot study with patient samples was run anyway and some difficulties arose. Low cell recovery from urine samples was addressed using a liquid fixative, whereas presence of mucus in samples was treated with a reducing agent. These optimisation actions improved the sample preparation, but autofluorescence interference could not be overcome. Luminescent tools for conjugation with MIL38 are explored in the following chapters.

# 3. UPCONVERTING NANOPARTICLES

## 3.1. SUMMARY

In this chapter, the development of a secondary reagent, using antibody-binding peptides and upconverting nanoparticles (UCNP), is described. Peptides were conjugated to single strand DNA via click chemistry. These conjugates were incorporated onto upconversion nanoparticles (UCNP) via ligand exchange. The final conjugate resulted unstable in suspension and cell assays were unsuccessful. The development of the reagent and assay platform was not pursued further.

## 3.2. INTRODUCTION: UPCONVERSION AS A TOOL TO OVERCOME AUTOFLUORESCENCE

### UCNP or superdots

Upconverting nanoparticles are crystalline molecules, formed by a host (matrix), and a dopant (luminescent lanthanide ions, such as Erbium, Thulium, and europium), which are able to absorb light, typically in the Near Infra-Red (NIR) region, and emit photons of higher energy levels (shorter wavelength, anti-Stokes emission) through a process known as Energy Transfer Upconversion (ETU).[103] These properties, luminescence and ETU, make them ideal for highly autofluorescent samples, such as urine samples, given that most autofluorescence displays a normal Stokes emission profile of excitation at short wavelength and emission of longer wavelength light.

Lanthanides are very inefficient energy absorbers, resulting in very low quantum yields for these molecules: for UCNP, quantum yield is in the range of $10^{-5}$-1%[104]. Thus, the brightness of the particles is highly dependent on the energy input (laser power). To increase lanthanide poor light absorption, UCNP are synthesised with other metal ions (such as

Ytterbium and Gadolinium), called sensitizers, that transfer absorbed energy to the luminescent ions[105]. In this work, the UCNP $NaYF_4$:20%Yb,2%Er is used. The emission spectrum of this nanoparticle when excited with a 943 nm laser shows 4 peaks at 410 nm (blue), 520 and 550 nm (green) and 660 nm (red). Green luminescence consists on photon absorption by $Yb^{3+}$, followed by two-step energy transfer upconversion to $Er^{3+}$. The excited electrons rapidly relax to a more stable energy levels, the green emitting states[106]. This green luminescence is the one used in this work.

Concentration of lanthanides cannot be too high in the nanoparticle, because these ions quench each other's luminescence. On the other hand, concentrations of sensitizers are much higher, to increase the amount of energy absorbed. In other words, the proportion of every element in the nanoparticle needs to be carefully optimised[103, 105]. Host crystal shape and size, as well as its matrix composition, are also important in the efficiency of the nanoparticle as a label[105]. These parameters need to be controlled during particle synthesis.

**Ligands**

It is possible to generate water soluble particles during the synthesis by adding hydrophilic ligands to the organic solvent during the synthesis reaction. For example, addition of 6-aminohexanoic acid to oleic acid during the nanoparticle synthesis can generate products that are soluble both in water and organic solvents. However, the shape of the particle is affected, which is not desirable[104]. Chelators can also be used during the synthesis to control growth and encourage water solubility. But, in the case of EDTA, for example, the interaction with the lanthanides in the particle is strongly pH dependent, and particles tend to aggregate under physiological conditions[104]. The use of polymers such as polyacrylic acid

(PAA) during the synthesis also promotes water solubility and controls particle size and shape. In particular, PAA offers carboxylate groups, suitable for bioconjugation[104].

Despite all these advantages, the synthesis of UCNP in pure organic solvents is preferred, because of the higher level of control over the process, resulting in uniform particles of the desired size and shape as products. Different approaches have been described to either modify the surface part of the ligands, or to exchange them for other hydrophilic ones[104, 105]. However, for the purpose of this work, only the interchange of oleic acid for single strand DNA (ssDNA) for super dots solubilisation in water and bioconjugation is considered. The negatively charged DNA nucleotide's phosphate groups, which have a stronger affinity as chelators for the lanthanide ions at the surface of the nanoparticle than carboxylate groups of oleic acid, displace these to form a new layer, promoting solubility in water. Modifications in the DNA strand are then desirable for further bioconjugation.

**Conjugation to antibodies**

There are several works that describe different approaches in conjugating UCNPs to antibodies[104, 105]. For example, Wang *et al* crosslinked amino-modified silica coated $NaYF_4$;Yb;Er nanoparticles with EDC/NHS activated IgG. This conjugate was used successfully for cell imaging[107].

The use of DNA as crosslinker for bioconjugation with nanoparticles has been summarized by C. Niemeyer [108]. In particular, gold nanoparticles have been conjugated to biotinylated antibodies using DNA-streptavidin conjugates (DNA modified with sulfhydryl group was crosslinked to streptavidin using sulfo-SMCC) as crosslinker. This DNA-streptavidin-antibody complex is then bound to the gold nanoparticle using a DNA base pairing to a

complementary DNA sequence, modified with a thiol group that is adsorbed by the gold nanoparticle[109]. This reagent proved to be efficient in a sandwich ELISA.

More recently, Li (et al, 2013) used ssDNA as substitute ligand and crosslinker for UCNP [110]. Their method is very simple and consists of mixing ssDNA in water with oleic acid capped nanoparticle in chloroform. After incubation with vigorous agitation, the nanoparticles covered with the new ligand are extracted to the aqueous phase. For further applications, they used the complementary ssDNA sequence of this DNA-ligand for crosslinking with drugs to test their utility for intracellular delivery[110].

In this work, the approach for bioconjugation is slightly different, but based in some of these principles. ssDNA was conjugated with small peptides (6-8 aminoacids) capable of binding to the Fc region of IgG antibodies, which have been shown to be useful for IgG purification from different matrixes[111-115]. Sequence of these peptides are shown in table 3.2.1

**Table 3.2.1.-** Characteristics of peptides used for bioconjugation

| **Peptide Nº** | **Design Source** | **Sequence** | **$K_D$ (M)** | **Binding conditions** | **Comments** |
|---|---|---|---|---|---|
| 1 | Fcγ-Receptor[111] | NKFRGKYK | $1.1x10^{-7}$ | 20mM phosphate buffer pH 7.0, 0-0.5 M NaCl. | Bind to both human and mouse IgG. Binding stable at pH 6 |
| 2 | | NARKFYKG | $1.5x10^{-7}$ | | |
| 3 | Combinatorial Chemistry[112] | HWRGWV | $1x10^{-5}$ | PBS, pH 7.4 0.5-1 M NaCl | Binds to both human and mouse IgG and IgM. No sensitive to deglycosilation. |

The crosslinking was done via “biofriendly” click chemistry[116], which consists of the cycloaddition of an azide group (N-terminal of the peptide, with a tetraethylene glycol spacer

arm) with an alkyne group (3' of DNA) catalysed by Cu(I) ions (Figure 3.4.1). To avoid biuret reactions between Cu(II) ions and peptide bonds, the Cu(I) was generated by *in situ* reduction with an excess of a reducing agent (ascorbic acid), and then chelated with a particular ligand to protect the reduced copper from being oxidised by the atmospheric oxygen, previous to the coupling reaction. Two ligands were investigated: tris(3-hydroxypropyltriazolylmethyl)amine (THPTA), which has been widely used for this application, although with relatively low efficiency[32, 117], and bicinchoninic acid, which has recently been shown to have better yields for this copper assisted cycloaddition, but with less application history[118]. The former one was ultimately chosen for the synthesis method. The final product was tested for antibody binding and then used for UCNP ligand exchange. The final conjugate was tested as a secondary detection reagent in a cell immunoassay similar to the one described in the previous chapter, with MIL38 antibody as a primary reagent.

## 3.3. MATERIALS AND METHODS

### 3.3.1. Equipment and Supplies

i. Micro-reaction tubes (Eppendorf).

ii. Glass vials with aluminium cap.

iii. Parafilm.

iv. Automatic pipettes and tips.

v. pH-meter.

vi. Sonicator.

vii. Nanodrop spectrophotometer.

viii. Micro-reaction tube shaker with controlled temperature (heat block).

ix. HPLC system (Agilent).

x. RP-HPLC column: PLRP-S 300A, 3 µm, 150x2.1 mm (520 µL bed volume), Agilent.

xi. FPLC system (BioRad)

xii. Gel filtration column Superdex S-200 10/300 GL. GE

xiii. Dynamic Light Scattering instrument (ZetaSizer).

xiv. Confocal Microscope, Olympus, equipped with a 980 nm NIR laser.

### 3.3.2. Reagents

All chemicals used were analytical grade. Acetic acid (glacial); acetone; acetonitrile (HPLC grade); aminoguanidine hydrochloride; ascorbic acid; bicinchoninic acid potassium salt; Bovine Serum Albumin (BSA); copper (II) sulphate; EDTA; ethanol; 4-morpholineethanesulfonic acid (MES); potassium chloride; potassium phosphate dibasic; potassium phosphate monobasic; sodium acetate; sodium chloride; triethylammonium acetate (TEAA); trifluoroacetic acid (TFA); Trizma base; ultra-pure water (MQ).

Single strand DNA with a 3'alkyne group (sequence: GGG GGA AAA AAA AAA AAA AAA), was purchased from Integrated DNA Technologies (USA).

Peptides sequences (see table 3.2.1) were conjugated at the N-terminus to an azide group through a Lysine-tetraethylene glycol linker. These peptides were synthesized by GenScript (USA).

Oleic acid capped UCNP ($NaYF_4$:$Er^{3+}$, $Yb^{3+}$) were kindly provided by Professor Dayong Jin.

### 3.3.3. Solutions

All solutions were prepared in MQ water, unless specified otherwise.

i. Peptide-DNA coupling:

i. Phosphate buffer: 100 mM pH 7.

ii. Cupric sulphate ($CuSO_4$) 20 mM.

iii. BCA 100 mM

iv. sodium ascorbate 100 mM (fresh).

v. Aminoguanidine hydrochloride 100 mM.

vi. Peptide-azide, 5 mM in MQ water.

vii. DNA-alkyne: 0.5 mM in MQ water.

viii. EDTA 50 mM, pH 7.

ii. Peptide-DNA conjugate purification:

i. Sodium acetate: 3 M, pH 5.5

ii. Solution A: TEAA 100 mM, pH 5.5

iii. Solution B: 75% acetonitrile in solution A.

iv. Solution C: TFA 0.1%, Acetonitrile 5%.

v. Solution D: 90% Acetonitrile, 0.01% TFA.

iii. Peptide-DNA-UCNP conjugation:

i. MES buffer: 50 mM, pH 5.5

ii. Tris buffered saline, (50 mM Tris pH 7.5, 150 mM sodium chloride)

iii. Acetate buffered saline, (50 mM acetate pH 5.5, 150 mM sodium chloride)

iv. MES buffered saline (50 mM MES pH 6.5, 150 mM sodium chloride)

v. DNA-peptide conjugate: 1 nmol/µL in MES buffer

iv. Cell assay:

i. Tris buffered saline (TBS) pH 7.5

ii. 1% BSA in TBS

### 3.3.4. Procedure

i. DNA-Peptide Coupling:

In a 2 mL tube, 5 µL of DNA-alkyne solution were mixed with 425 µL of phosphate buffer. 10 µL of Peptide-azide solution were added. 2.5 µL of $CuSO_4$ solution were mixed with 5 µL of BCA solution and this mixture was added to the reaction solution above, followed by 25 µL of aminoguanidine solution and 25 µL of sodium ascorbate solution. Reaction tubes were closed, wrapped in parafilm and incubated with agitation (about 60 r.p.m) overnight at 45°C protected from light. 10 µL of EDTA solution were added to stop the reaction.

ii. DNA-Peptide conjugate purification:

i. *DNA-peptide precipitation*: for 100 µL of DNA-peptide coupling mixture, 2 µL of sodium acetate solution and 500 µL of absolute ethanol at -80$^{o}$C, were added and mixed well by vortexing. The mixture was incubated at -80$^{o}$C for 15 min, then centrifuged at 25,000 g for 10 min, discarding the supernatant. This step was repeated once or twice to obtain a cleaner pellet. The final DNA-peptide conjugate was reconstituted in 100 µL of MQ water and frozen until purification.

ii. *Reverse phase HPLC*: the PLRP-S column was equilibrated with Solution A, at 0.1 mL/min. 20-40 µL of conjugation reaction mixture were injected per run. The run consisted of the following steps:

1. 15 min isocratic flow Solution A.
2. 20 min gradient to 100% Solution B.

3. 10 min isocratic flow Solution B.
4. 10 min isocratic flow Solution C.
5. 10 min gradient to 100% Solution D.
6. 10 min isocratic flow Solution D.

260 nm peaks were collected, dried by vacuum centrifugation, resuspended in 100 µL MQ water and stored at -20$^{o}$C until used for UCNP ligand exchange.

- Concentration of DNA-peptide conjugate was estimated using NanoDrop spectrophotometer. All the peptides to be tested contain aromatic aminoacids that contribute to the absorbance at 260 nm. However, given that the number of nucleotides per conjugate is larger than the aromatic aminoacid (20 to 2), estimation assuming 20 nucleotides was used for the concentration estimate.

iii. <u>UCNP Ligand Exchange</u>:

10 µL of oleic acid capped UCNPs were diluted in 500µL of chloroform in a glass vial with aluminium cap. 500 µL of 0.5 nmol/µL ssDNA-peptide conjugate in MES buffer pH 5.5 were slowly added to the UCNP suspension, vortexing occasionally. The reaction mixture was capped and incubated overnight at room temperature with shaking. The reaction mixture was allowed to sit on the bench until aqueous (top) and organic (bottom) phases were clearly separated. The aqueous phase containing the nanoparticles was transferred to a clean Eppendorf tube and centrifuged for 15 min at 20,000 g. The nanoparticle pellet was washed twice with buffer to remove unbound ssDNA-

peptide conjugate. Final pellet was resuspended in 100-500 µL of different storage buffers by sonication.

iv. Transmission Electron Microscopy:

TEM images were kindly obtained by Dr Deming Lu, from the Physics Department at Macquarie University. Original sample solution (10 µL) were mixed with 20 µL ultrapure water and 10 µL of ethanol and sonicated for 10 s prior to imaging. Instrument settings: voltage 100 kV, Spot size 6, camera exposure time 1 s.

v. Cell assay:

DU145 and C3 cells were cultured and slides prepared as described in Chapter 2; for the basic assay see 2.2.5. Fixed cells were incubated with MIL38 antibody in TBS/BSA for 30 min, then washed with TBS. Different dilutions of the UCNP-ssDNA-peptide conjugate in TBS/BSA were incubated with MIL38 probed cells or unlabelled cells (for non-specific binding control), then washed with TBS. Images were taken with 980 nm NIR laser equipped confocal microscope.

## 3.4. CONJUGATION AND PURIFICATION OF SSDNA AND IGG BINDING PEPTIDES

Conjugation of the IgG binding peptides to the single strand DNA chain (ssDNA) was done through click chemistry, as described in Section 3.3.4. Peptides were linked to an azide group by a lysine residue side chain through a tetra-ethylene glycol crosslinker. The ssDNA chain had an alkyne group linked at the 3' terminal. The reaction scheme is shown in Figure 3.4.1

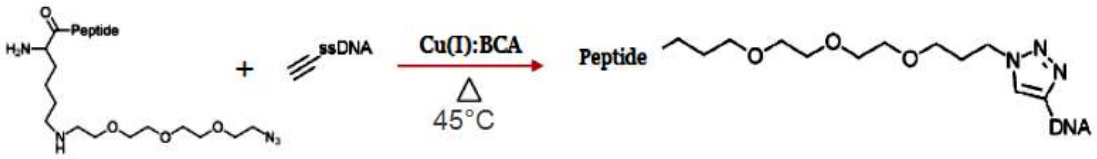


**Figure 3.4.1-** Reaction scheme for conjugation of IgG binding peptides to ssDNA through click chemistry.

To protect the peptide backbone from reduction during the cycloaddition, two different Cu(I) chelators were tested: tris(3-hydroxypropyltriazolylmethyl)amine (THPTA)[116] and bicinchoninic acid (BCA)[118]. Both gave similar results (not shown) and BCA was ultimately chosen, because given the intense purple colour the Cu(I):BCA complex gives to the reaction mixture, it is convenient to monitor the sample clean-up for further purification. Previous works have carried out this reaction at room temperature[116], or at 37°C [32]. However, it was found in this work that overnight incubation at 45°C was optimal (data not shown).

To purify the final product from unreacted reagents, samples were precipitated with cold ethanol and then purified by reverse phase HPLC. During the method development it was noticed that an acidic buffered system (TEAA) favoured elution of ssDNA and ssDNA-peptide conjugates with acetonitrile, but unreacted peptides would remain in the column. On the other hand, aqueous TFA would favour elution of peptides with acetonitrile, but ssDNA and ssDNA-peptide conjugates would remain in the column. The interest was on separating the ssDNA-peptide conjugates from the unreacted ssDNA, therefore the method was designed to perform this separation first, followed by two extra steps with TFA to remove unreacted peptide from the column.

Typical chromatograms from ssDNA species is shown in the Figure 3.4.2

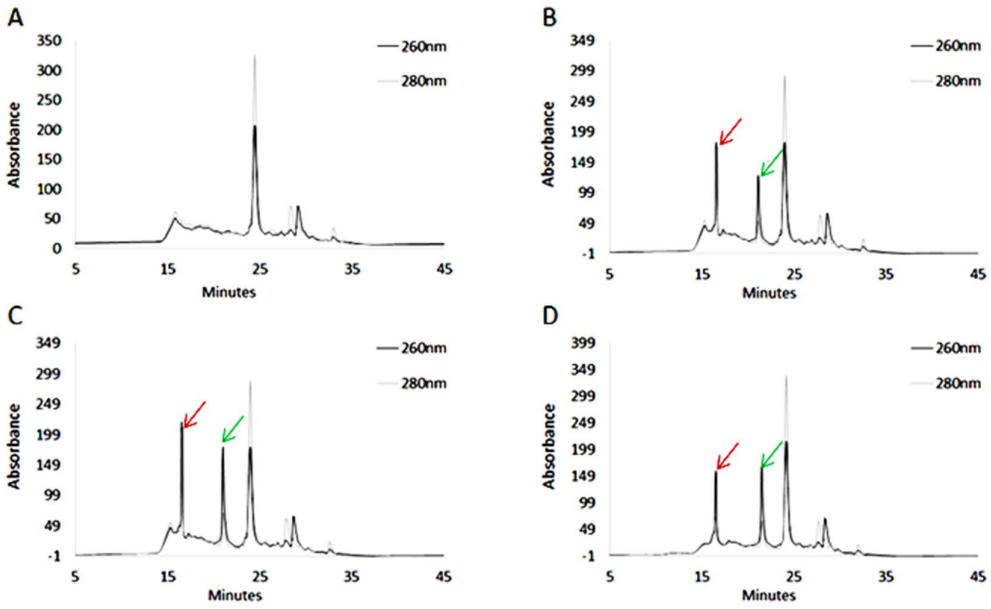


**Figure 3.4.2-** Representative examples of HPLC profiles for ssDNA and ssDNA-peptide conjugates with the final purification method. Traces recorded at 260nm (black) and 280nm (grey) are shown. Unreacted ssDNA (red) and ssDNA conjugated to the different peptides (green) are signalled by arrows. **A**. Blank of reaction mixture. **B.** Conjugate 1. **C.** Conjugate 2. **D.** Conjugate 3. (Conjugates 1,2 and 3 correspond to those of the peptides 1-3 described on Table 3.2.1.)

ssDNA and ssDNA-peptide conjugate peaks were manually collected, dried and resuspended in ultra-pure water. UV-Visible spectra were measured with a NanoDrop Spectrophotometer (Figure 3.4.3).

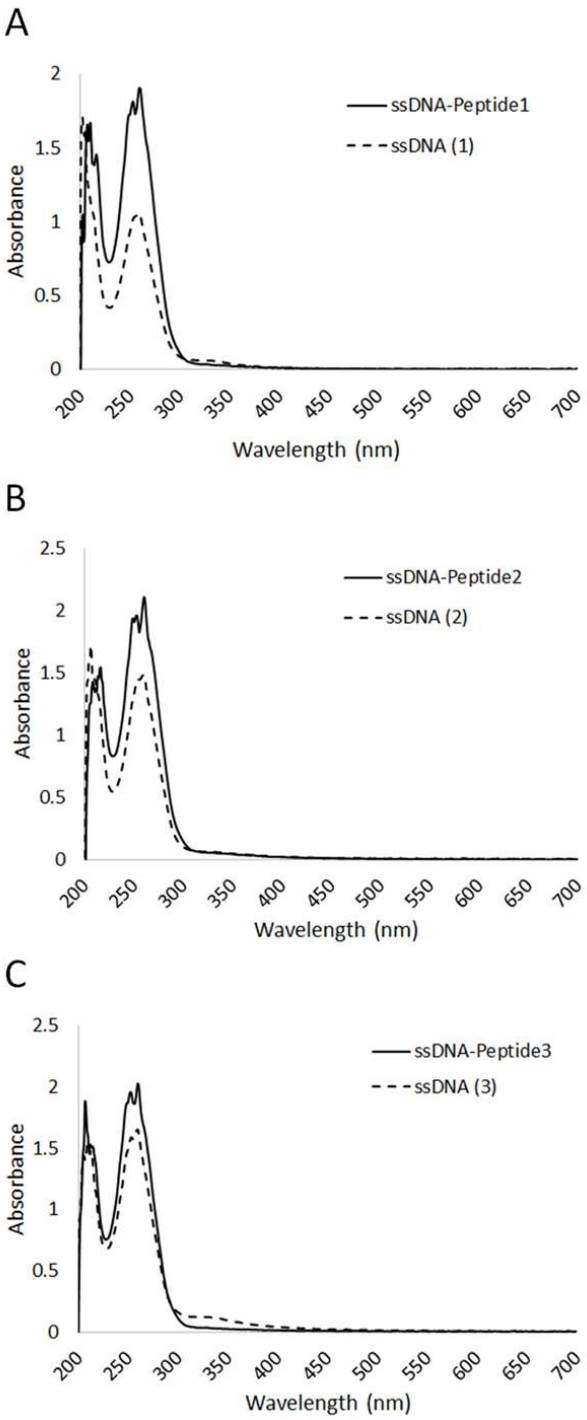


**Figure 3.4.3-** Spectra of purified ssDNA-peptide conjugates (solid line) and the unreacted ssDNA (broken line) peaks collected. **A**. Conjugate 1. **B**. Conjugate 2. **C**. Conjugate 3.

The spectra profile corresponding to the ssDNA conjugated to the different peptides look similar, despite the differences of the peptide sequences all containing aromatic aminoacids. These profiles are also like the unconjugated ssDNA. Based on these similarities, it was assumed that the absorbance at 260 nm was mostly due to the nucleotides in the DNA, and using its sequence, the concentrations of the purified samples were determined by Nanodrop to estimate the yield of the reaction. The data is summarised in the table 3.4.1.

**Table 3.4.1** ssDNA and IgG binding peptides conjugation yield estimation.

| Sample | Conjugate recovered (nmol) | Total recovered* (nmol) | Yield (%) |
|---|---|---|---|
| Conjugate 1 | 8.0 | 12.0 | 66.7 |
| Conjugate 2 | 9.2 | 15.2 | 60.5 |
| Conjugate 3 | 8.5 | 14.6 | 58.2 |

* The total nmol of conjugate and unreacted DNA collected from HPLC elution.

The yields obtained in the conjugation reactions are comparable with the 60% range reported before for click chemistry using BCA[118].

The differences in 280 nm / 260 nm absorbances and molecular size of both antibody and ssDNA-peptide conjugates were used to examine, by gel filtration chromatography, whether the conjugate would bind to MIL38 antibody. Roughly equimolar amounts of antibody and either ssDNA-peptide conjugate or unconjugated ssDNA (to test for non-specific interactions) were mixed in TBS (pH 7.5), incubated for 10 minutes and injected onto a Superdex S-200 (GE) column equilibrated with TBS/glycerol (5%). The antibody alone was run as control and reference. Absorbance traces at 280 nm and 260 nm were recorded. Chromatograms are shown in Figure 3.4.4.

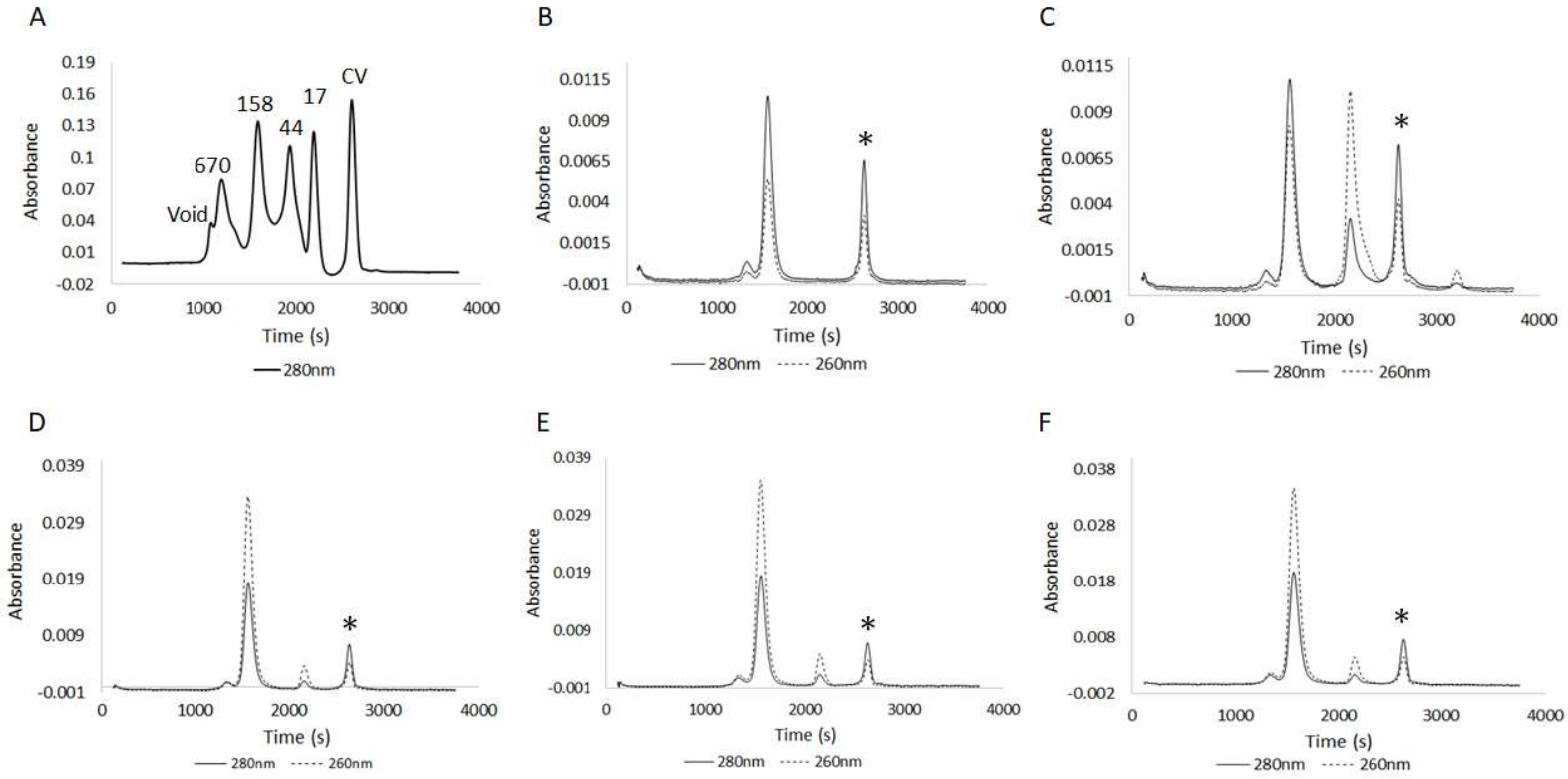


**Figure 3.4.4-** Antibody/DNA-Peptide conjugates binding assay: gel filtration chromatograms. Traces recorded at 280 nm (solid line) and 260 nm (broken line) are shown. Peaks marked with a star (*) indicate an artefact caused by the density difference between running buffer and sample buffer. **A.** Molecular weight standards run on the same conditions are shown. Molecular weights are in kDa. Void volume and column volume (CV) are also shown. **B** Antibody alone. **C**. Antibody and unconjugated DNA mixed. **D, E, F** Conjugates 1, 2 and 3 respectively.

In the figure a set of molecular weight standards are shown for reference. MIL38 alone elutes at the expected retention time. The Antibody and unconjugated DNA chromatogram shows the elution of two individual peaks. The resolution of the column is, according to the specifications of the manufacturer, from 10-600 kDa. The retention time of the ssDNA (which is around 6.6 kDa) is expected to be the same or very close to the 1 CV mark, but it comes out a bit earlier. This could be due to formation of dimers by weak interactions, or just simply an artefact due to the shape of the molecule, which is linear rather than globular. In any case, the result suggests that there are not important non-specific interactions between the ssDNA sequence used as crosslinker and the antibody. On the other hand, for conjugates 1, 2 and 3, the chromatograms show a similar profile, in which the peak corresponding to the antibody retention time has an increased absorbance at 260 nm. Note that the molecular weight shifts due to the binding of 1 or 2 ssDNA-peptide conjugates (7 and 14 kDa extra respectively) would not be resolved by this column. The evidence of binding is the change in the relative absorbance at 260 nm and 280 nm. With this experiment it is concluded that, at the conditions tested, the three ssDNA-conjugates prepared are capable of binding the MIL38 antibody.

## 3.5. ssDNA-PEPTIDE CONJUGATES AND UCNP CONJUGATION - LIGAND EXCHANGE

Following the IgG-binding peptides conjugation to ssDNA and purification, the conjugates were used to coat UCNP, via a process known as ligand exchange (see process scheme in Figure 3.5.1). UCNP are synthesized in the presence of oleic acid, to control shape and size. The final product is, therefore, coated with oleic acid molecules, which make the particles insoluble in aqueous solutions. The goal of ligand exchange is to substitute the oleic acid ligands for the peptide-ssDNA conjugates, which are negatively charged. To achieve this, the conjugates are diluted into MES buffer (pH 5.5) and mixed with the UCNP suspended in

chloroform. The exchange occurs in the interface between the aqueous and the organic media, given that phosphate groups in the ssDNA molecule have a higher affinity for the lanthanides on the surface of the nanoparticles. Once enough oleic acid has been displaced, the particles gain negative charge that transfers them to the aqueous phase.

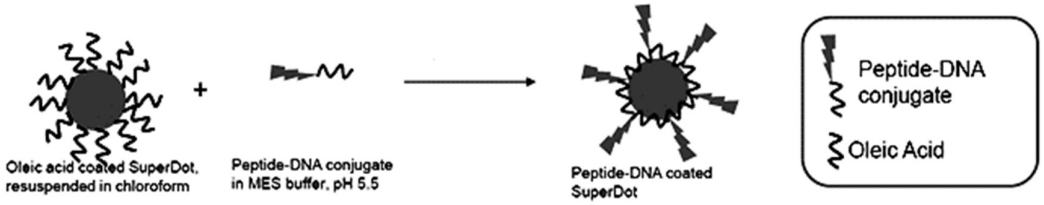


**Figure 3.5.1-** UCNP ligand exchange scheme representation.

After the exchange, the particles are washed with MES buffer by centrifugation, to remove unbound conjugate, and the final product was resuspended in a storage buffer. Initially, TBS (pH7.5) was selected, as it was being used for cells assays and phosphate containing buffers were avoided, as phosphate ions could displace the ligands from the particle's surface.

Particles suspension in TBS were characterised with different methods. First, a UV-Visible spectrum was measured, using Nanodrop spectrophotometer. Figure 3.5.2 shows a typical spectrum profile of UCNP coated with ssDNA-peptides conjugates. The UV-visible spectrum has a typical scattering absorbance profile, with characteristic 260 nm absorbance peak of the DNA bound to the nanoparticle superimposed. The UCNP, on the other hand, absorb in the NIR part of the spectrum (980nm), which is out of the range of the instrument.

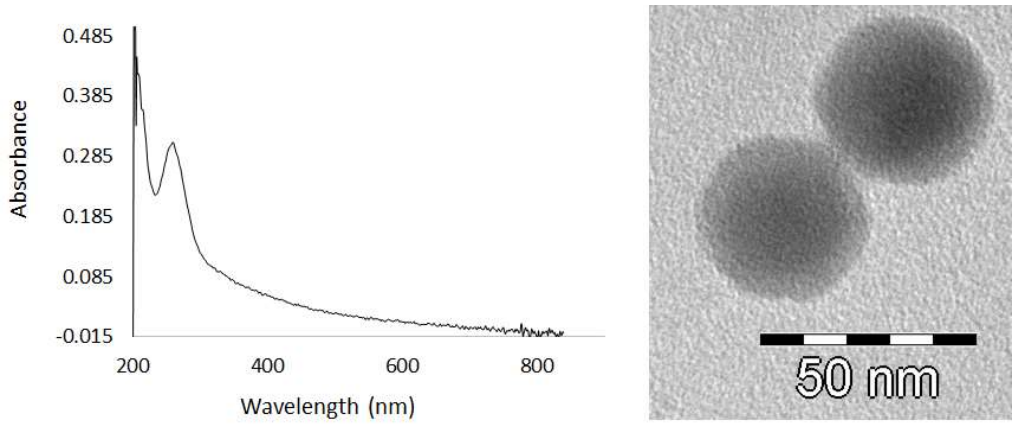


**Figure 3.5.2.** Left: Typical UV-Visible spectrum of UCNP in suspension after ligand exchange. Right: Transmission Electron Microscopy Image of UCNP after ligand exchange.

To visualise the particle's shape and the uniformity of the coating, transmission electron microscopy images were taken. Figure 3.5.2 shows a typical zoom image. The core particle, that looks darker, is around 25-30 nm in diameter, and the coat around 7-10 nm thick. The whole particle measured 40-50 nm in diameter. These dimensions corresponded to what was expected for UCNP, which are around 40nm in diameter.

The UCNP coated with ssDNA-peptide conjugates were stored in TBS buffer at 4°C as mentioned above. It was noticed however, that the particles would aggregate and precipitate on time, and that aggregates would not disaggregate with sonication. This was the next problem to be addressed.

## 3.6. UCNP-PEPTIDE CONJUGATES STABILITY – AGGREGATION PROBLEMS

The first hypothesis considered when addressing the UCNP aggregation in storage was that the ligand exchange was incomplete and that the leftovers of oleic acid on the surface of the particles were driving the aggregation. To solve this, a second incubation step with the ssDNA-peptide conjugate in the presence of a non-ionic surfactant was tested. The rationale behind this additional step was that the surfactant would help the oleic acid to be replaced by the phosphate groups in the ssDNA molecule in aqueous solution. This step was carried on at room temperature with agitation for 2h. Polysorbate 20 (Tween-20) was chosen as its polar group, which consists on ether and hydroxyl groups, has a lower affinity for the lanthanides on the surface of the particle, compared with the phosphate groups, and therefore would not compete for binding. Also, Tween-20 is widely used in immunoassays and would not interfere with the final application of the conjugate. After this additional incubation, the particles were washed from unbound ssDNA-peptide conjugate and resuspended in TBS for storage. UV-visible spectra were examined, and particle size was observed by TEM and Light Scattering (Zeta-Sizer), as shown in figure 3.6.1.

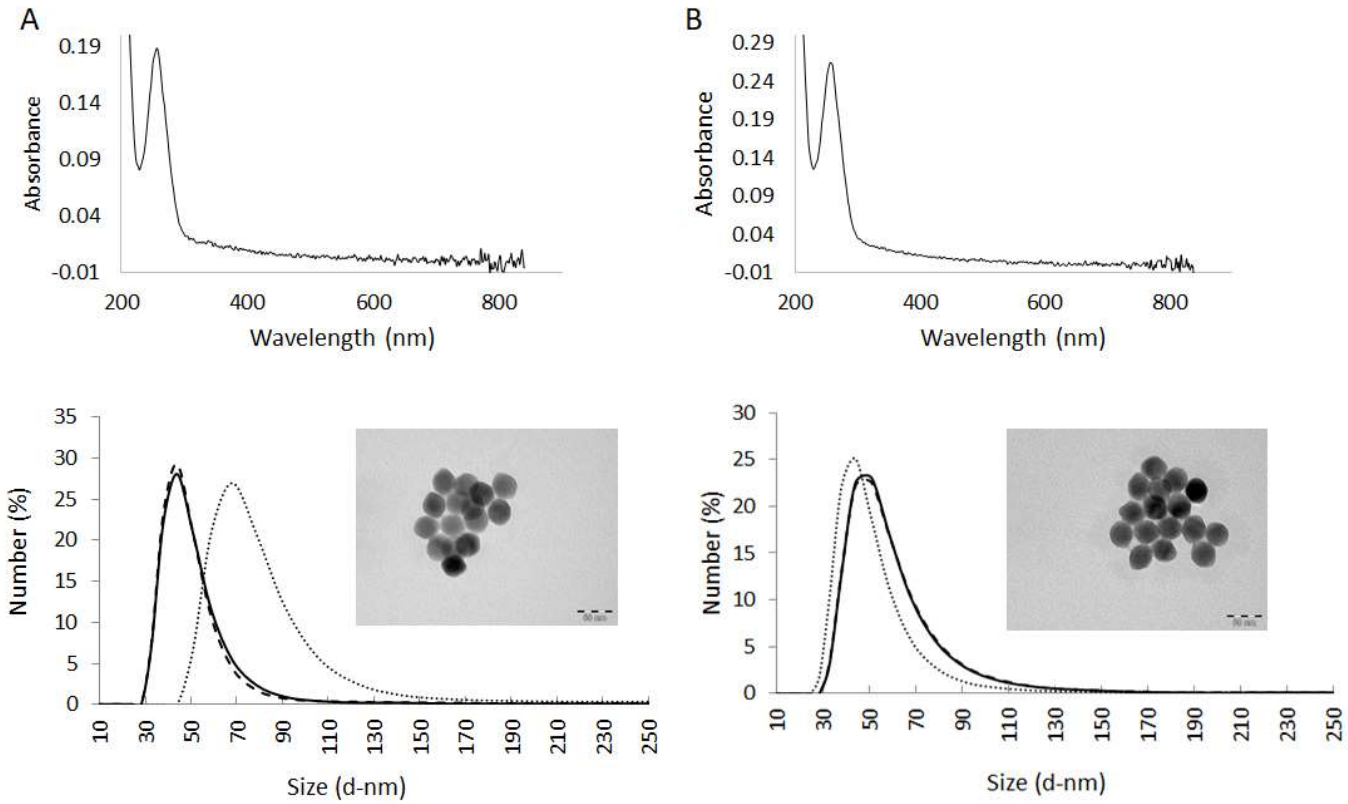


**Figure 3.6.1**- Effect of surfactant Tween-20 in the stability of monodisperse UCNP suspension. Results for conjugate 2 are shown. Incubation without **(A)** and with **(B)** Tween-20 was done after ligand exchanged UCNP were collected in the aqueous phase. **Top**: UV-Visible spectra of UCNP in suspension in TBS. **Bottom:** Zeta-Sizer particle size distributions (triplicates) and the corresponding TEM image.

The UV-spectra showed a similar pattern for both preparations. Light-Scattering results also show similar particle size, except that one of the replicates for the preparation in which Tween-20 was not used shows a higher particle size. For both preparations, however, TEM images look similar. Stability during storage did not improve either, as aggregation was again observed in time.

Storage buffer was therefore addressed. The Tween-20 preparation was sonicated in water bath for 10 min, split into aliquots and spun down. Particles were then resuspended by sonication in MQ water and three different buffers: TBS (pH 7.5); acetate buffered saline (pH 6.5) and MES-buffered saline (pH5.5). Light Scattering measurements of particle sizes were then taken, as shown in Figure 3.6.2.

Particle size distribution shows that lower pHs buffers favours a monodisperse suspension of the particles, and that water only is not an adequate storage medium. Note that the particles, originally aggregated, did not reverse to a truly monodisperse distribution, around 50 nm, which confirmed that the aggregation of these particles Cannot be totally reversed, as was observed before.

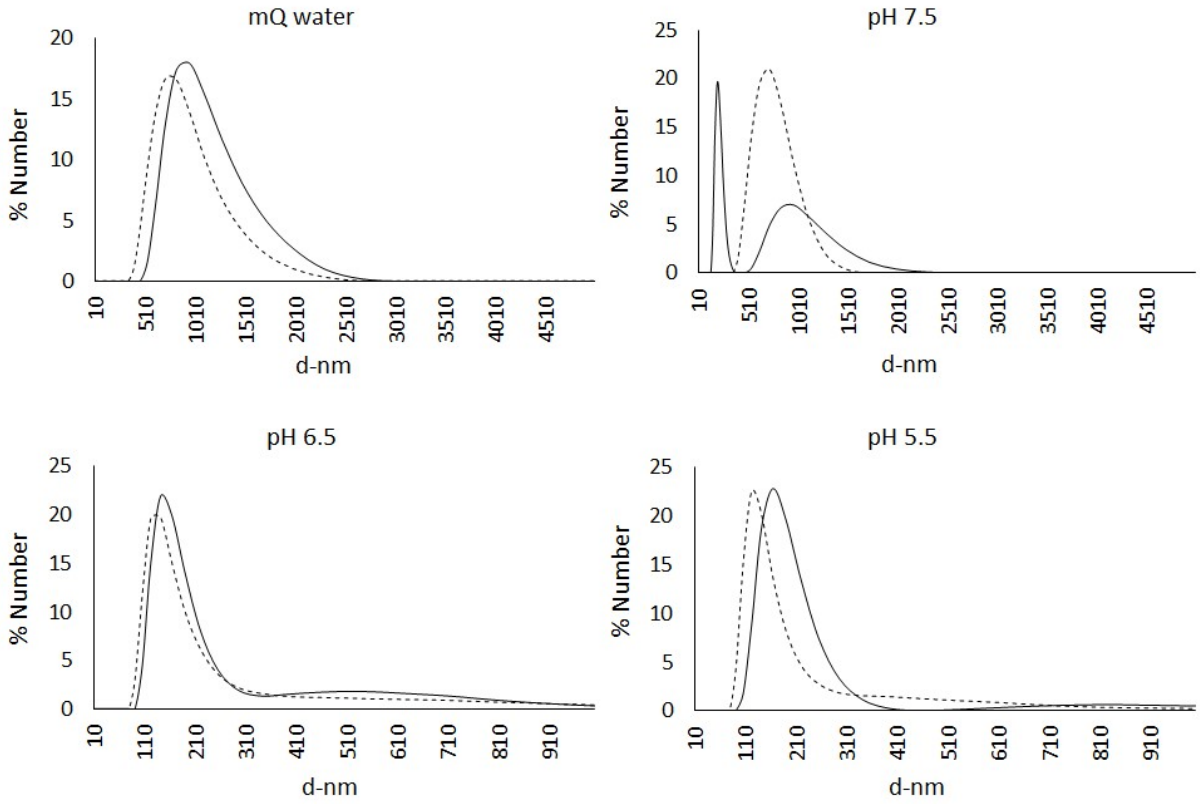


**Figure 3.6.2.** Zeta-Sizer particle size distributions (duplicates) of UCNP in suspension in ultrapure water and buffers with different pHs.

Despite the aggregation and broad distribution of sizes of the conjugated UCNPs, a cell assay was attempted, nonetheless. The method developed in chapter 2 with MIL38 as primary antibody and the conjugated nanoparticles as a secondary reagent was followed, but using TBS buffer instead, as it complies with the binding conditions for the IgG-binding peptides (see Table 3.2.1 and Figure 3.4.4). A few attempts of this assay were unsuccessful, as particle aggregates would predominate in the images and no binding to the cells was observed. Figure 3.6.3 shows a typical image obtained using the UCNP conjugated IgG binding peptides as Secondary reagent.

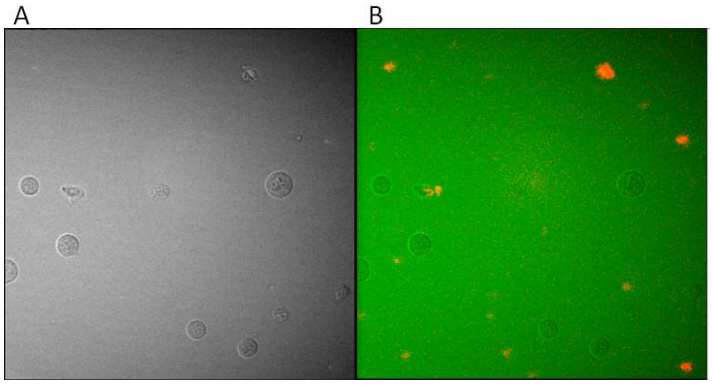


**Figure 3.6.3.** Typical image of cell assay performed on DU145 cells, with MIL38 as primary antibody and Peptide-ssDNA-UCNP conjugates as secondary reagent. **A** Bright field. **B** Merge of bright field and UCNP emission. Image was taken using a 980 nm NIR laser equipped confocal microscope.

Results so far suggest that the cell assay conditions used are incompatible with stability conditions of the conjugated nanoparticles, which tend to form aggregates during storage.

## 3.7. DISCUSSION

In this stage of the work, it was intended to explore the use of Upconversion Nanoparticles (UCNP) as a tool to overcome autofluorescence in urine samples being examined for GPC1 by immunoassay using MIL38 antibody. The approach taken consisted of the preparation of a secondary reagent that would be useful for immunoassays targeting antibodies against other biomarkers as well. The use of peptides to capture antibodies had been shown to be an effective and less expensive alternative to traditional molecules, such as Protein A and Protein G [111, 113, 114, 119, 120]. Three of these peptides were selected to test for the reagent. On the other hand, one step ligand exchange using ssDNA molecules[110] was appealing to incorporate the antibody binding peptides to UCNP. In order to conjugate the IgG binding peptides to the ssDNA crosslinker, click chemistry was chosen as it is clean and specific, compared for example with the widely used EDC-NHS system, which would target any free amino group available, leading to undesirable reactions. Biofriendly click chemistry methods have been developed in order to protect the protein/peptide backbone from undesired reactions with copper [116, 118, 121]. A method using bicinchoninic acid was slightly modified to use with peptide-tetraethyleneglycol-azide and ssDNA-alkyne conjugation successfully. Purification of the conjugates from the unreacted material was done by reverse phase HPLC and the purified products were shown to bind to MIL38 antibody. The conjugates were then incorporated by one step ligand exchange, but the final conjugates were unstable at the storage conditions used, tending to aggregation over time, through an unknown process that seems to be pH dependent. Muhr *et al* (2014)[122], have summarised different approaches that have been attempted in order to turn hydrophobic UCNP in functionalised water soluble UCNP stable in aqueous solutions. In

particular, the use of the amphiphile Poly(maleic anhydridealt-1-octadecene) (PMAO) to transfer oleic acid coated UCNP to aqueous phase, followed by crosslinking with bis(hexamethylene)triamine (BHMT) stabilised UCNP in pHs from 3 to 13 for several weeks[123]. This approach generated stable particles that can be used for cell uptake experiments. However, aggregation of bioconjugated UCNP for immunoassays seems to be still an unsolved problem[122].

If the aggregation of the particles was due to a non-uniform ligand exchange process, perhaps a purification and enrichment of more uniform particles could improve the stability of the final product. However, for UCNP, given their size and tendency to aggregation, it is not trivial. In most of the works revised, modified nanoparticles were separated from the non-bound modifiers by simple centrifugation or ultrafiltration. However, these methods do not discriminate between the different populations of nanoparticles, such as aggregates, partially modified particles, etc. Different methods have been described for the separation of nanoparticles of different sizes. Density gradients have been used to separate polydisperse nanoparticles. Chen *et al* were able to separate different levels of aggregates of encapsulated gold nanoparticles using CsCl gradient centrifugation[124]. Also, gold nanoparticles of different sizes (20-250 nm) were separated using glycerol gradient centrifugation[125]. Viscosity gradients have also been used for separation of nanoparticles of different sizes: Qiu and Mao prepared a polyvinylpyrrolidone (PVP) gradient to generate a viscosity gradient, and with it they were able to separate PVP coated gold nanoparticles up to 50 nm[126]. On the other side, size exclusion chromatography has also been reported for separation of gold nanoparticles of different sizes (~10-60 nm), using a Nucleogel column, which according to the manufacturer can be used to separate polymers up to about 1 MDa[127]. However,

without the understanding of the actual process that drives the conjugated UCNPs aggregation, development of a separation step would be a very empirical process of trial and error.

Given that the preparation of this reagent was becoming more complex and ultimately would result in an expensive process that would not be transferrable to a larger scale, the pursuit of the optimisation of the reagent preparation and an appropriate cell assay was abandoned. Additionally, it was later considered that human specimens often present antibodies from the patients. Thus, the use of this conjugate as a detection reagent for the analysis of human samples, such as blood circulating tumour cells (CTC) or cancer cells in urine, is ill advised: as the peptides cannot discern between human and mouse IgG, this cross-reactivity would potentially generate false positives.

Autofluorescence interference of urine samples was still a problem, though, and a new approach was then tested: the use of lanthanide chelates as labels for antibody labelling. The work developed in this stage is described in the next chapter.

## 4.8. CONCLUSION

IgG-Fc binding peptides were conjugated to single strand DNA and purified by RP-HPLC. The ssDNA-peptide conjugates were then conjugated with oleic acid capped UCNP ($NaYF4:Er^{3+}$, $Yb^{3+}$). Although the ssDNA-peptide conjugates were proven to bind to MIL38 antibody, the whole UCNP-ssDNA-peptide conjugates would aggregate in the assay conditions used. It was shown that aggregation is affected by pH, being acidic conditions more favourable to keep particles in suspension. However, these conditions are not compatible with assay conditions. Additionally, the antibody-binding peptides would likely bind to antibodies that could be present in patient samples because they are not species specific (i.e. it would bind to both human and mouse IgG). Given the complexity of the production process and the high risk of low specificity, this reagent and assay was not pursued further.

# 4. EUROPIUM CHELATE CONJUGATES

## 4.1. SUMMARY

In this chapter, the development of an immunoluminescent reagent and optimisation of storage and plate and cell immunoassay conditions are discussed. Two europium chelates were trialled for conjugation with MIL38 antibody. Conjugation, storage and assay conditions were optimised with the selected ligand. Amplification of the signal using biotin-streptavidin system was also explored.

## 4.2. INTRODUCTION: BHHBCB AND BHHBTEGSB

Nanoparticles, despite their numerous advantages, are difficult to work with, and in particular UCNP require specific equipment that is not widely available. As an alternative, Lanthanide chelates were explored.

As mentioned above, Lanthanides are very poor energy absorbers, but their sharp emission peaks and luminescence properties are useful for analytical purposes. As explained for the UCNP, this weakness can be overcome with the interaction with a more efficient energy absorber molecule which transfers the energy to the lanthanide, so it can luminesce. Many molecules have been designed which allow conjugation with biomolecules, such as proteins, and energy absorbance and transfer to a chelated lanthanide ion[128-130]. These molecules have three primary components: a chelator moiety, which coordinates with the lanthanide ion; an antenna group, which consist of a structure with multiple conjugated double bonds, very efficient in photon absorption; and a reactive group, which allows the conjugation with other molecules, such as antibodies. Due to the nature of the energy flow,

these complexes show a large Stokes shift (difference between absorption and emission peaks), and given the sharp emission peaks of lanthanide ions, there is no overlap between excitation and emission wavelengths, as occurs in other common fluorescent molecules, such as FITC (see Figure 4.2.1). Therefore, these complexes do not exhibit any self-quenching effect that other fluorophores, such as FITC, show, what constitutes a problem for antibody labelling and cell staining[131]. This allows the enhancement of the sensitivity by increasing the number of labels per biomolecule, being restricted only by the binding sites present. Also, decay times are in the orders of micro and milliseconds; therefore, time resolved spectroscopy techniques can be used for detection, contributing to the elimination of interference by autofluorescence of the samples. In Figure 4.2.1 B a diagram of emission decay times for luminescent and fluorescent molecules is shown. A period of time between a pulse of excitation light and emission acquisition, called gate delay, is left for the excited fluorescent molecules to decay.

Due to the higher brightness and longer lifetime when compared with other lanthanides, europium is the most commonly used for analytical purposes. Its emission peak is around 615 nm, which is easily detected with common emission filters[132]. For this project, Zhang's *et al* compound BHHBCB (1,2 bis[4'-(1",1",1",2",2",3",3"-heptafluoro-4",6"-hexanedion-6"-yl)-benzyl]-4-chlorosulfobenzene) [133] and its derivative BHHBTEGSB (1,2-bis[4'-(1",1",1",2",2",3",3"-heptafluoro-4",6"-hexanedion-6"-yl)-benzyl]-4- sulfonylamino-tetraethyleneglycol-succinimidyl carbonate-benzene)[134] were used. Structures of these molecules are shown in Figure 4.2.2.

A

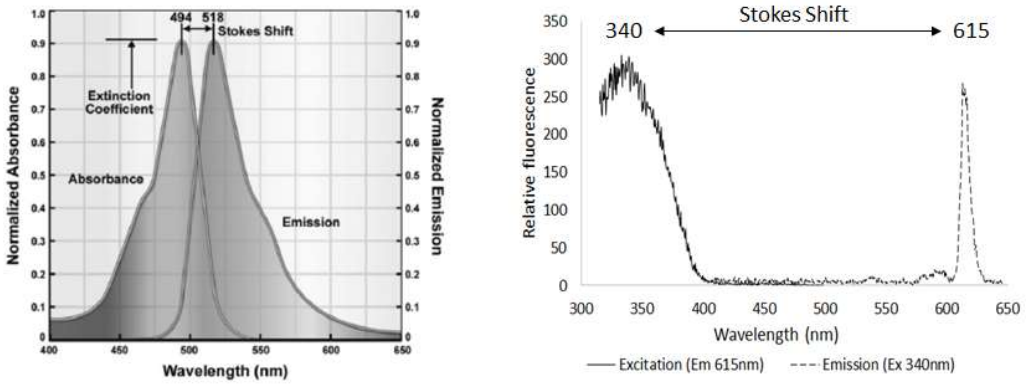


B

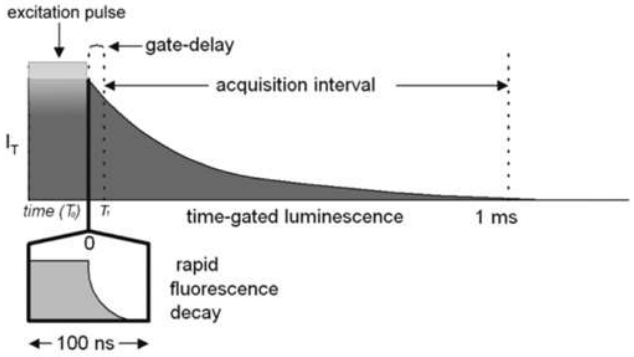


**Figure 4.2.1.** Comparison of fluorescence and luminescence emissions **A.** Absorption and emission spectra of FITC, a common fluorescent molecule used for antibody labelling, (Left, image original from [135]) and excitation and emission spectra of the BHHBCB-Eu complex (Right, spectra obtained with a Cary Eclipse Fluorescence Spectrophotometer). **B.** Emission decay times for luminescent (top) and fluorescent (bottom) molecules (modified from the original in [136]).

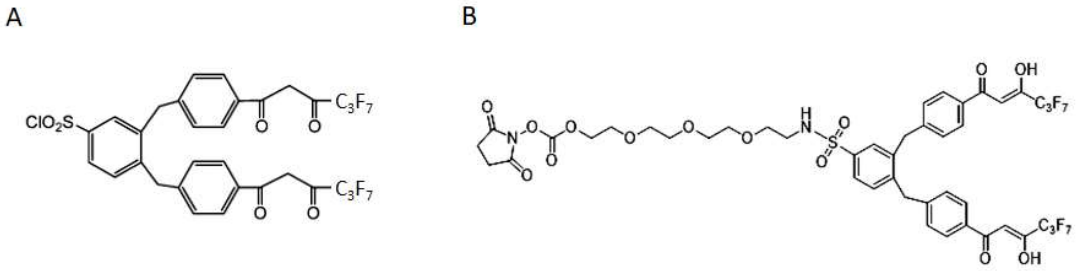


**Figure 4.2.2.** Structures of europium chelates used for MIL38 labelling. **A.** BHHBCB. **B**. BHHBTEGSB.

The reactive groups for bioconjugation, chlorosulfonyl in BHHBCB and N-hydroxysuccinimide ester (NHS) in BHHBTEGBS, react with primary amines in the antibody. BHHBTEGBS has a tetraethylene glycol (TEG) chain that increases hydrophilicity in a highly hydrophobic molecule[134]. The three benzene rings form the antenna group and the carbonyl groups coordinate with $Eu^{3+}$ ion. europium has 9 coordination sites that must be filled completely with ligands to avoid quenching by water[132]. BHHBCB is a tetradentate ligand, meaning it only occupies 4 coordination sites of europium. This problem can be overcome using some additives, such as triphosphine oxide (TOPO)[137], to occupy those free coordination sites and isolate the europium from water molecules.

In this chapter it is shown the optimisation process for labelling the MIL38 antibody with BHHBCB and BHHBTEGSB, stabilisation in aqueous solution and cell assay. These chelators were selected because they are improved versions of a popular europium chelate BHHCT (4,4'-bis(1",1",1",2",2",3",3"-heptafluoro-4",6"-hexanedione-6"-yl) - chlorosulfo-o-terphenyl) used in the development of time resolved immunoassays[138-141]. The instrumentation used for cell imaging was kindly facilitated by Dr Russell Connally [136]. The work presented here was developed as part of a project depicting the synthesis,

characterisation and use of BHHBTEGSB as an alternative europium chelator[134]. The publication can be found in Appendix A-3.

## 4.3. MATERIALS AND METHODS

### 4.3.1. Equipment and Materials

i. Automatic pipettes ranging from 2 to 1000 µL
ii. Epoxy-coated slides for IHC or IFA, one or two 8 mm wells (Medical Packaging Corporation # CPS-0108 (1 well per slide) or # CPS-0208 (2 wells per slide).
iii. Fluorescence microscope with mercury lamp and filters for 490 nm and 350 nm.
iv. FPLC system (BioRad)
v. GALD device adapted fluorescence microscope (kindly provided by Prof. Russell Connally.
vi. Gel filtration column Superdex S-200 10/300 GL (GE)
vii. Microcentrifuge tubes, pipettes tips, transfer pipettes and other general plastic.
viii. Microplate reader with time resolved acquisition, with filters for Excitation 340 nm and Emission 615 nm.
ix. Nanodrop Spectrophotometer (Thermo).
x. Cary Eclipse Fluorescence Spectrophotometer (Agilent).
xi. Sephadex G-25 in PD-10 Desalting Columns (GE)
xii. White high protein binding ELISA plates (Greiner)
xiii. Black no binding microtitration plate (Greiner)
xiv. Precast gels bis-tris 4-12% acrylamide (NuPAGE, Thermo-Invitrogen)
xv. Trans-Blot Turbo RTA Midi Nitrocellulose Transfer Kit (BioRad)

### 4.3.2. Reagents

All chemicals used were analytical grade. Acetic acid; acetone; BHHBCB (kindly provided by Prof. Dayong Jin); BHHBTEGBS (kindly provided by Dr. Nima Sayyadi); bovine serum albumin (BSA); CytoLyt solution (ThinPrep); dimethyl formamide (DMF); ethanolamine; europium chloride hexahydrate; glycerol; Hoechst 33342 (Invitrogen); hydrochloric acid; MIL38 antibody (kindly provided by Minomic); Saccomanno fluid (Thermo); Rabbit anti-Mouse IgG (H+L) Cross-Adsorbed Secondary Antibody, Biotin (Thermo); sodium acetate; sodium bicarbonate; sodium carbonate; sodium chloride; streptavidin, unconjugated (Invitrogen); trioctylphosphine oxide (TOPO); Triton X-100; Trizma Base; Tween-20; Skim milk powder used was purchased in the supermarket. XT Sample Buffer (BioRad); Precision Plus Protein Western Standards (BioRad); Precision Protein StrepTactin-HRP Conjugate (BioRad); Clarity Western ECL Substrate (BioRad); EZ-Link NHS-PEG4-Biotin (Thermo Fisher Scientific); high sensitivity streptavidin conjugated to HRP (Thermo-Pierce); Heparinase I from *Flavobacterium heparinum* (Sigma).

### 4.3.3. Solutions

All solutions were prepared in MQ water, unless specified otherwise.

i. Antibody Labelling

   a. Labelling Buffer: carbonate buffer 50 mM pH8.5; 0.1% Tween-20

   b. BHHBCB or BHHBTEGSB: 10 mg/mL in DMF

   c. Ethanolamine: 0.1 M pH8.0

   d. Tris buffered saline (TBS): 50 mM Tris-HCl pH 7.5; 150 mM sodium chloride

e. acetate buffer saline (ABS): 50mM sodium acetate/acetic acid, pH 5.0; 150 mM sodium chloride

ii. Gel filtration

a. Running buffer: TBS + 10% glycerol.

iii. ELISA:

a. Coating buffer: 100 mM sodium bicarbonate, pH 8.5

b. Blocking solution: 1% BSA, 0.05% Tween-20 in TBS

c. Wash buffer: TBS-Tween-20 (0.05%)

d. Fluorescence Enhancement Buffer (FEB) 10X: acetate buffer 100 mM pH 5; Tween-20 1%; trioctylphosphine oxide (TOPO) 0.5 mM (Note: dissolve TOPO in ethanol to a stock of 20 mM, then dilute in acetate-Tween to 0.5 mM).

iv. Cell Assay

a. Phosphate buffered saline: 10 mM phosphate pH 7.4, 150 mM sodium chloride.

b. TBS-T: TBS + 0.1% Tween-20

c. Blocking/sample buffer: BSA 1% in TBS-T

d. Counterstaining solution: 1 µg/mL Hoechst 33342 in TBS.

e. europium chloride 1 mM

f. Fluorescence Enhancement Buffer (FEB) 10X: see iii-d above.

v. Western blot

a. Lysis buffer 1: 20 mM MES pH 6.5, 0.5 mM EDTA, 0.005% Triton X-100, protease inhibitor cocktail 5 µL/mL; approximately $1x10^7$ cells/mL.

b. Lysis buffer 2: 20mM HEPES pH 7.5, 0.5 mM EDTA, 0.5% Triton X-100, protease inhibitor cocktail 5 µL/mL.

c. Blocking solution: 10% skim milk in DPBS + 0.1% Tween-20 (DPBS-T)

d. Washing solution: DPBS-T

### 4.3.4. Antibody Labelling

i. Antibody buffer exchange: 1 mg of MIL38 was applied onto a PD-10 desalting column pre-equilibrated with Labelling Buffer. Protein was eluted with this buffer and 50 µL fractions were collected and inspected in the NanoDrop spectrophotometer. Antibody containing fractions were pooled for subsequent labelling.

ii. Conjugation:

a. Immediately before use, 1 mg of BHHBCB or BHHBTEGSB were dissolved in 100 µL of DMF.

b. The appropriate volume of chelator solution was added to the antibody solution, according to the desired antibody-chelator ratio, and mixed by vortexing.

c. Reaction was incubated for 1-2h at room temperature protected from light.

d. Once the reaction time has been completed, 50 µL of ethanolamine solution were added to stop the reaction.

e. Labelled antibody was separated from unreacted chelator by purification through PD-10 desalting column, equilibrated with either TBS or ABS. Antibody containing fractions were pooled.

f. The Antibody concentration was estimated using Nanodrop spectrophotometer. To eliminate the contribution of the chelator to the absorbance at 280 nm for antibody concentration calculation, the equation below, derived from the Beer-Lambert law, was used:

$$C_{Ab} = \frac{A_{T\ 280} - A_{Ch\ 335}(^{\varepsilon_{Ch\ 280}}/_{\varepsilon_{Ch\ 335}})}{\varepsilon_{Ab\ 280}}$$

$C_{Ab}$ = Antibody concentration in mg/mL

$A_{T\ 280}$ = Total absorbance of antibody and chelator at 280 nm

$A_{Ch\ 335}$ = Absorbance at 335 nm. The contribution of the antibody to this parameter is assumed to be zero.

$\boldsymbol{\varepsilon}_{Ch\ 280}$ = Extinction coefficient of the chelator at 280 nm ($1.64\times10^4$ $M^{-1}.cm^{-1}$ [134])

$\boldsymbol{\varepsilon}_{Ch\ 335}$ = Extinction coefficient of the chelator at 335 nm ($3.10\times10^4$ $M^{-1}.cm^{-1}$ [134])

$\boldsymbol{\varepsilon}_{Ab\ 280}$ = Extinction coefficient of the antibody at 280 nm (1.4 $mL.mg^{-1}$). This value is a common approach to estimate concentration of IgG in solution.

g. Preparation was divided in working aliquots and either stored at -80°C or freeze dried and stored at -80°C

### 4.3.5. Labelled Antibody Quality Control

i. Gel Filtration chromatography: 20-50 µg of samples were injected into a 25 mL Superdex S-200 column equilibrated with TBS + 10% glycerol, at a flow of 0.5 mL/min. Traces at 280 nm and 340 nm were recorded.

ii. ELISA: assay development is described in the results section. Briefly, analyte in Coating Buffer was immobilised onto a high protein binding white plate (Greiner), followed by blocking with Blocking Solution and then incubating with the different antibodies in blocking solution and europium- FEB, as described. Time resolved fluorescence (Luminescence) readings were taken with a PHERAstar FS multi-mode microplate reader (BMG Labtech), with HTRF optic module (excitation:337 nm and dual emission: 665 nm and 620 nm) and a flash lamp. According to emission decay measured (see Figure 4.3.5.1), gating was set at 40 µs after light pulse and 400 µs of integration time, with 400 flashes per well.

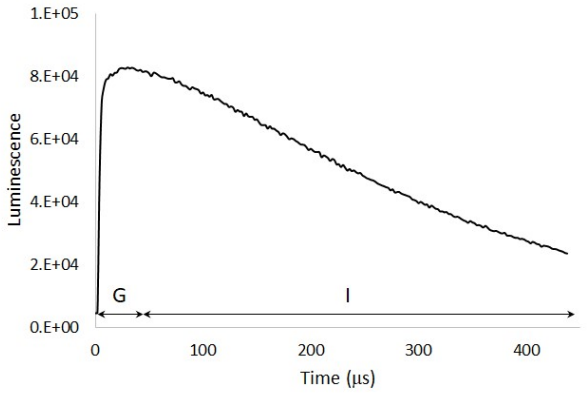


**Figure 4.3.5.1** Luminescence decay curve of BHHBTEG-MIL38-Eu used to establish reading parameter for time resolved fluorescence (TRF) in the plate reader. Gating time (G) was set to 40 µs and integration time (I) was set to 400 µs.

### 4.3.6. Cell Immunoluminescence Assay

i. Preparation of cell slides: cells were prepared as described in Chapter 2, with the modifications defined by the method optimisation. Briefly, cells (DU145, C3 or urine cells) were washed with CytoLyt solution and spotted onto the slides, air dried and further fixed with ice-cold acetone for 3 min. The CytoLyt wash was eventually changed for the addition of 1:1 volume of Saccomanno fluid (a fixative used for liquid samples in pathology labs) on the urine samples upon arrival, as described in a similar immunofluorescence assay[39]. Cells were left in this fixative for at least 1 h up to 24 h at room temperature (to avoid precipitation of mineral crystals in the samples that often occurs with storage at 4$^{o}$C). After incubation with the fixative, cells were spun down and spotted onto slides, air dried and either stored at 4$^{o}$C or immunostained.

ii. Immunostaining: 2 different immunoluminescence assays were tested: a one-step direct assay, where the primary antibody, MIL38, was labelled with the chelator; and a 3-step indirect assay with a biotinylated anti-mouse antibody and streptavidin labelled with the chelator. In all cases, cells were counterstained with the nuclear dye Hoechst 33342, by incubating with counterstaining solution for 5 min, protected from light.

   a. Blocking: in all cases, fixed cells were blocked with blocking solution (1% BSA in TBS-T) for 1 h at room temperature.

   b. Direct assay: cells were incubated with 10 µg/mL of MIL38 antibody, labelled with Eu-chelator, in blocking solution for 30 min at room

temperature. Slides were then washed with TBS-T, counterstained and then washed with TBS, then air dried for imaging.

c. Three step indirect assay: cells were incubated with 10 µg/mL of unlabelled MIL38 antibody in blocking solution for 1 h at room temperature, washed with TBS-T and then incubated with 10 µg/mL of biotinylated rabbit-anti-mouse antibody in blocking solution at room temperature for 30 min. Slides were washed with TBS-T and then incubated with Streptavidin labelled with Eu-chelator in blocking solution for 30 min at room temperature protected from light. Slides were then washed with TBS-T, counterstained and then washed with TBS and airdried for imaging.

d. Cell mounting and imaging: just before imaging, FEB and europium solutions were mixed (1:1) and spotted onto the immunostained cells and covered with a coverslip. Further examination showed that the addition of europium solution after counterstaining would show europium luminescence in the nuclei (discussed in section 4.6). Therefore, incubation of labelled cells with europium was done before counterstaining, followed by mounting the slides with FEB just prior imaging. Slides were inspected under the microscope, then time-gated luminescence (TGL) imaging was performed on an Olympus BX51 fluorescence microscope using the Gated Autosynchronous Luminescence Detector (GALD)[136], which was inserted into the DIC slot of the microscope. Images were captured without a fluorescence filter using a DP72 colour camera set for ASA speed of 200 and exposure period between 5 and 10 s. Following TGL images, fluorescence images for nuclear counterstaining (blue

filter, 10 ms exposure) and autofluorescence (green filter, 100-200 ms exposure) were taken using a 100 W mercury arc lamp in the same microscope.

### 4.3.7. Western blot

i. Preparation of cell membrane protein extracts: detached cultured cells (see 2.3.4-i) were lysed by incubation with lysis buffer 1 for 10 min onto a tube rotator, and membranes were separated from water soluble proteins by centrifugation at 16,000 g for 15 minutes. Supernatant was discarded and pellet was resuspended in lysis buffer 2 and incubated for 30 minutes onto a tube rotator. Solubilised membrane proteins were separated from DNA and other nuclear components by centrifugation at 16,000g for 15 min. Pellet was discarded, and supernatant was collected and stored in working aliquots (50-100µL) at -80˚C.

ii. SDS-PAGE: 20 µg of protein from cell membrane protein extracts were mixed with 4 times concentrated loading buffer, boiled at 95°C for 5 min and centrifuged at 10,000 g for 5 min. Protein standard and samples were served onto precast gels, and run in MOPS-SDS buffer at 200 V for 45-60 min.

iii. Protein transfer: proteins separated by SDS-PAGE were transferred to nitrocellulose membrane by semi-dry transference using a BioRad trans-blot turbo machine. BioRad transfer buffer (5 times concentrated, containing SDS) was diluted to one time concentrated with methanol (20% final concentration) and mQ water. Filter papers and nitrocellulose membrane were pre-wet with transfer buffer in advance. Transfer sandwich was assembled on the transfer

machine cassette and run at 25 V for 10 min. Gel was discarded, and blotted membrane was rinsed with mQ water.

iv. Western Blot: After transfer, membranes were blocked with blocking solution for 1 h at room temperature. Primary antibody (MIL38-biotin) was diluted to 1 µg/mL in blocking solution and incubated for 1 h at room temperature. After 3 times 5min washes with washing solution, membranes were incubated with streptavidin-HRP and protein standard probe (StrepTactin-HRP) diluted in blocking solution. Membranes were then washed 4 times by 10min with washing solution. Clarity ECL Western substrate (1:1 mixture) was added onto the membrane, and this was covered with a plastic film before imaging using a GE ImageQuant LAS 4000 imager, with exposure time of 5 sec 1 min.

## 4.4. ANTIBODY LABELLING STRATEGIES

In order to label MIL38 antibody with the europium chelator, two different amine targeted chemistries were used. The first approach was attempted using BHHBCB directly on MIL38. The reactive group in BHHBCB is a sulfonyl chloride, which targets primary amines from lysine residues and the N-terminus. The reaction scheme is shown in Figure 4.4.1(A). The second approach was to use BHHBTEGBS, a derivative of BHHBCB which contains a tetraethylene glycol spacer, to increase solubility, and contains a N-hydroxysuccinimide (NHS) ester as a reactive group, which also targets primary amino groups, as shown in Figure 4.4.1(B).[132]

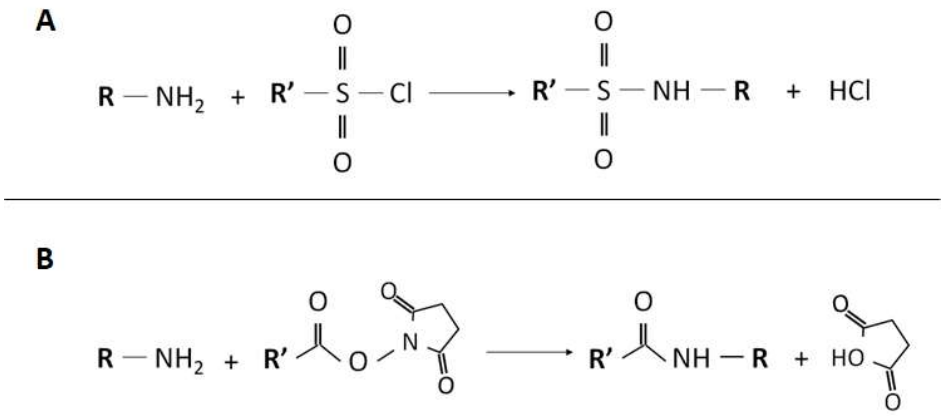


**Figure 4.4.1.** Scheme of conjugation reactions used to label MIL38 antibody with the europium chelator. R = Antibody; R' = europium chelator. **A**. Sulfonyl chloride reaction with amino group in antibody. **B**. NHS ester reaction with amino group in antibody.

According to its sequence (kindly provided by Minomic for this study, but not shown due to intellectual property restrictions), MIL38 has a total of 49 lysine residues, 14 in the light chain and 35 in the heavy chain. Together with 4 amino termini from the heavy and light chains, there are 53 theoretical available primary amino groups. However, it is not likely that all of them are readily accessible for conjugation. Initially, a molar ratio chelator/antibody of 20 was used as a starting point. Both conjugation reactions were conducted in a slightly basic pH environment (pH 8.5), in order to reduce the competition of hydrolysis breakdown of the reactive groups, particularly the sulfonyl chloride group, without compromising the availability of reactive deprotonated amines. Under these conditions, both conjugations were successful. However, the level of conjugation using BHHBTEGBS was higher than that using BHHBCB. In Figure 4.4.2 (bottom) are shown the UV-visible spectra of the unlabelled antibody (A), and the conjugates MIL38-BHHBCB (B) and MIL38-BHHBTEGBS (C). The levels of conjugation can be qualitatively observed in the intensity of the peaks at 340 nm, which

corresponds to the absorbance of the chelator: the absorbance intensity is higher for the BHHBTEGBS conjugate, compared to the BHHBCB conjugate.

At the top of Figure 4.4.2 it can be seen gel filtration chromatograms corresponding to the unlabelled MIL38 (A), MIL38-BHHBCB (B) and MIL38-BHHBTEGBS (C). Traces for 280 nm and 340 nm were recorded to monitor labelled protein. The antibody alone shows a small peak that could be either some aggregate or a contaminant protein, as the antibody had been only purified by affinity (Protein G). It is present in all the antibody alone chromatograms run, at roughly the same proportion. The major peak comes at the expected retention volume for IgG, according to the standards run. The MIL38-BHHBCB conjugate chromatogram shows three overlapping peaks with different 340 nm / 280 nm absorbance ratios. This profile suggests that the labelling with BHHBCB was not homogeneous. Moreover, the higher the 340 nm / 280 nm ratio is, the sooner the peak came out of the column. The same occurs with the MIL38-BHHBTEGBS conjugate (C), which comes at the void volume. This was unexpected for MIL38-BHHBTEGBS, as this derivative of BHHBCB contains a tetraethyleneglycol chain that would potentially increase the hydrophilicity of the conjugate. These results show that the conjugated protein aggregates as labelling efficiency increases.

Based on these results, as BHHBTEGBS appeared to achieve a higher labelling efficiency, the conjugation of the antibody with this chelator was optimised further, also addressing the protein aggregation problem.

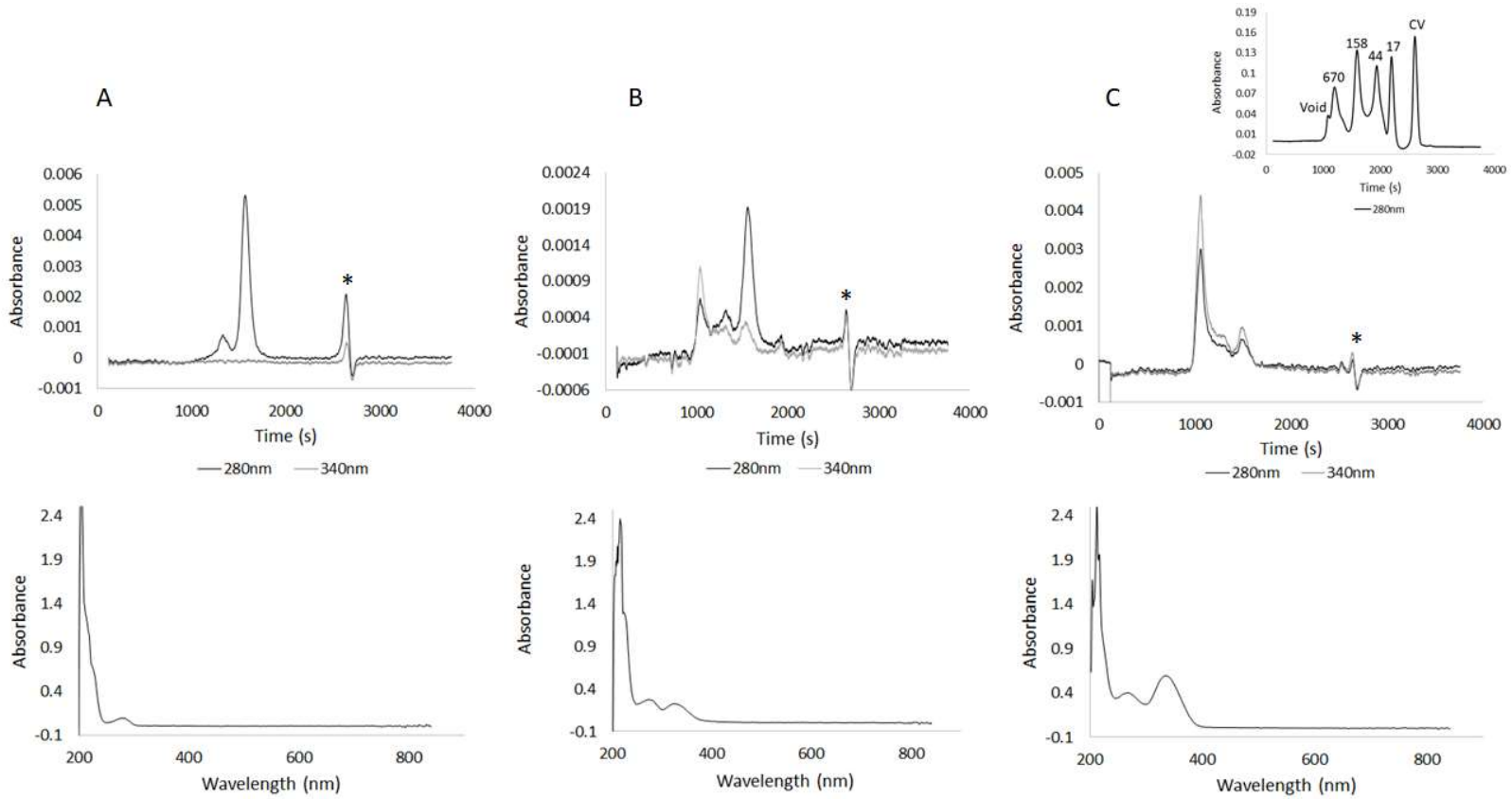


**Figure 4.4.2** Comparison of MIL38 labelling with BHHBCB and BHHBTEGBS. **Top**: Gel filtration chromatograms of labelled antibodies. At the top right, standards for reference. Molecular weights of protein peaks are shown in kDa. Void and column volume (CV) are also shown. * Density artefact. **Bottom**: UV-visible spectra of labelled antibodies. **A**. Non-labelled MIL38. **B.** MIL38-BHHBCB **C.** MIL38-BHHBTEGBS.

Following the choice of label, the conjugation ratio was optimised. Three different chelator to antibody molar ratios were tested: 10, 20 and 50. The reaction conditions were similar to the ones used above, except that 0.1% of the surfactant Tween-20 were added to both the reaction solution and the storage solution (TBS pH 7.5) to promote solubility of the conjugate. Following buffer exchange, purified conjugates UV-visible spectra were analysed by NanoDrop. Molar concentrations (C) of both antibody and chelator were determined using the Beer-Lambert law:

$$C = \frac{A_\lambda}{b.\varepsilon_\lambda}$$

Being $A_{\boldsymbol{\lambda}}$ the absorbance at wavelength $\boldsymbol{\lambda}$, b is the path of light in cm ($b = 1$ cm) and $\boldsymbol{\varepsilon_\lambda}$ is the extinction coeficient at wavelength $\boldsymbol{\lambda}$. Extinction coefficients for antibody of $\boldsymbol{\varepsilon}_{\text{Ab 280}}$ = 2.1x10$^5$ M$^{-1}$.cm$^{-1}$, and chelator of $\boldsymbol{\varepsilon}_{\text{Ch 280}}$ = 1.6×10$^4$ M$^{-1}$.cm$^{-1}$ and $\boldsymbol{\varepsilon}_{\text{Ch 335}}$ = 3.1×10$^4$ M$^{-1}$.cm$^{-1}$ were used. Results are summarised in Table 4.4.1.

**Table 4.4.1** Number of chelators per antibody with the different chelator/IgG ratio used for labelling. T = total; Ch = chelator; Ab = Antibody

| Ratio | $A_{280}$T | $A_{280}$(T-Ch) | [Ab] (M) | $A_{335}$ | [Ch] (M) | Ch/Ab ratio |
|---|---|---|---|---|---|---|
| 10 | 0.161 | 0.096 | 4.6E-07 | 0.123 | 4.0E-06 | 9 |
| 20 | 0.228 | 0.103 | 4.9E-07 | 0.236 | 7.6E-06 | 16 |
| 50 | 0.249 | 0.108 | 5.2E-07 | 0.266 | 8.6E-06 | 17 |

In the table it can be observed that a maximum of labels is reached with a ratio of 20 times. The 50 times ratio, on the other hand, precipitated within few hours. UV visible spectrum profiles are shown in Figure 4.4.3.

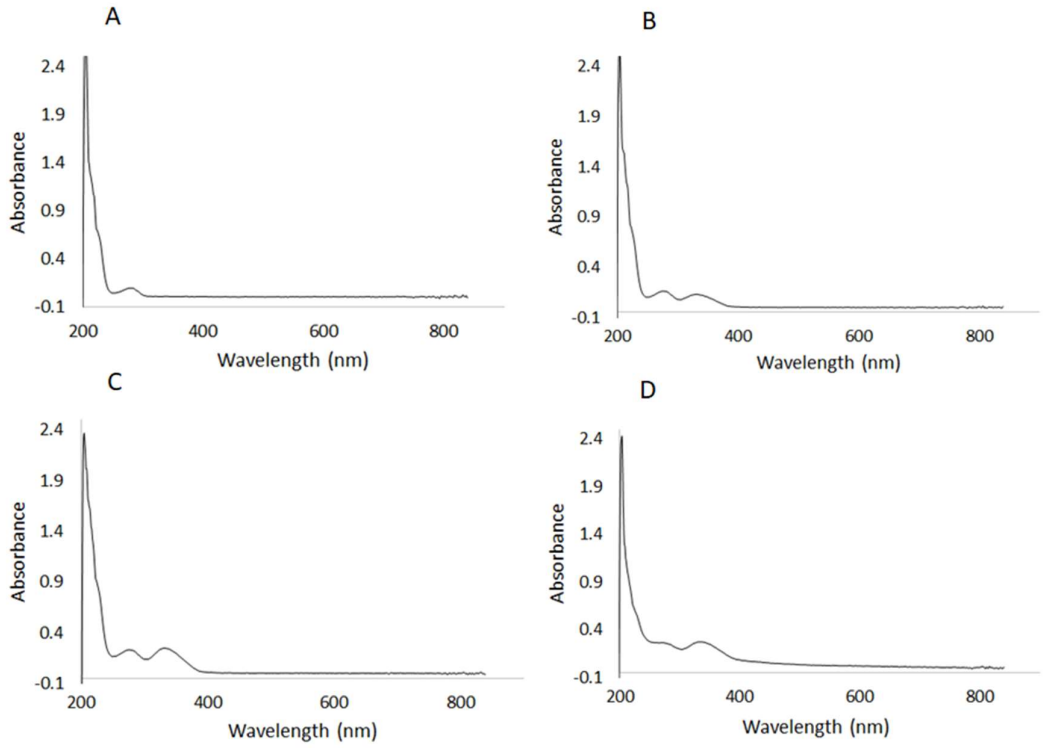


**Figure 4.4.3**. UV-visible spectra profiles for different chelator/antibody labelling ratios. **A.** Non-labelled MIL38. **B**. 10X. **C.** 20X. **D.** 50X

Gel filtration chromatography was performed to check on aggregation states of the conjugates. Same running conditions were used. The chromatograms are shown in Figure 4.4.4. It is observed that at any level of conjugation tested, the conjugate tends to aggregate at the storage conditions used. The 10X preparation seems to show two peaks, one of them not labelled at all. This result is intriguing, as one would expect that conjugation occurrs as a semi-random process in which the amino groups react according to their expossure and reactivity, in every molecule of antibody. This non-labelled peak looks smaller in the other preparations. As the labelling was maximised at the highest conjugation ratios and the 20X did not visibly precipitate, this conjugation level was chosen as optimal. Further studies on the storage conditions were conducted to improve the solubility of the conjugate.

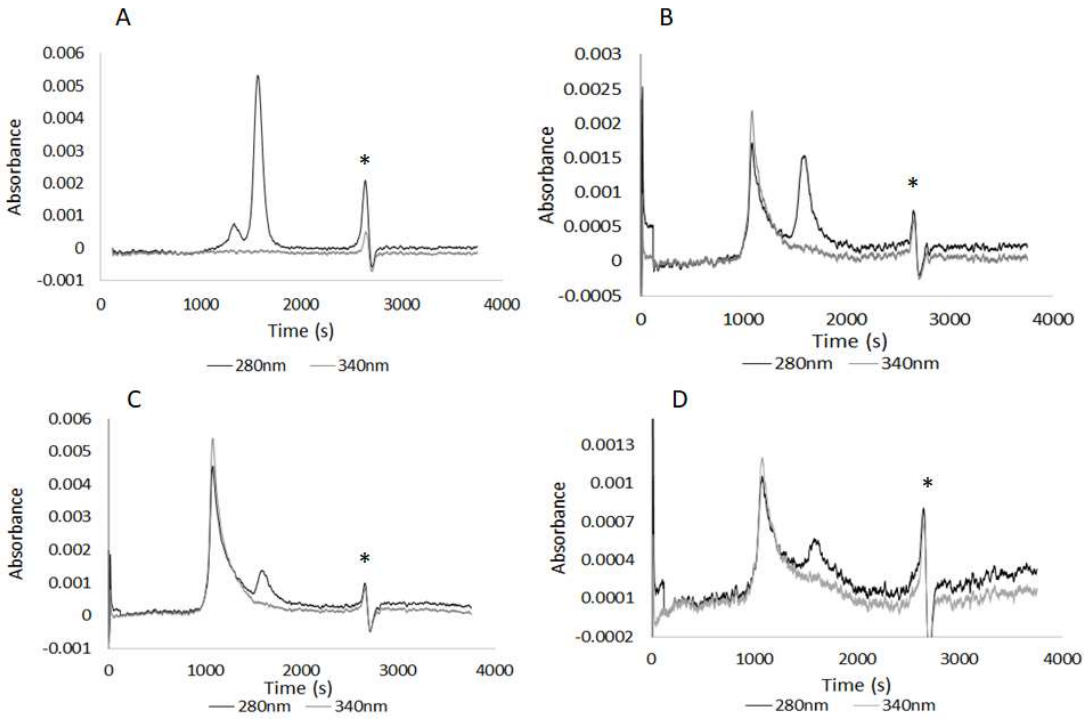


**Figure 4.4.4**. Gel filtration chromatograms for different chelator/antibody labelling ratios. * Density artefact. **A.** Non-labelled MIL38. **B**. 10X. **C.** 20X. **D.** 50X

## 4.5. REAGENT STABILITY: SOLUBILITY AND CHELATOR STABILITY

In the previous section it was clear that the storage conditions for the MIL38-BHHBTEGBS conjugate were not appropriate, as it tended to aggregate, as observed in the gel filtration chromatograms, and eventually form a visible precipitate. The theoretical isoelectric point of MIL38 antibody was estimated using the Kozlowski *et al* calculator[142], (http://isoelectric.org/) and the *Compute pI/Mw* tool from ExPASy (https://web.expasy.org/compute_pi/), using the sequences of heavy and light chains of the antibody. Theoretical isoelectric points calculated using these tools were 7.19 and 8.35 respectively. Antibody glycosylation modifies the isoelectric point as the sugar residues can be charged too. As solubility is lowest at the isoelectric point, and the storage buffer used is

close to this point, it is possible that the addition of a highly hydrophobic molecule such as BHHBTEGBS or BHHBCB further reduces the solubility of the conjugate in aqueous solutions.

Based on the premise that the aggregation was being caused by the proximity of the antibody isoelectric point to the storage buffer pH, a low pH buffer (pH = 5.5) was tested for storage. Two pH units below the average isoelectric point was used to ensure that the conjugate is sufficiently charged to be kept in solution. MIL38 was therefore conjugated with BHHBTEGBS using the labelling conditions optimised above and exchanging the buffer to acetate buffered saline (ABS) pH 5.5. Gel filtration chromatography was run at the same conditions as the previous preparations, using TBS-glycerol as running buffer, to check on the conjugate aggregation. Figure 4.5.1 shows the gel filtration chromatogram of this preparation (C), compared to the non-labelled antibody (A) and the conjugate stored in TBS (pH 7.5). It can be observed that most of the antibody remained in solution and the aggregation process started as soon as the sample was at a higher pH, forming a wide peak at a slightly higher molecular weight than the labelled antibody.

With this result it was concluded that pH 5.5 was optimal for storage to prevent the aggregation of the antibody conjugate.

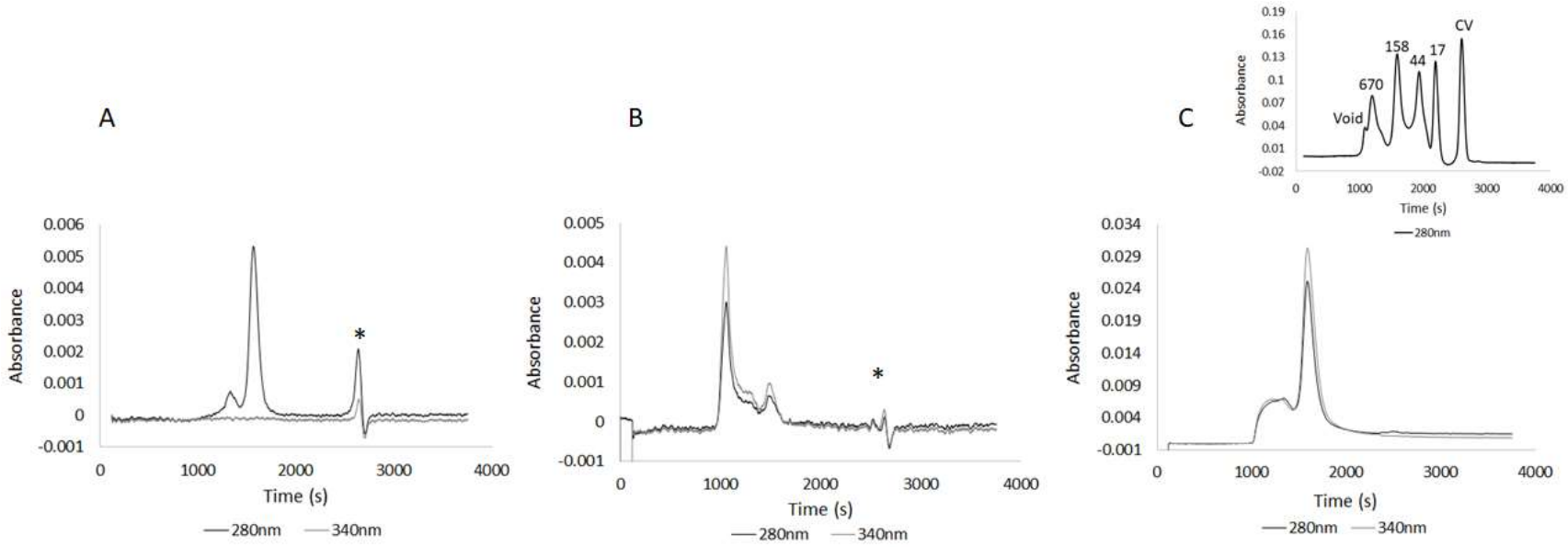


**Figure 4.5.1.** Aggregation state of MIL38-BHHBTEG conjugates stored at different pH, observed via gel filtration chromatography. Running buffer used in all cases: TBS pH 7.5, 10% glycerol. **A.** Non-labelled MIL38. **B.** MIL38-BHHBTEG stored in TBS (pH 7.5). **C**. MIL38-BHHBTEG stored in ABS (pH 5.5). Top right, gel filtration standards for reference, with molecular weight of protein peaks in kDa, void and CV volumes shown. * Density artefact.

The next step to finalise the storage conditions optimisation was to compare freeze-drying with simple freezing small working aliquots. For this, 0.1% w/v BSA, a carrier protein, were added to the final preparation as an additive. 50 µL aliquots were made and half were freeze dried and stored at -80ºC or simply stored at -80ºC.

To check on the activity and integrity of the conjugation, two assays were performed. First, the labelled antibodies were immobilised onto an opaque high protein binding plate, and then incubated with europium chloride and the fluorescence enhancement buffer (FEB). Second, the activity of the conjugate was checked by ELISA, immobilising the protein target, GPC1, onto the plate, blocking, and detecting with MIL38-BHHBTEGBS conjugate (The optimisation of these assays is described on section 4.6). After incubating with europium chloride and FEB, time resolved fluorescence (Luminescence) readings were taken with a PHERAstar FS multi-mode microplate reader. Results are shown in Figure 4.5.2

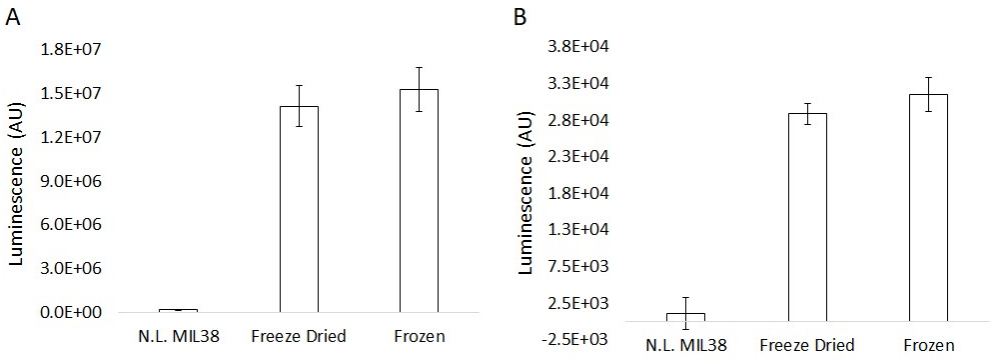


**Figure 4.5.2.** Comparison of freeze dried and frozen preparations. Samples run in duplicates (n=2). Error bars show standard deviation. **A.** 10 ng of antibody-non-labelled (N.L.), freeze dried or frozen- immobilised onto a high binding plate and enhanced with Eu-FEB **B**. ELISA response of 100 ng of GPC1 immobilised onto a high binding plate, enhanced with Eu-FEB. ELISA assay as per section 4.6 below.

The results show that there are no major differences in the activity of the conjugate when either frozen or freeze-dried. This last one was chosen as a final storage condition for the conjugate.

In summary, in this section it was determined that to promote solubility of the MIL38-BHHBTEGBS conjugate in aqueous solution, a lower pH buffer (pH5.5) was optimal. The addition of a carrier (BSA) and finally freeze-drying were also chosen for the final product storage.

## 4.6. IMMUNOASSAY OPTIMISATION FOR EUROPIUM CHELATE CONJUGATES

Once a stable product was achieved, the MIL38-BHHBTEGBS conjugate was trialled in immunoassays. Firstly, composition of the FEB was revised. The FEB composition was originally described by Arnaud and Georges (1997)[137], and consists on a solution of the ligand trioctylphosphine (TOPO) at low pH (4.7) in the presence of the detergent TritonX-100. Given that the final goal was to develop an immunoassay for urine cells, the composition of the buffer seemed harsh for the cells. In particular, the presence of Triton X-100, which is routinely used for cell permeabilisation, could disrupt the integrity of the cell membranes at the assay development step. As a surfactant is necessary to keep the highly hydrophobic TOPO in solution, Triton was substituted by Tween-20, which is milder. Also, low pHs are likely to disrupt the antibody-antigen interactions, and therefore, higher pHs were tested as buffer systems. The FEB was tested in an ELISA type immunoassay, with the MIL38 protein target, GPC1, immobilised onto a high binding plate, blocked with blocking solution (1%BSA in TBS-Tween) and incubated with the MIL38-BHHBTEGBS conjugate. After washes, the plate was incubated 10 min with 0.1 mM europium chloride in different buffers (acetate, pH 5.5; MES,

pH 6.5; TBS, pH 7.5 and carbonate, pH 8.5). A first set of time resolved fluorescence (luminescence) readings were taken with a PHERAstar FS multi-mode microplate reader as described in the methods. This first reading without enhancement was taken as a reference of the basal luminescence of the europium-chelate complex. Following, europium chloride solution was discarded and FEB (50 µM TOPO, 0.1% Tween-20) prepared with these buffers was incubated up to 30 min, luminescence readings at different time points. Results are shown in Figure 4.6.1(A).

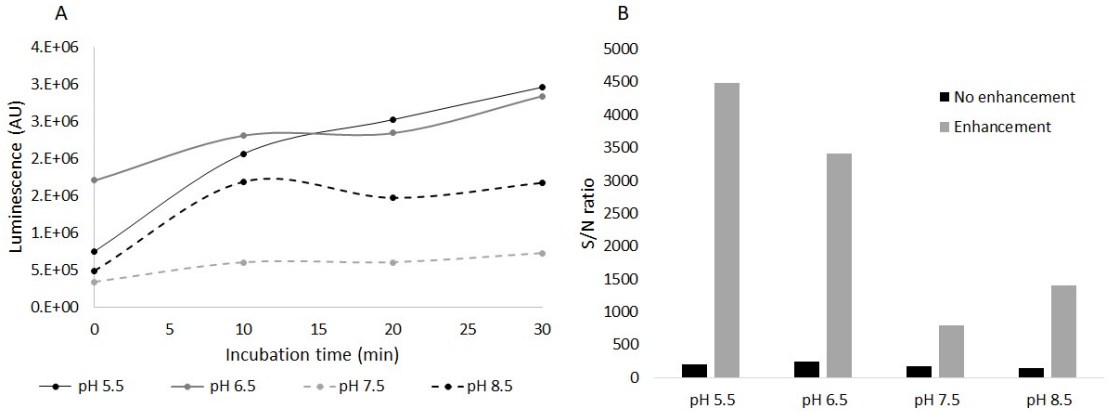


**Figure 4.6.1.** Effect of pH in the Fluorescence Enhancement Buffer (FEB) performance. **A**. Luminescence as a function of incubation time with the FEB solution. Point 0 corresponds to the signal of the europium chelate without enhancement. **B**. Signal to noise (S/N) ratio of the samples incubated with FEB (grey, readings at 30 min incubation time), compared to readings with europium alone (black).

The best performing buffers were the more acidic ones, pHs 5.5 and 6.5. This result is in agreement with what was observed by Arnaud and Georges[137], who found that the luminescence intensity peaked at pH 4.5, between 3 and 5.5, and then started to slightly

decline. In Figure 4.6.1(B) it is shown the signal to noise ratio achieved when only europium is added (black) compared with that after 30 min incubation with FEB. It is clearly seen the very significative signal increment when water quenching is avoided using the external ligand TOPO. Based on these results, acetate buffer pH 5.5 with an incubation of at least 10 min were selected for enhancement of the signal of the europium chelate complex. These conditions were used for ELISA like assays and for the cell immunoluminescence assay in development.

## 4.7. IMAGING USING MIL38-BHHBTEG

The cell assay platform used for labelling urine cells was described in detail on chapter 2. Briefly, fixed cells (either with CytoLyt or Saccomanno solutions) are spun down and resuspended 0.1-1 mL of DPBS, depending on the size of the pellet. Then, 5-10 µL of this cell suspension is spotted onto an epoxy-coated slide, let to air-dry and then incubate into ice-cold acetone for further fixation. This is followed by blocking with 1% BSA in TBS and incubation with primary and secondary antibodies, and finally nuclear counterstaining using Hoechst. Slides were mounted with 70% glycerol in DPBS, and then inspected under epifluorescence microscope. Figure 4.7.1-A shows a typical staining using this method.

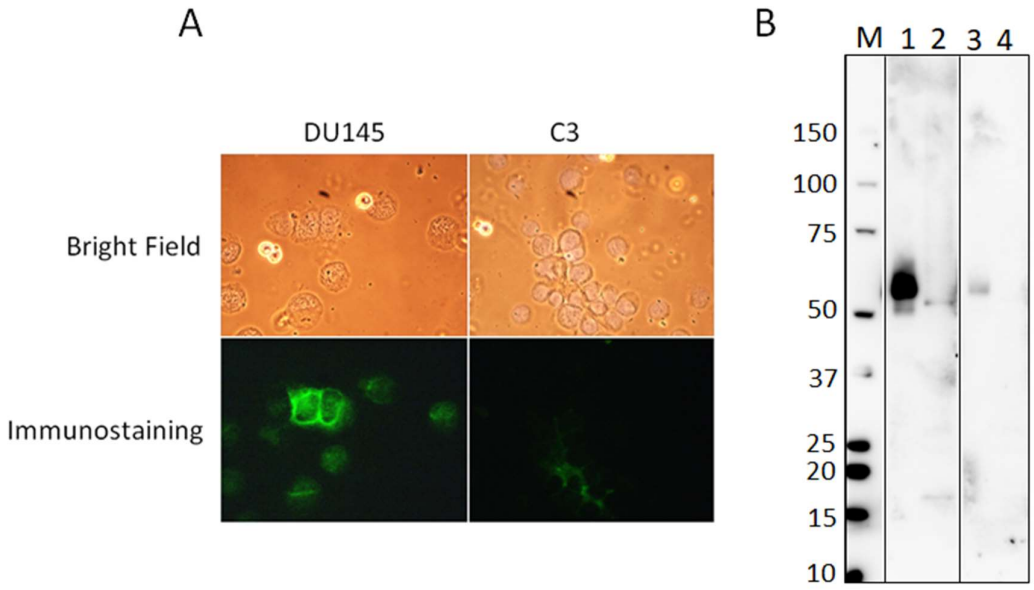


**Figure 4.7.1. A** Typical indirect immunofluorescence assay (IFA) using MIL38 as primary antibody and a secondary antibody (anti-mouse) labelled with Alexa Fluor-488 (exposure time: 200 ms), against prostate cancer cell line (DU145, positive control) and bladder cancer cell line (C3, negative control). 40X objective was used. **B**. Western blot of DU145 and C3 cell lines MIL38 crude extracts treated with heparinase I (1 and 3 respectively) or untreated (2 and 4 respectively). Biotinylated MIL38 and streptavidin-HRP conjugate were used as probes. 20 µg of protein were loaded per lane. Exposure time: 5s.

The prostate cancer cell line DU145 was routinely used as a positive control for these urine cells assays. As it can be seen in the figure, the expression of GPC1 is not uniform in all the cells, nor all the cells are stained. The bladder cancer cell line C3, on the other hand, is used as a negative control for the assay. However, the cells are not entirely negative, but the expression levels of GPC1 are so low, they often look negative. In Figure 4.7.1-A, slightly positive C3 cells are observed, and this is consistent with weak bands corresponding to GPC1

observed in western blots done with membrane extracts of these cell lines (Figure 4.7.1-B). It is worth noting that treatment with heparinase I in order to digest the long and bulky heparan sulphate chains allows the glycoprotein to go into the SDS-PAGE gel, as it is observed when comparing lanes 1 and 2 for DU145 and 3 and 4 for C3. Two bands are observed for DU145: one wide band at around 60 kDa, which corresponds to the mature form with what remains from heparan sulphate chains, and one of around 55kDa, which corresponds to the non-glycosylated and N-glycosylated protein core (see structure features in Figure 1.4.2.1.- A). For C3, only the high molecular weight form is detected when treating with heparinase I, and levels of the protein core are below of detection limits.

To decide whether an immunofluorescence assay is valid based on the controls, the majority of the DU145 cells in each field of view are strongly stained and the majority of C3 are negative, and the few positives if any, are weakly stained, as shown in the figure. Invalid assays were very rare.

With this information in mind, a similar cell assay was carried on DU145 and C3 cells but using the MIL38-BHHBTEGBS conjugate (direct immunoluminescence assay) and some modifications. Immunostaining was done as described above. After counterstaining, cells were incubated with europium and then FEB was used as mounting solution, added at least 10 min before inspection under the microscope equipped with a GALD unit. It was noticed

that if counterstaining was done before the addition of europium chloride, the nuclei were non-specifically stained (Figure 4.7.2).

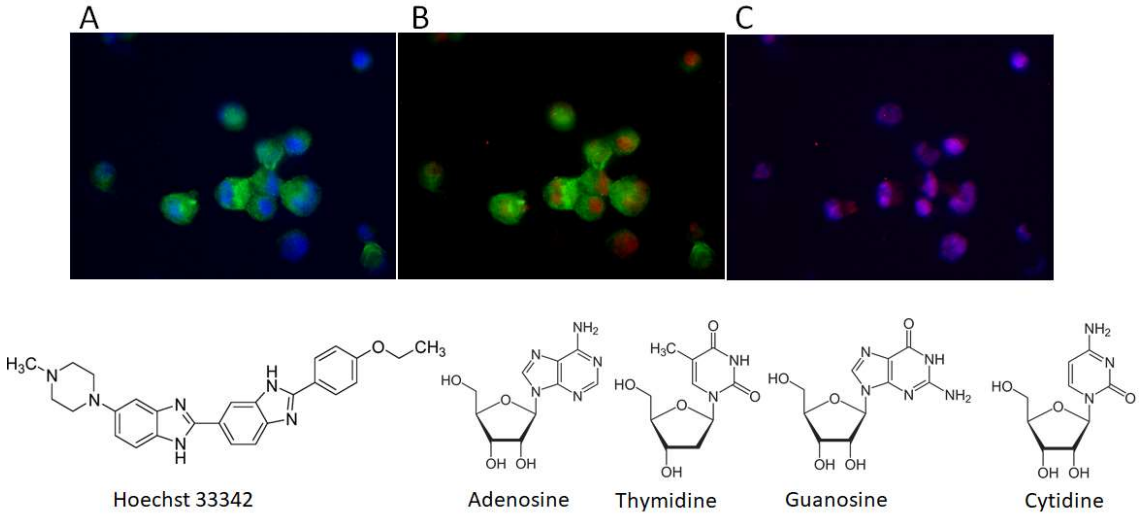


**Figure 4.7.2.** Europium incorporation into the cell nuclei in the presence of Hoechst. **Top**: cell staining with MIL38-BHHBCB as primary antibody (time gated image, 10s exposure) and anti-mouse-Alexa488 (exposure 200s) as secondary antibody, doing Hoechst nuclear counterstaining (exposure 10s) before the addition of europium. 40X objective was used **A** Hoescht-Alexa488 merge. **B** Alexa488-europium merge. **C** Hoechst-europium merge. **Bottom**: chemical structures of Hoechst and DNA nucleosides.

In figure 4.7.2 a typical result of the luminescence pattern of europium when nuclear counterstaining was done before the addition of the lanthanide. The weakly labelled MIL38-BHHBCB was used for this experiment, and the binding of the conjugate to the cell was monitored using an anti-mouse-Alexa488 antibody. It was observed that the labelling didn't impair the conjugate binding to the cells (4.7.2-A), but it was also noticed that the emission

of europium didn't match the conjugate binding sites, but the cells' nuclei (4.7.2-B and C). The BHHBCB labelling level of the antibody was so low that europium emission from the conjugate was below detection limits and the only signal observed was from the europium in the nuclei.

To overcome the chelation of europium by the Hoechst-DNA complex, the cell assay was slightly modified. After the MIL38 conjugate, the cells were incubated first with europium solution, then counterstaining with Hoechst and, finally, FEB was used as mounting media before microscope inspection as described above. Figure 4.7.3 shows a typical staining using this method. The pattern of staining is consistent with what is observed with the indirect IFA, shown in Figure 4.7.1.

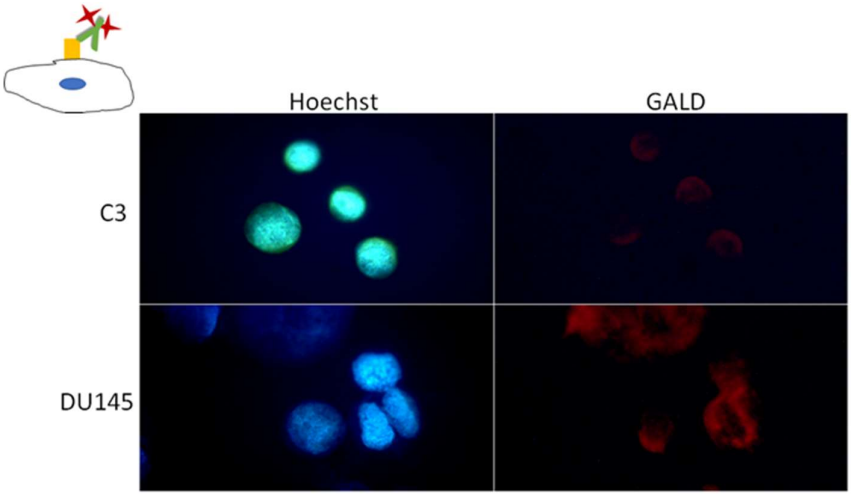


**Figure 4.7.3.** Direct Immunoluminescence Assay, using MIL38 antibody labelled with BHHBTEGBS, against a bladder cancer cells (C3, negative control) and prostate cancer cells (DU145, positive control). Exposure times: Hoechst, 10 ms; GALD: 10 s. Top left shows a diagram of the assay: Antibody (green, MIL38) is labelled with BHHBTEGBS (red), targeting the antigen (yellow, GPC1) on the surface of the cell. 40X objective was used.

Despite the success of the staining, there was a strong photobleaching effect caused by the UV light used for excitation, and therefore, the signal was lost quickly. This is not desirable when positive cells are being searched in a patient sample. Trying to address this new difficulty, amplification of the signal via an indirect assay was tested, using a biotin-streptavidin system.

## 4.8. AMPLIFICATION – USE OF BIOTIN-STREPTAVIDIN SYSTEM

Streptavidin is a homo-tetrameric protein complex that binds biotin with high affinity. For this work it was used a recombinant form. According to the manufacturer (Thermo Scientific Pierce), it has a mass of 53 kDa and neutral isoelectric point (pI = 6.8 to 7.5). For the labelling, the chelator/protein molar ratio used was 20X, and given the similar isoelectric point to MIL38 antibody, the same storage conditions were employed. UV-visible spectrum and gel filtration chromatography as described before were run as quality control tests before checking for activity. Results are shown in Figure 4.8.1.

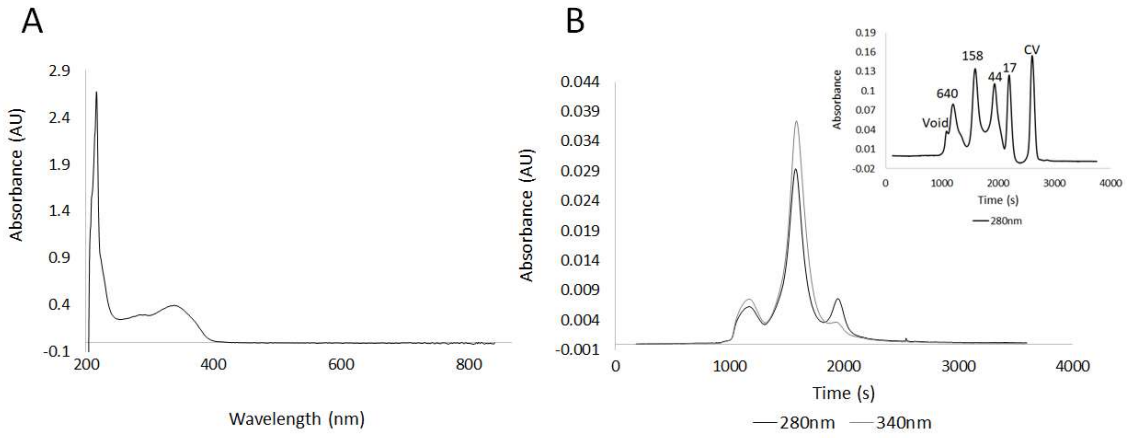


**Figure 4.8.1** Streptavidin-BHHBTEGBS conjugate. **A**. UV-visible spectrum. **B**. Gel filtration chromatogram. TBS pH 7.5, 10% glycerol was used as running buffer. Standards chromatogram is shown at the top right for reference, with void and column volume points and molecular weights shown in kDa.

The spectrum shows, as before for MIL38, a high level of conjugation. The number of chelators per protein was calculated as described before, using $\varepsilon_{280}$ = 1.8x10$^5$M$^{-1}$cm$^{-1}$ as specified by the manufacturer, with a result of 19. The chromatogram shows that the majority of the labelled protein comes out at about the expected retention time for 53 kDa, and some aggregation is already taking place during the chromatography (run TBS pH 7.5 10% glycerol to keep conditions comparable), as observed with MIL38-BHHBTEGBS conjugate. The small peak at a later retention time is probably some monomeric form of the streptavidin.

The new conjugate was tested on an indirect immunoluminescence cell assay, using MIL38 as primary antibody, an anti-mouse-biotin secondary antibody and the streptavidin-BHHBTEGBS conjugate, comparing this time with Streptavidin-DyLight (488), another photostable fluorescent dye (Thermo). The result is shown in Figure 4.8.2.

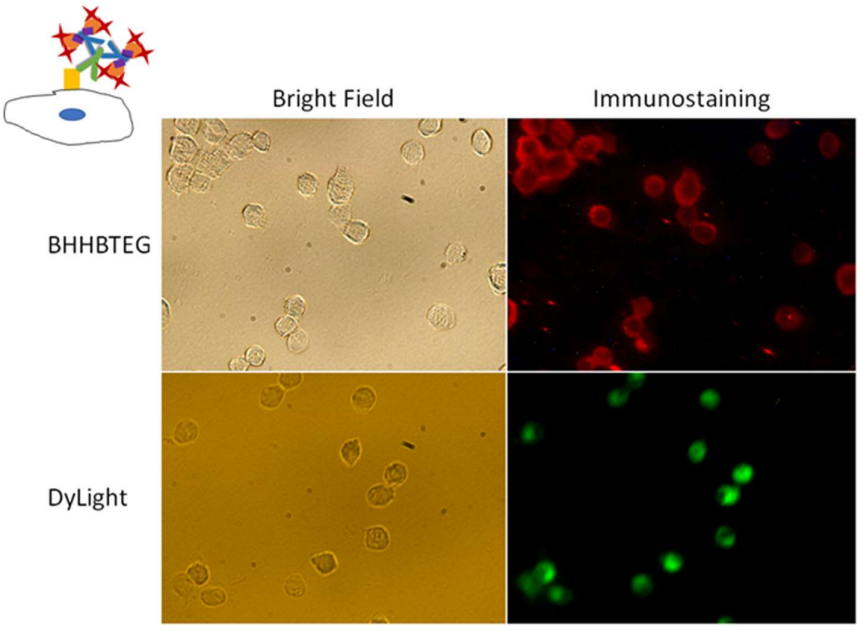


**Figure 4.8.2.** Indirect Immunoluminescence Assay (top) and Immunofluorescence Assay (bottom) on prostate cancer cells (DU145), using MIL38 as primary antibody, and an anti-mouse-biotin with Streptavidin-BHHBTEG (top) or Streptavidin-DyLight.488 (bottom) systems as secondary reagents for detection. Exposure times: GALD: 10 s; DyLight: 200 ms. Top left shows a diagram of the assay: Antibody (green, MIL38) is bound by a secondary antibody (blue) labelled with biotin (purple), which is detected by streptavidin (orange) labelled with BHHBTEG (red), targeting the antigen (yellow, GPC1) on the surface of the cell. 20X Objective was used.

The assay was successful. Cells were stained as expected, with higher intensity than the direct assay and the expected pattern for DU145. Photobleaching still occurred, but as the signal was more intense, it lasted longer giving enough time to search and photograph the cells.

Following this preliminary test, DU145 cells were spiked into normal urine to test for specificity in a real sample. Spiked samples were processed as patient samples and assayed using the optimised indirect immunoluminescence assay. The performance of Streptavidin-BHHBTEGBS was compared with Streptavidin-DyLight (488). Results are shown in Figure 4.8.3.

On panels A and B, it can be observed the performance of streptavidin-BHHBTEGBS and streptavidin-DyLight respectively. C and D show the streptavidin alone controls, BHHBTEGBS and DyLight conjugates respectively. For the time gated image, only some of the cells are stained, the spiked DU145 cells. For the fluorescence image, however, both DU145 and epithelial urine cells fluoresce. The secondary alone controls show that there is no non-specific binding of the europium chelate conjugate, whereas cells show fluorescence for the DyLight conjugate, most likely autofluorescence.

On panel E, results for a similar assay using streptavidin is shown. Bright-field and time-gated luminescence images of *Cryptosporidium muris* were immunostained in suspension with anti-cryptosporidium antibody, biotinylated secondary antibody, and the BHHBCB-$Eu^{3+}$ labelled BSA-streptavidin complex in a fruit juice sample.[133] The time gated image is also clear of autofluorescence but required 3 min exposure to reach similar intensity levels that were reached with 10 s exposure with the system developed and used in this work.

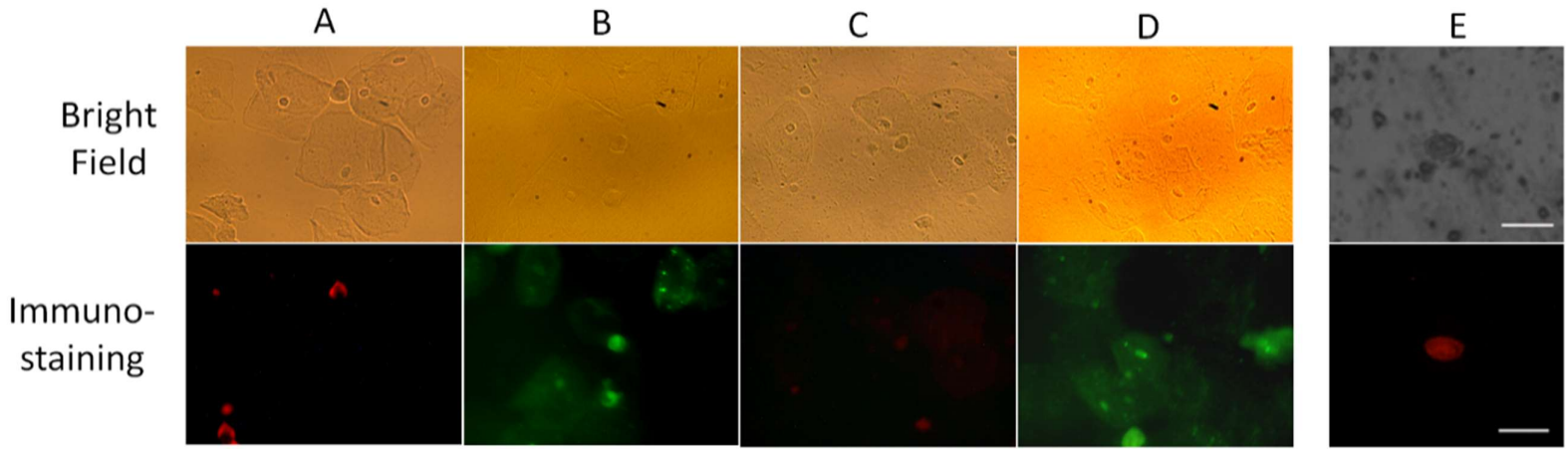


**Figure 4.8.3.** Indirect Immunoluminescence Assay (**A, C**) and Immunofluorescence Assay (**B, D**) on prostate cancer cells (DU145) spiked in normal urine. MIL38 was used as primary antibody (**A, B)**, and anti-mouse-biotin with streptavidin-BHHBTEG (**A**) or streptavidin-Dylight.488 (**B**) as detection systems. Secondary alone controls (**C, D** respectively) were run to test for non-specific binding and autofluorescence. Exposure times: GALD: 10 s; DyLight: 200 ms. 20X objective was used. **E**. Image modified from [133]. Bright-field (top), time-gated (bottom; exposure time, 3 min) luminescence images of *Cryptosporidium muris* oocysts immunostained by BHHBCB-labelled BSA-Streptavidin complex in fruit juice.

Running this final test, it is concluded that the system developed for urine assays seems suitable to analyse patient urine samples, with stable reagents and a clean assay. However, during the imaging it was noticed that the manual system in place would make the analysis of individual slides tedious and time consuming.

## 4.9. DISCUSSION

The development of this new platform for urine cells immunoassay was devided in two major stages: reagents development and assay optimisation. The achievement of a stable reagent that can be prepared in reproducible batches and the optimisation of a robust immunoassay are desirable in order to transfere the technology to commercial pathology laboratories for routine analysis.

The first step consisted in choosing the best europium chelator for conjugation to the MIL38 antibody. BHHBTEGBS showed better performance when compared with BHHBCB in terms of level of labelling. BHHBCB has a sulfonyl chloride as a reactive group, which hydrolyses very quickly in aqueous conditions. Although the hydrolysation rate was not determined empirically, it is likely that this high reactivity with water contributed with the low labelling efficiency observed. On the other hand, BHHBTEGBS, a derivative of BHHBCB, has a tetraethylene glycol (TEG) spacer which increases the hydrophilicity of the molecule, otherwise highly hydrophobic. The presence of this spacer increases the accessibility of the chelator to less exposed amino groups from the antibody, that BHHBCB would not be able to access. Additionally, BHHBTEGBS has N-hydroxysuccinimide ester (NHS) as a reactive group, which is more stable in aqueous solutions than the sulfonyl chloride. The higher stability of the reactive group in water and the enhanced accessibility of amino groups thanks to the TEG

spacer could explain the higher degree of labelling when using BHHBTEGBS, compared with BHHBCB.

While the TEG linker facilitates the attachment of a high number of chelators to the antibody, the best ratio of chelator to protein that maintains the activity and the stability of the conjugated protein remained to be investigated. A series of conjugations of BHHBTEGBS to MIL38 were carried out by increasing the molar ratio of ligand to antibody from 10:1 (10X) to 50:1 (50X). It was determined that the optimal molar ratio for MIL38 is 20:1.

The presence of TEG did not guarantee the solubility of the conjugate, however, as evidenced by the short retention times observed for the conjugates in gel filtration chromatography tests, suggesting aggregation. Examination of the isoelectric point of MIL38 antibody using the heavy and light chains sequences showed that it was close to the pH of the storage buffer used. This was suspected to contribute to aggregation and eventually the precipitation of the conjugate during storage. A two pH units lower buffer was used for storage, and further analysis by gel filtration showed that the antibody-chelator conjugate was stable in solution. The use of two pH units below the isoelectric point for storage of antibodies used in therapeutics is not uncommon. For example, the storage buffer of the commercial antibody Trastuzumab, according to the drug insert (Herceptin) is 6, while the isoelectric point of the antibody is near 8.

Once a stable reagent was achieved, the next step followed was to modify the original assay used for the patient trial to be adapted to the europium chelate emission conditions. First, the mounting medium needed to be replaced, as europium emission is quenched by water and it was observed that the glycerol based mounting medium was not optimal either. The previously described FEB[137], was adapted to more gentle conditions compatible with

cells immunoassays, which included the use of a slightly less acid buffer and a milder detergent. The optimised FEB was lately used as mounting medium for cell imaging. The immunoassay steps were kept the same up to the counterstaining step. It was observed that if the nuclear dye Hoechst was used first, europium used either by itself or mixed with FEB in the mounting medium, the nuclei would be stained red (Figure 4.7.2). The complex formed by the dye and the DNA, which makes the dye fluoresce blue when excited at the same wavelength interval that BHHBTEGBS/BHHBCB do, may be creating a coordination space surrounded by an aromatic environment (see the structures of Hoechst and DNA nucleosides in Figure 4.7.2 bottom), where europium is chelated and excited during irradiation. When adding europium before the counterstaining, it would be captured only by the chelator and perhaps other groups in the cells that do not have an antenna well positioned for energy transfer and therefore, the non-specific nuclear staining is not observed. This was not found to be reported yet in the literature, thus the interactions between nuclear dyes, DNA and europium, and perhaps other lanthanides, remain to be studied.

A major disadvantage of the use of europium chelators is the strong photobleaching by the UV radiation that reduces the europium emission, often impairing the sample examination and the imaging process. This problem was addressed by increasing the signal intensity via amplification by streptavidin-biotin system. However, recently, two highly luminescent and water-soluble europium chelates have been reported to display UV-light stability in solution, remaining highly emissive after 100 min of strong UV irradiation[143]. These developed probes could be used as an alternative in future developments of this type of assays in the future.

Similar conjugation, storage and assay conditions used for the MIL38-BHHBTEGBS were found to be optimal for the Streptavidin-BHHBTEGBS conjugate. An assay over a urine sample spiked with prostate cancer cells showed that the optimised assay was adequate to analyse autofluorescent samples, as selectively stained the GPC1 expressing cells. A comparison with a similar assay done over *Cryptosporidium muris* oocysts in a fruit juice sample[133] showed that the assay developed in this work seemed to be more efficient. In this work, the streptavidin was directly labelled with BHHBTEGBS with a total of 19 chelators per protein, whereas the streptavidin conjugate used for the detection of the oocytes was in a complex with BSA labelled with BHHBCB, to improve the solubility of the chelator, with a labelling ratio of 47:1. This preparation already contains the europium in coordination to the complex before the immunoassay and do not use any enhancement, therefore they required a longer exposure time to reach similar levels of luminescence intensity in their image (3 min, compared with 5-10 s for the optimised assay). Another factor of improved signal is the different instrumentation used. For this work, a microscope with a Gated Autosynchronous Luminescence Detection (GALD)[136] was used, which among its components contains a high-power UV-led unit as a light source and a DP72 colour camera for imaging, whereas for the imaging of the oocytes a 30 W xenon flashlamp was used as light source, with UV-2A and V-2A filters and a time-resolved digital black-and-white CCD camera system for image acquisition. The differences in the reagents, the assay method and the instrumentation used account for the improved performance of the immunoassay. On the other hand, time gated luminescence instruments to be used for cell imaging are still being developed.

The europium chelate platform optimised in this work has been shown to be successful as an assay that overcame the problems that affected the initial

immunofluorescence assay trial with MIL38 antibody over urine cells for the detection of prostate cancer. However, during the analysis of the samples it was noticed that the instrumentation used is not optimal for sample slides screening: as the operation is highly manual, the analysis of patient samples that requires the screening of a wide area of the slide, would be a time consuming and tedious task. Other similar technologies that promise to overcome this particular problem by automatization are being developed, such as the Time-Gated Orthogonal Scanning Automated Microscopy (OSAM) [144], which has been reported to detect protein of low expression on cells using europium containing nanoparticles for enhancement[145]. This technology could be adapted to the assay developed in this work for a more reliable sample analysis.

## 4.10. CONCLUSION

Luminescence has been proven useful to overcome the autofluorescence interference in cell immunofluorescence assays. MIL38 antibody was successfully labelled with the europium chelator BHHBTEGBS, and it was found that the conjugate was more stable for storage in acidic conditions. The original IFA developed at the beginning of the study was adapted for luminescence. It was found during the optimisation process that europium can be incorporated non-specifically in the cell nucleus when the nuclear dye Hoechst is present. Due to the susceptibility of BHHBTEGBS (and BHHBCB for that matter) to photobleaching, a biotin-streptavidin system was incorporated to the assay in order to amplify the signal. Streptavidin was then labelled with BHHBTEGBS, using same conditions used for MIL38, and the assay was successful. An assay run with urine spiked with DU145 cells showed that the platform was useful in overcoming autofluorescence, but the instrumentation used was not adequate for screening. It is recommended to continue the development of the assay with a

scanning system such as the Time-Gated Orthogonal Scanning Automated Microscopy (OSAM)

# 5. GENERAL CONCLUSIONS

Thanks to the advances of modern medicine, life expectancy is increasing. With an aging population, many ailments linked to age are to become more common, and it is of interest to find accurate ways of diagnosis and prognosis, as well as effective treatments. One of these age-related illnesses is prostate cancer. Thanks to the implementation of screening policies, early detection is a possibility, increasing the chances of survival of those with malignancies. However, the current screening protocols have low specificity, and require invasive confirmatory tests that can bring complications. Additionally, many indolent tumours are overtreated, and therefore, improvement in prognosis tools are also required. Much effort is focused on the finding of new biomarkers that complement the current ones for a more accurate risk stratification of prostate cancer. Also, the development of new technologies to assist the improvement of specificity and sensitivity of cancer detection and prognosis are continuously in progress.

In the present work, the relevance of Glypican 1 as a biomarker for detection of cancer cells in urine of prostate cancer patients was explored, as a proof of concept of a support test for cytological examination of urine sediments. A mouse monoclonal antibody, MIL38, was used as a central tool for the development of an immunoassay to detect Glypican 1 positive cells. As a first approach, an immunofluorescence assay was optimised, and a small pilot study was performed with 4 different groups of patients: confirmed prostate cancer; prostate cancer negative but confirmed BPH (notorious to be positive for gold standard PSA); radical prostatectomy (previous prostate cancer, without evidence of metastasis, prostate removed); and normal (either healthy or with non-cancer related illnesses). The expectation in this study

is that only the confirmed prostate cancer group will be positive for Glypican-1 in urine sediments unless there is undiagnosed cancer in the other three groups.

Analysis of the data from these four groups indicated that the specificity of the test, 73.4%, was found to be moderate-high, when compared with the gold standard PSA, which is around 40%. The sensitivity, however, was 55.6%, which is relatively low. The samples collected for the pilot study were voided mid-stream, as was recommended at the time. Investigation of urine sampling techniques for prostate related diagnostics, in particular for RNA based tests such as PCA3, showed that it is better to perform a digital rectal examination (DRE), or prostate massage, prior the sample collection, and that first catch urine should be collected. This approach maximises the prostate derived material for testing but is not the normal method recommended for other tests conducted on urine. The requirement for DRE for the urine collection is controversial, because it is uncomfortable for both patients and physicians, in particular for healthy participants of any clinical study. The use of imaging techniques where few cancer cells can be detected could potentially bypass the need of DRE, and a simple voided first-catch sample might be sufficient. This remains to be investigated.

The patient samples presented two major interference problems that introduced bias in the results. One of the problems was the low number of cells recovered, in particular for normal samples. This was addressed modifying the sample preparation using different fixatives, which improved the cells integrity and recovery. More recently, although not for the work presented here, cell recovery was maximised by using 8µm polycarbonate filters to collect the sediments by filtration[39]. The cells containing filters are then put on polylysine coated slides and stained using the standard protocol. The presence of mucus in urine was also found to impair the analysis of the samples, but a simple incubation with a reducing agent

was shown to be sufficient to disrupt the mucins matrix without damaging the antibody epitope, improving the performance of the assay. Finally, the most difficult problem to address was the autofluorescence of the samples, in particular those of prostate cancer patients. The rest of the work is devoted to the solution of this interferent.

Fluorescence of natural occurring molecules from the cells and their external matrixes or due to fixation treatments, which is called here autofluorescence, is a well-known problem. In the present work, two different tools were explored as an alternative of the common fluorophores used, FITC and Alexa Fluor, for the urine cells immunoassay under development.

Initially, upconversion nanoparticles (UCNP) were explored. They overcome autofluorescence by the emission of wavelengths shorter than the excitation light, contrary to what is observed in common fluorophores, thanks to the stable excited electronic states of lanthanides embedded into the nanoparticle matrixes. As a bioconjugation strategy, three IgG binding peptides were selected to be conjugated to the nanoparticle, using a short (20 bases) single strand DNA (ssDNA) chain as crosslinker. The peptides and the ssDNA were coupled to the peptides via click chemistry, purified by HPLC and then it was demonstrated that the conjugates effectively bind to MIL38 antibody, using gel filtration chromatography. The ssDNA-peptide molecules were then conjugated to the nanoparticles through a process known as ligand exchange, and it was proven to be successful. However, the final conjugate was unstable and easily formed aggregates, impairing its function in immunoassays. It was shown that low pHs were optimal for storage, but the optimal assay conditions for cell analysis was not achieved. The cause of the aggregation was not determined, however, and further optimisation was abandoned at this point.

It is worth noting, though, that given that the ssDNA-peptide conjugate successfully bound to the antibody, it might be worth to characterise further antibody-peptide/ssDNA interaction using isothermal titration calorimetry (ITC) or surface plasmon resonance (SPR), in order to determine a range of conditions within which these peptides would bind to IgG for other purposes. This peptide could also be modified to allow for different chemical couplings. For example, direct conjugation of other molecules to the Fc region of the antibody mediated by a covalently coupled Fc binding peptide containing a photoactivable molecule such as BPA could be used when the Fv binding site is sensitive to commonly used conjugation chemistries.

Following the UCNP attempt, a europium chelate was explored. The europium-chelate complex as a whole functions as the reporter molecule: the chelator or ligand, has an aromatic system that acts like an antenna group to absorb photons, and transfers this energy to europium, a lanthanide, which then emits light. This system overcomes autofluorescence by the delayed emission of light after an excitation pulse, in a process known as luminescence. By gating the acquisition of emitted light from the time the fluorescent molecules have emitted their photons, the non-specific background is eliminated.

Two derivatives of the same ligand, BHHBCB and BHHBTEGBS, were tested for direct conjugation to the MIL38 antibody with the labelling by BHHBTEGBS being more efficient. The conjugation conditions, as well as storage and assay conditions were also further optimised. A direct immunoluminescence assay was performed successfully on cultured cells, using a standard fluorescence microscope with a GALD unit for cell imaging. However, due to rapid loss of emission by photobleaching, amplification of the signal was necessary and was realised using a biotin-streptavidin system. This final assay was tested over normal urine samples spiked with prostate cancer cells. Prostate cancer cells were readily and specifically

detected from normal cells without the problem of autofluorescence observed with normal fluorophores. However, it was noted that because of the highly manual operation of the GALD adapted microscope, it would be very laborious and time consuming when analysing real patient samples, as it often requires the search of positive cells over a wide sample area. It is therefore recommended the use of automated scanning system such as the OSAM for a high throughput assay. Work is underway with this optimisation, and once completed, a new pilot study to reassess the utility of Glypican 1 as a biomarker for detection of prostate cancer can be conducted.

# 6. REFERENCES


1. Nargund, V.H., D. Raghavan, and H.M. Sandler, *Urological Oncology*, ed. V.H. Nargund, D. Raghavan, and H.M. Sandler. 2008, London: London: Springer London.
2. Gleason, D.F. and G.T. Mellinger, *Prediction of Prognosis for Prostatic Adenocarcinoma by Combined Histological Grading and Clinical Staging.* J Urol, 2017. **197**(2s): p. S134-s139.
3. Axel, S.M., A.K. Markus, and W.M. Judd, *Urology at a Glance*. 2014 ed, ed. A.S. Merseburger, M.A. Kuczyk, and J.W. Moul. 2014, Berlin, Heidelberg: Berlin, Heidelberg: Springer Berlin Heidelberg.
4. Australian Institute of, H. and Welfare, *Cancer in Australia: Actual incidence data from 1982 to 2013 and mortality data from 1982 to 2014 with projections to 2017.* Asia Pac J Clin Oncol, 2018. **14**(1): p. 5-15.
5. Yu, X.Q., et al., *Prostate cancer prevalence in New South Wales Australia: a population-based study.* Cancer Epidemiol, 2015. **39**(1): p. 29-36.
6. Haines, I.E., R.J. Ablin, and G.L. Miklos, *Screening for prostate cancer: time to put all the data on the table.* Bmj, 2016. **353**: p. i2574.
7. Barh, D., et al., *Cancer Biomarkers : Minimal and Noninvasive Early Diagnosis and Prognosis*. 2014, Baton Rouge: Baton Rouge: Chapman and Hall/CRC.
8. Chamie, K., et al., *The role of magnetic resonance imaging in delineating clinically significant prostate cancer.* Urology, 2014. **83**(2): p. 369-75.
9. Loeb, S., et al., *Systematic review of complications of prostate biopsy.* Eur Urol, 2013. **64**(6): p. 876-92.
10. Nadler, R.B., et al., *Effect of inflammation and benign prostatic hyperplasia on elevated serum prostate specific antigen levels.* J Urol, 1995. **154**(2 Pt 1): p. 407-13.
11. Gann, P.H., C.H. Hennekens, and M.J. Stampfer, *A prospective evaluation of plasma prostate-specific antigen for detection of prostatic cancer.* Jama, 1995. **273**(4): p. 289-94.
12. Egawa, S., et al., *Prospective evaluation of prostate cancer detection by prostate specific antigen related parameters: comparison in serum and plasma samples.* J Urol, 2002. **167**(1): p. 97-102.
13. Verma, A., et al., *PSA density improves prediction of prostate cancer.* Can J Urol, 2014. **21**(3): p. 7312-21.
14. Carter, H.B., et al., *Detection of life-threatening prostate cancer with prostate-specific antigen velocity during a window of curability.* J Natl Cancer Inst, 2006. **98**(21): p. 1521-7.
15. Ankerst, D.P., et al., *Serial Percent Free Prostate Specific Antigen in Combination with Prostate Specific Antigen for Population Based Early Detection of Prostate Cancer.* J Urol, 2016. **196**(2): p. 355-60.
16. Prcic, A., E. Begic, and M. Hiros, *Actual Contribution of Free to Total PSA Ratio in Prostate Diseases Differentiation.* Med Arch, 2016. **70**(4): p. 288-292.

17. Djavan, B., et al., *Complexed prostate-specific antigen, complexed prostate-specific antigen density of total and transition zone, complexed/total prostate-specific antigen ratio, free-to-total prostate-specific antigen ratio, density of total and transition zone prostate-specific antigen: results of the prospective multicenter European trial.* Urology, 2002. **60**(4 Suppl 1): p. 4-9.
18. Mikolajczyk, S.D., et al., *A precursor form of PSA (pPSA) is a component of the free PSA in prostate cancer serum.* Urology, 1997. **50**(5): p. 710-4.
19. Mikolajczyk, S.D., et al., *A precursor form of prostate-specific antigen is more highly elevated in prostate cancer compared with benign transition zone prostate tissue.* Cancer Res, 2000. **60**(3): p. 756-9.
20. Lepor, A., W.J. Catalona, and S. Loeb, *The Prostate Health Index: Its Utility in Prostate Cancer Detection.* Urol Clin North Am, 2016. **43**(1): p. 1-6.
21. Darson, M.F., et al., *Human glandular kallikrein 2 (hK2) expression in prostatic intraepithelial neoplasia and adenocarcinoma: a novel prostate cancer marker.* Urology, 1997. **49**(6): p. 857-62.
22. Stephan, C., et al., *Serum human glandular kallikrein 2 (hK2) for distinguishing stage and grade of prostate cancer.* Int J Urol, 2006. **13**(3): p. 238-43.
23. Magklara, A., et al., *The combination of human glandular kallikrein and free prostate-specific antigen (PSA) enhances discrimination between prostate cancer and benign prostatic hyperplasia in patients with moderately increased total PSA.* Clin Chem, 1999. **45**(11): p. 1960-6.
24. Partin, A.W., et al., *Use of human glandular kallikrein 2 for the detection of prostate cancer: preliminary analysis.* Urology, 1999. **54**(5): p. 839-45.
25. Stattin, P., et al., *Improving the Specificity of Screening for Lethal Prostate Cancer Using Prostate-specific Antigen and a Panel of Kallikrein Markers: A Nested Case-Control Study.* Eur Urol, 2015. **68**(2): p. 207-13.
26. Vickers, A.J., et al., *A four-kallikrein panel predicts prostate cancer in men with recent screening: data from the European Randomized Study of Screening for Prostate Cancer, Rotterdam.* Clin Cancer Res, 2010. **16**(12): p. 3232-9.
27. Bussemakers, M.J., et al., *DD3: a new prostate-specific gene, highly overexpressed in prostate cancer.* Cancer Res, 1999. **59**(23): p. 5975-9.
28. de Kok, J.B., et al., *DD3(PCA3), a very sensitive and specific marker to detect prostate tumors.* Cancer Res, 2002. **62**(9): p. 2695-8.
29. Salagierski, M. and J.A. Schalken, *Molecular diagnosis of prostate cancer: PCA3 and TMPRSS2:ERG gene fusion.* J Urol, 2012. **187**(3): p. 795-801.
30. Leyten, G.H., et al., *Identification of a Candidate Gene Panel for the Early Diagnosis of Prostate Cancer.* Clin Cancer Res, 2015. **21**(13): p. 3061-70.
31. Jiang, Z., et al., *P504S: a new molecular marker for the detection of prostate carcinoma.* Am J Surg Pathol, 2001. **25**(11): p. 1397-404.
32. Besanceney-webler, C., et al., *Increasing the Efficacy of Bioorthogonal Click Reactions for Bioconjugation: A Comparative Study.* Angewandte Chemie International Edition, 2011. **50**(35): p. 8051-8056.
33. Meid, F.H., et al., *The use of telomerase activity for the detection of prostatic cancer cells after prostatic massage.* J Urol, 2001. **165**(5): p. 1802-5.

34. Vicentini, C., et al., *Detection of telomerase activity in prostate massage samples improves differentiating prostate cancer from benign prostatic hyperplasia.* J Cancer Res Clin Oncol, 2004. **130**(4): p. 217-21.
35. Martignano, F., et al., *Urinary RNA-based biomarkers for prostate cancer detection.* Clin Chim Acta, 2017. **473**: p. 96-105.
36. Fujita, K. and N. Nonomura, *Urinary biomarkers of prostate cancer.* Int J Urol, 2018. **25**(9): p. 770-779.
37. Wu, D., et al., *Urinary biomarkers in prostate cancer detection and monitoring progression.* Crit Rev Oncol Hematol, 2017. **118**: p. 15-26.
38. Fujita, K., et al., *Specific detection of prostate cancer cells in urine by multiplex immunofluorescence cytology.* Hum Pathol, 2009. **40**(7): p. 924-33.
39. Nickens, K.P., et al., *Prostate cancer marker panel with single cell sensitivity in urine.* Prostate, 2015. **75**(9): p. 969-75.
40. Walker, K.Z., et al., *Detection of malignant cells in voided urine from patients with bladder cancer, a novel monoclonal assay.* J Urol, 1989. **142**(6): p. 1578-83.
41. Russell, P.J., et al., *Immunohistochemical characterisation of the monoclonal antibody BLCA-38 for the detection of prostate cancer.* Cancer Immunol Immunother, 2004. **53**(11): p. 995-1004.
42. Russell, P.J., et al., *Monoclonal antibodies for intravesical radioimmunotherapy of human bladder cancer.* Cell Biophys, 1993. **22**(1-3): p. 27-47.
43. Russell, P.J., et al., *Growth and metastasis of human bladder cancer xenografts in the bladder of nude rats. A model for intravesical radioimmunotherapy.* Urol Res, 1991. **19**(4): p. 207-13.
44. Carter, T., et al., *Biodistributions of intact monoclonal antibodies and fragments of BLCA-38, a new prostate cancer directed antibody.* Cancer Immunol Immunother, 2004. **53**(6): p. 533-42.
45. Quach Truong, I.O.J., Aline L. Nocon, Julie T. Soon, Sandra Wissmueller, and D.H.C.a.B.J. Walsh, *Glypican-1 as a Biomarker for Prostate Cancer: Isolation and Characterization.* Journal of Cancer, 2016. **7**(8): p. 1002-1009.
46. Svensson, G., et al., *The structural role of N-linked glycans on human glypican-1.* Biochemistry, 2011. **50**(43): p. 9377-87.
47. Svensson, G., et al., *Crystal structure of N-glycosylated human glypican-1 core protein: structure of two loops evolutionarily conserved in vertebrate glypican-1.* J Biol Chem, 2012. **287**(17): p. 14040-51.
48. Pettersen, E.F., et al., *UCSF Chimera--a visualization system for exploratory research and analysis.* J Comput Chem, 2004. **25**(13): p. 1605-12.
49. Awad, W., et al., *Structural Aspects of N-Glycosylations and the C-terminal Region in Human Glypican-1.* J Biol Chem, 2015. **290**(38): p. 22991-3008.
50. Malave, C., et al., *Role of glypican-1 in the trophic activity on PC12 cells induced by cultured sciatic nerve conditioned medium: identification of a glypican-1-neuregulin complex.* Brain Res, 2003. **983**(1-2): p. 74-83.
51. Ding, K., et al., *Growth factor-induced shedding of syndecan-1 confers glypican-1 dependence on mitogenic responses of cancer cells.* 2005.

52. Matsuda, K., et al., *Glypican-1 is overexpressed in human breast cancer and modulates the mitogenic effects of multiple heparin-binding growth factors in breast cancer cells.* Cancer Res, 2001. **61**(14): p. 5562-9.
53. Kleeff, J., et al., *The cell-surface heparan sulfate proteoglycan glypican-1 regulates growth factor action in pancreatic carcinoma cells and is overexpressed in human pancreatic cancer.* The Journal of clinical investigation, 1998. **102**(9): p. 1662.
54. Su, G., et al., *Glypican-1 is frequently overexpressed in human gliomas and enhances FGF-2 signaling in glioma cells.* Am J Pathol, 2006. **168**(6): p. 2014-26.
55. Qiao, D., K. Meyer, and A. Friedl *Glypican 1 stimulates S phase entry and DNA replication in human glioma cells and normal astrocytes*. Molecular & Cellular Biology, 2013. **33**, 4408 DOI: 10.1128/MCB.00238-13.
56. Qiao, D., et al., *Glypican-1 regulates anaphase promoting complex/cyclosome substrates and cell cycle progression in endothelial cells.* Mol Biol Cell, 2008. **19**(7): p. 2789-801.
57. Whipple, C.A., A.L. Young, and M. Korc, *A KrasG12D-driven genetic mouse model of pancreatic cancer requires glypican-1 for efficient proliferation and angiogenesis.* Oncogene, 2012. **31**(20): p. 2535-2544.
58. Whipple, C.A., A.D. Lander, and M. Korc, *Discovery of a novel molecule that regulates tumor growth and metastasis.* ScientificWorldJournal, 2008. **8**: p. 1250-3.
59. Suhovskih, A.V., et al., *Proteoglycan expression in normal human prostate tissue and prostate cancer.* ISRN Oncol, 2013. **2013**: p. 680136.
60. Bologna-Molina, R., A. Mosqueda-Taylor, and N. Molina-Frechero, *Differential Expression of Glypican-1 in Ameloblastoma Variants.* Appl Immunohistochem Mol Morphol, 2014.
61. Garcia-Suarez, O., et al., *Neuroendocrine tumors show altered expression of chondroitin sulfate, glypican 1, glypican 5, and syndecan 2 depending on their differentiation grade.* Front Oncol, 2014. **4**: p. 15.
62. Mordente, A., et al., *Cancer Biomarkers Discovery and Validation: State of the Art, Problems and Future Perspectives.* Adv Exp Med Biol, 2015. **867**: p. 9-26.
63. Rifai, N., M.A. Gillette, and S.A. Carr, *Protein biomarker discovery and validation: the long and uncertain path to clinical utility.* Nat Biotechnol, 2006. **24**(8): p. 971-83.
64. Goossens, N., et al., *Cancer biomarker discovery and validation.* Transl Cancer Res, 2015. **4**(3): p. 256-269.
65. Barkan, G.A. and E.M. Wojcik, *Genitourinary cytopathology (kidney and urinary tract).* Cancer Treat Res, 2014. **160**: p. 149-83.
66. Barkan, G.A., et al., *The Paris System for Reporting Urinary Cytology: The Quest to Develop a Standardized Terminology.* Acta Cytol, 2016. **60**(3): p. 185-97.
67. Yafi, F.A., et al., *Is the performance of urinary cytology as high as reported historically? A contemporary analysis in the detection and surveillance of bladder cancer.* Urologic Oncology: Seminars and Original Investigations, 2014. **32**(1): p. 27.e1-27.e6.
68. McCroskey, Z., et al., *Accuracy and interobserver variability of the cytologic diagnosis of low-grade urothelial carcinoma in instrumented urinary tract cytology specimens.* Am J Clin Pathol, 2015. **144**(6): p. 902-8.
69. Kim, L., et al., *Cytologic Features of Prostatic Adenocarcinoma in Urine: Comparison with Urothelial Carcinoma.* J Pathol Transl Med, 2011. **45**(1): p. 79-86.

70. Son, S.M., et al., *Evaluation of Urine Cytology in Urothelial Carcinoma Patients: A Comparison of CellprepPlus(R) Liquid-Based Cytology and Conventional Smear.* Korean J Pathol, 2012. **46**(1): p. 68-74.
71. Voss, J.S., et al., *Changes in specimen preparation method may impact urine cytologic evaluation.* Am J Clin Pathol, 2008. **130**(3): p. 428-33.
72. Fetsch, P.A., et al., *Comparison of three commonly used cytologic preparations in effusion immunocytochemistry.* Diagn Cytopathol, 2002. **26**(1): p. 61-6.
73. Laucirica, R., et al., *Do Liquid-Based Preparations of Urinary Cytology Perform Differently Than Classically Prepared Cases?* Arch Pathol Lab Med, 2010. **134**: p. 19-22.
74. Layfield, L.J., et al., *Review of the state of the art and recommendations of the Papanicolaou Society of Cytopathology for urinary cytology procedures and reporting : the Papanicolaou Society of Cytopathology Practice Guidelines Task Force.* Diagn Cytopathol, 2004. **30**(1): p. 24-30.
75. Cibas, E.S. and B.S. Ducatman, *Cytology E-Book : Diagnostic Principles and Clinical Correlates*. 2014, Philadelphia: Philadelphia: Elsevier.
76. Zhou, A.G., et al., *Clinical implications of current developments in genitourinary pathology.* Arch Pathol Lab Med, 2013. **137**(7): p. 887-93.
77. Marin-Aguilera, M., et al., *Utility of a multiprobe fluorescence in situ hybridization assay in the detection of superficial urothelial bladder cancer.* Cancer Genet Cytogenet, 2007. **173**(2): p. 131-5.
78. Khalbuss, W. and S. Goodison, *Immunohistochemical detection of hTERT in urothelial lesions: a potential adjunct to urine cytology.* Cytojournal, 2006. **3**: p. 18.
79. Dimashkieh, H., et al., *Evaluation of UroVysion and Cytology for Bladder Cancer Detection: A Study of 1,835 Paired Urine Samples with Clinical and Histological Correlation.* Cancer cytopathology, 2013. **121**(10): p. 591-597.
80. He, H., et al., *ImmunoCyt test compared to cytology in the diagnosis of bladder cancer: A meta-analysis.* Oncol Lett, 2016. **12**(1): p. 83-88.
81. Vergara-Lluri, M.E., et al., *Comparative evaluation of ProEx C and ImmunoCyt/uCyt assays in atypical urine cytology.* Arch Pathol Lab Med, 2014. **138**(9): p. 1215-22.
82. Pal, R.P., et al., *Immunocytochemical detection of ERG expression in exfoliated urinary cells identifies with high specificity patients with prostate cancer.* BJU Int, 2016. **117**(4): p. 686-96.
83. Trabulsi, E.J., et al., *Development of a voided urine assay for detecting prostate cancer non-invasively: a pilot study.* BJU Int, 2017.
84. Nakai, Y., et al., *Photodynamic diagnosis of shed prostate cancer cells in voided urine treated with 5-aminolevulinic acid.* BMC Urol, 2014. **14**: p. 59.
85. Nakai, Y., et al., *Protoporphyrin IX induced by 5-aminolevulinic acid in bladder cancer cells in voided urine can be extracorporeally quantified using a spectrophotometer.* Photodiagnosis Photodyn Ther, 2015. **12**(2): p. 282-8.
86. Todenhofer, T., et al., *Prognostic relevance of positive urine markers in patients with negative cystoscopy during surveillance of bladder cancer.* BMC Cancer, 2015. **15**: p. 155.
87. Li, Y., et al., *Antigenic expression of human metastatic prostate cancer cell lines for in vitro multiple-targeted alpha-therapy with 213Bi-conjugates.* Int J Radiat Oncol Biol Phys, 2004. **60**(3): p. 896-908.

88. Nguyen-Khuong, T., et al., *Alterations to the protein profile of bladder carcinoma cell lines induced by plant extract MINA-05 in vitro.* Proteomics, 2009. **9**(7): p. 1883-92.
89. Cao, W., et al., *Prostate specific G protein coupled receptor is associated with prostate cancer prognosis and affects cancer cell proliferation and invasion.* BMC Cancer, 2015. **15**: p. 915.
90. Rodriguez, M., S. Siwko, and M. Liu, *Prostate-Specific G-Protein Coupled Receptor, an Emerging Biomarker Regulating Inflammation and Prostate Cancer Invasion.* Curr Mol Med, 2016. **16**(6): p. 526-32.
91. Srinivasan, M. and A.V. Parwani, *Diagnostic utility of p63/P501S double sequential immunohistochemical staining in differentiating urothelial carcinoma from prostate carcinoma.* Diagn Pathol, 2011. **6**: p. 67.
92. Kusumi, T., et al., *Immunohistochemical detection of carcinoma in radical prostatectomy specimens following hormone therapy.* Pathol Int, 2008. **58**(11): p. 687-94.
93. Kristiansen, I., et al., *Sensitivity of HOXB13 as a Diagnostic Immunohistochemical Marker of Prostatic Origin in Prostate Cancer Metastases: Comparison to PSA, Prostein, Androgen Receptor, ERG, NKX3.1, PSAP, and PSMA.* Int J Mol Sci, 2017. **18**(6).
94. Jiang, J., et al., *NK3 homeobox 1 (NKX3.1) up-regulates forkhead box O1 expression in hepatocellular carcinoma and thereby suppresses tumor proliferation and invasion.* J Biol Chem, 2017. **292**(47): p. 19146-19159.
95. Dijkstra, S., et al., *Prostate cancer biomarker profiles in urinary sediments and exosomes.* J Urol, 2014. **191**(4): p. 1132-8.
96. Fontenete, S., et al., *Controversies in using urine samples for Prostate Cancer detection: PSA and PCA3 expression analysis.* Int Braz J Urol, 2011. **37**(6): p. 719-26.
97. Dudderidge, T.J., et al., *Diagnosis of prostate cancer by detection of minichromosome maintenance 5 protein in urine sediments.* Br J Cancer, 2010. **103**(5): p. 701-7.
98. Quek, S.I., et al., *Processing of voided urine for prostate cancer RNA biomarker analysis.* Prostate, 2015. **75**(16): p. 1886-95.
99. Donovan, M.J., et al., *A molecular signature of PCA3 and ERG exosomal RNA from non-DRE urine is predictive of initial prostate biopsy result.* Prostate Cancer Prostatic Dis, 2015. **18**(4): p. 370-5.
100. Monici, M., *Cell and tissue autofluorescence research and diagnostic applications*, in *Biotechnology Annual Review*. 2005, Elsevier. p. 227-256.
101. Palmer, S., et al., *Detection of urinary bladder cancer cells using redox ratio and double excitation wavelengths autofluorescence.* Biomed Opt Express, 2015. **6**(3): p. 977-86.
102. Georgakoudi, I., et al., *NAD(P)H and collagen as in vivo quantitative fluorescent biomarkers of epithelial precancerous changes.* Cancer Res, 2002. **62**(3): p. 682-7.
103. Haase, M. and H. Schäfer, *Upconverting nanoparticles.* Angewandte Chemie (International ed. in English), 2011. **50**(26): p. 5808.
104. Sedlmeier, A. and H.H. Gorris, *Surface modification and characterization of photon-upconverting nanoparticles for bioanalytical applications.* Chem Soc Rev, 2014.
105. Gnach, A. and A. Bednarkiewicz, *Lanthanide-doped up-converting nanoparticles: Merits and challenges.* Nano Today, 2012. **7**(6): p. 532-563.
106. Berry, M.T. and P.S. May, *Disputed Mechanism for NIR-to-Red Upconversion Luminescence in NaYF4:Yb(3+),Er(3+).* J Phys Chem A, 2015. **119**(38): p. 9805-11.

107. Wang, M., et al., *Immunolabeling and NIR-excited fluorescent imaging of HeLa cells by using NaYF(4):Yb,Er upconversion nanoparticles.* ACS nano, 2009. **3**(6): p. 1580.
108. Niemeyer, C.M., *Semisynthetic DNA-protein conjugates for biosensing and nanofabrication.* Angew Chem Int Ed Engl, 2010. **49**(7): p. 1200-1216.
109. Niemeyer, C.M. and B. Ceyhan, *DNA-Directed Functionalization of Colloidal Gold with Proteins This work was supported by Deutsche Forschungsgemeinschaft and Fonds der Chemischen Industrie. We thank Prof. D. Blohm for helpful discussions and generous support.* Angewandte Chemie International Edition, 2001. **40**(19): p. 3685.
110. Li, L.L., et al., *An exceptionally simple strategy for DNA-functionalized up-conversion nanoparticles as biocompatible agents for nanoassembly, DNA delivery, and imaging.* J Am Chem Soc, 2013. **135**(7): p. 2411-4.
111. Sugita, T., et al., *Screening of peptide ligands that bind to the Fc region of IgG using peptide array and its application to affinity purification of antibody.* Biochemical Engineering Journal, 2013. **79**: p. 33-40.
112. Yang, H., P.V. Gurgel, and R.G. Carbonell, *Hexamer peptide affinity resins that bind the Fc region of human immunoglobulin G.* The journal of peptide research : official journal of the American Peptide Society, 2005. **66**: p. 120.
113. Yang, H., P.V. Gurgel, and R.G. Carbonell, *Purification of human immunoglobulin G via Fc-specific small peptide ligand affinity chromatography.* Journal of Chromatography A, 2009. **1216**(6): p. 910-918.
114. Zhao, W.-W., et al., *Octapeptide-based affinity chromatography of human immunoglobulin G: Comparisons of three different ligands.* Journal of Chromatography A, 2014. **1359**: p. 100-111.
115. Zhao, W.-W., et al., *Biomimetic design of affinity peptide ligands for human IgG based on protein A-IgG complex.* Biochemical Engineering Journal, 2014. **88**: p. 1-11.
116. Presolski, S.I., V.P. Hong, and M.G. Finn, *Copper-Catalyzed Azide-Alkyne Click Chemistry for Bioconjugation.* Curr Protoc Chem Biol, 2011. **3**(4): p. 153-162.
117. Presolski, S.I., et al., *Tailored ligand acceleration of the Cu-catalyzed azide-alkyne cycloaddition reaction: practical and mechanistic implications.* Journal of the American Chemical Society, 2010. **132**(41): p. 14570.
118. Christen, E.H., et al., *Evaluation of bicinchoninic acid as a ligand for copper(I)-catalyzed azide-alkyne bioconjugations.* Org Biomol Chem, 2012. **10**(33): p. 6629-32.
119. Yu, F., P. Jarver, and P.A. Nygren, *Tailor-making a protein a-derived domain for efficient site-specific photocoupling to Fc of mouse IgG(1).* PLoS One, 2013. **8**(2): p. e56597.
120. Zhao, W.-W., Q.-H. Shi, and Y. Sun, *FYWHCLDE-based affinity chromatography of IgG: Effect of ligand density and purifications of human IgG and monoclonal antibody.* Journal of Chromatography A, 2014.
121. Khatwani, S.L., et al., *Covalent protein-oligonucleotide conjugates by copper-free click reaction.* Bioorganic and Medicinal Chemistry, 2012. **20**(14): p. 4532-4539.
122. Muhr, V., et al., *Upconversion nanoparticles: from hydrophobic to hydrophilic surfaces.* Acc Chem Res, 2014. **47**(12): p. 3481-93.
123. Jiang, G., et al., *An effective polymer cross-linking strategy to obtain stable dispersions of upconverting NaYF4 nanoparticles in buffers and biological growth media for biolabeling applications.* Langmuir, 2012. **28**(6): p. 3239-47.

124. Chen, G., et al., *High-purity separation of gold nanoparticle dimers and trimers.* Journal of the American Chemical Society, 2009. **131**(12): p. 4218.
125. Steinigeweg, D., et al., *Fast and Cost-Effective Purification of Gold Nanoparticles in the 20–250 nm Size Range by Continuous Density Gradient Centrifugation.* Small, 2011. **7**(17): p. 2443-2448.
126. Qiu, P. and C. Mao, *Viscosity gradient as a novel mechanism for the centrifugation-based separation of nanoparticles.* Adv Mater, 2011. **23**(42): p. 4880-5.
127. Liu, F.-K., *Using Size-Exclusion Chromatography to Monitor Variations in the Sizes of Microwave-Irradiated Gold Nanoparticles.* ISRN Chromatography, 2012. **2012**: p. 1-7.
128. Hovinen, J. and P.M. Guy, *Bioconjugation with Stable Luminescent Lanthanide(III) Chelates Comprising Pyridine Subunits.* Bioconjugate Chem., 2009. **20**: p. 404–421.
129. Maindron, N., et al., *Synthesis and luminescence properties of new red-shifted absorption lanthanide(III) chelates suitable for peptide and protein labelling.* Org Biomol Chem, 2011. **9**(7): p. 2357-70.
130. Neil, E.R., et al., *Synthesis, stereocontrol and structural studies of highly luminescent chiral tris-amidepyridyl-triazacyclononane lanthanide complexes.* Dalton Trans, 2014. **43**(14): p. 5490-504.
131. Deka, C., et al., *Analysis of fluorescence lifetime and quenching of FITC-conjugated antibodies on cells by phase-sensitive flow cytometry.* Cytometry, 1996. **25**(3): p. 271-9.
132. Hermanson, G., *Bioconjugate Techniques*. 3rd ed. 2013: Elsevier. 1146.
133. Zhang, L., et al., *New class of tetradentate beta-diketonate-europium complexes that can be covalently bound to proteins for time-gated fluorometric application.* Bioconjug Chem, 2012. **23**(6): p. 1244-51.
134. Sayyadi, N., et al., *Sensitive Time-Gated Immunoluminescence Detection of Prostate Cancer Cells Using a TEGylated Europium Ligand.* Anal Chem, 2016. **88**(19): p. 9564-9571.
135. Murphy, D.B. and M.W. Davidson, *Fundamentals of Light Microscopy and Electronic Imaging*. 2012, Somerset, UNITED STATES: Wiley.
136. Connally, R., *A device for gated autosynchronous luminescence detection.* Anal Chem, 2011. **83**(12): p. 4782-7.
137. Arnaud, N. and J. Georges, *Fluorimetric Determination of Europium Over a Large Dynamic Range Using its Ternary Complex with Thenoyltrifluoroacetone and Trioctylphosphine Oxide in a Micellar Solution of Triton X-100.* Analyst, 1997. **122**(2): p. 143-146.
138. Wu, F.B. and C. Zhang, *A new europium beta-diketone chelate for ultrasensitive time-resolved fluorescence immunoassays.* Anal Biochem, 2002. **311**(1): p. 57-67.
139. Majima, K., et al., *Quantitative measurement of 17 beta-estradiol and estriol in river water by time-resolved fluoroimmunoassay.* Anal Sci, 2002. **18**(8): p. 869-74.
140. Kimura, H., et al., *Highly sensitive quantitation of methamphetamine by time-resolved fluoroimmunoassay using a new europium chelate as a label.* J Anal Toxicol, 1999. **23**(1): p. 11-6.
141. Matsumoto, K., et al., *Simultaneous determination of alpha-fetoprotein and carcinoembryonic antigen in human serum by time-resolved fluoroimmunoassay.* Anal Biochem, 1999. **276**(1): p. 81-7.

142. Kozlowski, L.P., *IPC – Isoelectric Point Calculator.* Biology Direct, 2016. **11**(1): p. 55.
143. Wei, C., et al., *Water-Soluble and Highly Luminescent Europium(III) Complexes with Favorable Photostability and Sensitive pH Response Behavior.* Inorg Chem, 2016. **55**(20): p. 10645-10653.
144. Lu, Y., et al., *Time-gated orthogonal scanning automated microscopy (OSAM) for high-speed cell detection and analysis.* Sci Rep, 2012. **2**: p. 837.
145. Lu, J., et al., *Resolving low-expression cell surface antigens by time-gated orthogonal scanning automated microscopy.* Anal Chem, 2012. **84**(22): p. 9674-8.

# 7. APPENDIXES

## A-1. ETHICS AND BIOSAFETY

This research was conducted as part of a bigger project focused in the development of tools for diagnostics of cancer. Below letters of approval from two Human Research Ethics Committees of the University of New South Wales and Macquarie University; and the Biohazard Risk Assessment presented to and approved by the Biohazard Safety Committee of Macquarie University.

THE UNIVERSITY OF
NEW SOUTH WALES

HUMAN RESEARCH ETHICS
COMMITTEE (HREC)

5 August 2010

Dr Bradley Walsh
Minomic International Ltd
Po Box 6126
Frenchs Forest DF NSW 2086

Dear Dr Walsh,

**Use of a monoclonal antibody directed toward a cell surface biomarker to detect prostate cancer**
HREC 10174

Thank you for the email and attachments from Belinda Schiller to Mrs Annamarie D'Souza dated 2 August 2010.

The Executive of the HREC considered the above protocol at its executive meeting held on 3 August 2010 and is pleased to advise it is satisfied that this protocol meets the requirements as set out in the National Statement on Ethical Conduct in Human Research*.

Having taken into account the advice of the Committee, the Deputy Vice-Chancellor (Research) has approved the project to proceed.

Would you please note -:

- approval is valid for five years (from the date of the executive meeting i.e. 3 August 2010);
- you will be required to provide annual reports on the study's progress to the HREC, as recommended by the National Statement;
- you are required to immediately report to the Ethics Secretariat anything which might warrant review of ethical approval of the protocol (National Statement 3.3.22, 5.5.7) including:
    a) serious or unexpected outcomes experienced by research participants (using the Serious Adverse Event proforma on the University website at http://www.gmo.unsw.edu.au/Ethics/HumanEthics/InformationForApplicants/ProformasTemplates/C13_SAE%20Proforma.rtf) ;
    b) proposed changes in the protocol; and
    c) unforeseen events or new information (eg from other studies) that might affect continued ethical acceptability of the project or may indicate the need for amendments to the protocol;
- any modifications to the project must have prior written approval and be ratified by any other relevant Human Research Ethics Committee, as appropriate;

..1..

UNSW SYDNEY NSW 2052
AUSTRALIA
Telephone: +61 (2) 9385 4234
Facsimile: +61 (2) 9385 6648
Email: ethics.sec@unsw.edu.au
Location: Rupert Myers Building
C/o Research Office / Ethics,
Gate 14, Barker Street Kensington
ABN 57 195 873 179

- if there are implantable devices, the researcher must establish a system for tracking the participants with implantable devices for the lifetime of the device (with consent) and report any device incidents to the TGA;

- if the research project is discontinued before the expected date of completion, the researcher is required to inform the HREC and other relevant institutions (and where possible, research participants), giving reasons. For multi-site research, or where there has been multiple ethical review, the researcher must advise how this will be communicated before the research begins (National Statement 3.3.23 and 5.5.6);

- consent forms are to be retained within the archives of the School and made available to the Committee upon request.

Yours sincerely,

Professor Michael Grimm
Presiding Member
HREC

*http://www.nhmrc.gov.au

Office of the Deputy Vice-Chancellor
(Research)

Research Office
Research Hub, Building C5C East
Macquarie University
NSW 2109 Australia
T: +61 (2) 9850 4459
http://www.research.mq.edu.au/
ABN 90 952 801 237

MACQUARIE University
SYDNEY·AUSTRALIA

22 October 2015

Dear Prof Walsh

**Reference No:** 5201500707

**Title:** Biomarkers for early diagnosis and prognosis of cancer

Thank you for submitting the above application for ethical and scientific review. Your application was considered by the Macquarie University Human Research Ethics Committee (HREC (Medical Sciences)) at its meeting on 24 September 2015 at which further information was requested to be reviewed by the HREC (Medical Sciences) Executive.

The requested information was received with correspondence on 11 September 2015.

I am pleased to advise that ethical and scientific approval has been granted for this project to be conducted at:

- Macquarie University

This research meets the requirements set out in the *National Statement on Ethical Conduct in Human Research* (2007 – Updated March 2014) (the *National Statement*).

This letter constitutes ethical and scientific approval only.

**Standard Conditions of Approval:**

1. Continuing compliance with the requirements of the *National Statement,* which is available at the following website:

http://www.nhmrc.gov.au/book/national-statement-ethical-conduct-human-research

2. This approval is valid for five (5) years, subject to the submission of annual reports. Please submit your reports on the anniversary of the approval for this protocol.

3. All adverse events, including events which might affect the continued ethical and scientific acceptability of the project, must be reported to the HREC within 72 hours.

4. Proposed changes to the protocol must be submitted to the Committee for approval before implementation.

It is the responsibility of the Chief investigator to retain a copy of all documentation related to this project and to forward a copy of this approval letter to all personnel listed on the project.

Should you have any queries regarding your project, please contact the Ethics Secretariat on 9850 4194 or by email ethics.secretariat@mq.edu.au

The HREC (Medical Sciences) Terms of Reference and Standard Operating Procedures are available from the Research Office website at:

http://www.research.mq.edu.au/for/researchers/how_to_obtain_ethics_approval/human_research_ethics

The HREC (Medical Sciences) wishes you every success in your research.

Yours sincerely

**Professor Tony Eyers**
Chair, Macquarie University Human Research Ethics Committee (Medical Sciences)

This HREC is constituted and operates in accordance with the National Health and Medical Research Council's (NHMRC) *National Statement on Ethical Conduct in Human Research* (2007) and the *CPMP/ICH Note for Guidance on Good Clinical Practice*.

## SECTION A

# Biohazard Risk Assessment Form – NON GMO

| | |
|---|---|
| *Notification Number:* | *ROW190614BHA* |

| | | | |
|---|---|---|---|
| **Department** | **CBMS** | **Date:** | **19/06/2014** |
| **Chief investigator:** | **Robert Willows** | | |
| **Contact number/email:** | **9850-8146 / robert.willows@mq.edu.au** | | |
| **Title of research/practical** | **Detection of cancer cells in voided urine** | | |
| **Is additional approval required?** | **Animal Ethics ☐ Human Ethics X Fieldwork Manager ☐ Other ☐ (state)_____** | | |

**Exact location(s) of research:**

**E8A-210, E8C-264**

**Control measures: Eliminate risk ☐ Substitute the hazard ☐ Isolate the hazard X Implement engineering controls X Administration X** (e.g. Training) **PPE X**
E.g. Eliminate by irradiation prior to use, isolation by class II biological safety cabinets, administration by following SWP as below, PPE as listed below.

**Supporting documents which must be read in conjunction with this assessment.** (e.g. Safe Working Procedures, Safety Data Sheets, Guidelines/Protocols)

MQU - A guide to Biological Risk Management: http://staff.mq.edu.au/human_resources/health_and_safety/policies-procedures-guidelines_forms/

1.Human_Serum_and_Plasma_information data sheet.
2.Handling of Human Samples and Cultures. ASAM/SOP/004.

**What is the type of the biological material?**

**Bacteria ☐ Fungi ☐Virus ☐ Cell Line ☐ Tissue ☐ Parasite ☐ Animal ☐ Plant ☐ Soil ☐ Toxin ☐ Prions ☐ Nucleic Acid☐ other X** Blood derivatives (plasma, serum, PBMCs) and human urine (voided, catheterized).

**What is the name of the biological agent?**

**Blood plasma, blood serum, PBMCs, urine.**

**List the Personal Protective Equipment required:**

**Gloves X (**e.g. chemical resistant ) **Eye protection X (**e.g. safety glasses/goggles) **Clothing** Labcoat **X** (e.g. button up lab coat/coveralls/apron)

**Footwear ☐**_____(e.g. Enclosed/Gumboots/overshoe covers) **Respiratory Protection X**_Medical face mask (e.g.PF2 face mask) **Other ☐**_____

| **What are the risks associated with this Biological Agent.** (Can be more than one risk group depending on method) | | | |
|---|---|---|---|
| **Risk Group** | **Details of Biohazards including risks associate with biological agent** http://www.absa.org/riskgroups/index.html | **Biosafety level** | **Risk Reduction Measures** (must be followed by the researcher) |
| **Group 1- Low Individual and community risk** (Microorganism that is unlikely to cause human, plant or animal disease) | | | 1 Standard laboratory procedures will be followed in accordance with Laboratory Microbiological Standards AS/NZ 2243:3:2010 and university guidelines (see supporting documents - Section A above) and include spillage and emergency response.<br>2 Investigator has attended university Biosafety training course (see 3)<br>3 Chief Investigator identified in Section A confirms that the researchers have received appropriate training and instruction or has adequate supervision and understands safe laboratory practice according to AS/NZ2243:3:2010 and university guidelines (see supporting documents - Section A above ) |
| **Group 2- Moderate individual risk, limited community risk** (Microorganism that is unlikely to be a significant risk to laboratory workers, the community/livestock/environment. Laboratory exposures may cause infection but effective treatment and preventative measures are available and the risk of spread is limited). | **Blood**:<br>Risk: HIV, HCV and other diseases could be acquired by incorrect handling and accidentally puncture with sharp tools.<br>**Urine**:<br>Risk: some samples might carry bacterial or fungal infections that could be transferred to operator if handled incorrectly. | 2 | 1 Standard laboratory procedures will be followed in accordance with Laboratory Microbiological Standards AS/NZ 2243:3:2010 and university guidelines which are appropriate for **Risk Group 2** (see supporting documents - Section A above) and include spillage and emergency response.<br>2 Researcher has attended university Biosafety training course (see 3)<br>3 Chief Investigator identified in Section A confirms that the researcher has received appropriate training and instruction or has adequate supervision and understands safe laboratory practice according to AS/NZ 2243:3:2010 and university guidelines (see supporting documents - Section A above ) |
| **Group 3 -High individual risk, limited community risk** (Microorganisms that usually causes serious human or animal disease and may present a significant risk to laboratory workers. It could present a limited to moderate risk if spread in the community or the environment, but there are usually effective preventative measures or treatment available). | | | 1 Standard laboratory procedures will be followed in accordance with Laboratory Microbiological Standards AS/NZ 2243:3:2010 and university guidelines which are appropriate for **Risk Group 3** (see supporting documents - Section A above) and include spillage and emergency response.<br>2 Researcher has attended university Biosafety training course (see 3)<br>3 Chief Investigator identified in Section A confirms that the investigator has received appropriate training and instruction or has adequate supervision and understands safe laboratory practice according to AS/NZ 243:3:2010 and university guidelines (see supporting |

| | | | |
|---|---|---|---|
| | | | documents - Section A above ) |

| **Process and equipment to be used** | You must include: -<br>Brief description of work, control measures (including aerosols), sample storage, transport of samples, clean up procedures, disinfectant and waste disposal. |
|---|---|

**General**: gloves, safety glasses and lab coats to be used at all times.

**Risks and reduction measures associated with these procedures:**

**What are the possible hazard(s) and the likelihood and consequence of the hazard(s) occurring (*ie* the risk) from the proposed work with human samples?**

- Human Blood and tissue samples are considered medium risk and it is recommended to have vaccination against Hepatitis B Virus. Other medium level risks include the potential risk of infection by other agents such as Hepatitis C, Human Immunodeficiency Virus (HIV) and Creutzfeldt-Jakob disease (CJD). These agents require ingestion or transfer directly to the blood stream (e.g. needle stick injury). We will not be using needles in handling of these samples.
- Urine samples are considered low risk as infectious agents are usually absent from urine.

Other risk reduction measures will be as per the SOP attached (with thanks to ASAM) with the main points highlighted below.

**Equipment**:

- Automatic pipettes: to load samples, use filter-tips. Sterilise with 70% ethanol after use.
- Centrifuges: to centrifuge blood and urine samples use sealed tubes and sealed buckets/rotor. After centrifugation, leave stand for at least 2 minutes to let any aerosol settle. In case of spillage, treat contaminated area with 0.5% bleach, followed by 70% ethanol. Rotor, buckets and drum must be cleaned and disinfected with 70% ethanol after use.
- Flow cytometer: proceed as per equipment and facility instructions. Add enough volume of bleach to the waste reservoir for disinfection. Used tubes and tips must be autoclaved and discarded as biohazard.

**Samples processing:**

- Commercial blood derivatives (plasma, serum) are to be used for standardisation and control purposes. Data sheet attached to this application.
- Patient's blood samples will be collected by a qualified medical technician or nurse. Researcher would receive only the whole blood collected in a tube.
- Voided Urine will be collected by patient in urine container. Catheterized urine will be collected from the collection reservoir to the urine container by nurse or clinician. Researcher will receive the sample from the nurse or clinician.
- For sample manipulation and waste disposal, follow "Handling of Human Samples and Cultures" SOP (ASAM/SOP/004). Attached to this application. Same precautions will be taken for both blood and urine samples.

| SECTION B | |
|---|---|
| MACQUARIE UNIVERSITY | **Biohazard Safety Committee – Risk Assessment Decision** |

**Important Information**

For **non GMO** investigations email this assessment to biohazard@mq.edu.au for approval by the **Biohazard** Safety Committee.

**Individual Responsibilities**

By submitting this assessment the Chief Investigator identified in Section A, confirms that any supporting documents, training, guidance, instruction or protocols issued by the University will been followed so far as reasonably practicable to ensure the work is carried out without risk to health, safety or the environment. The Chief investigator is responsible for ensuring, so far as reasonably practicable the safety of researchers and others who may be affected by the work described within this document.

**Decision to be completed by the Biohazard Safety Committee:**

The Committee has agreed that this risk assessment is sufficient for investigations to commence? **Yes** ☐ **No** ☐ **Further action required** ☐

Further Action/Comments:
**Can you please change the Bleach concentration to 0.5% Sodium hypochlorite,**

| | |
|---|---|
| Name of Approver (Committee Rep): | J Cuomo |
| Date Approved: | 23rd of July 2014 |

This Risk Assessment must be approved for work to commence

## A-2. PILOT STUDY RESULTS SUMMARY

Abbreviatures:

CaP = Prostate Cancer

BPH = Benign Prostate Hyperplasia

N = Normal

RP = Radical Prostatectomy

F/NC = Few or no cells

AF = Autofluorescence

OI = Other interferent

| | ID number | Sample type | Result | | | | Discarded | | |
|---|---|---|---|---|---|---|---|---|---|
| | | | True + | True - | False + | False - | F/NC | AF | OI |
| 1 | CAP108 | N | | | | | X | | |
| 2 | CAP306 | N | | X | | | | | |
| 3 | CAP550 | N | | | | | | | X |
| 4 | CAP352 | N | | X | | | | | |
| 5 | CAP417 | N | | | | | | X | |
| 6 | CAP229 | BPH | | | | | X | | |
| 7 | CAP300 | BPH | | X | | | | | |
| 8 | CAP163 | BPH | | X | | | | | |
| 9 | CAP328 | BPH | | X | | | | | |
| 10 | CAP487 | N | | X | | | | | |
| 11 | CAP403 | N | | | | | | X | |
| 12 | CAP411 | N | | | X | | | | |
| 13 | CAP289 | BPH | | X | | | | | |
| 14 | CAP224 | N | | | | | X | | |
| 15 | CAP383 | N | | | X | | | | |
| 16 | CAP392 | N | | X | | | | | |
| 17 | CAP469 | N | | X | | | | | |
| 18 | CAP154 | BPH | | X | | | | | |
| 19 | CAP346 | BPH | | | | | | X | |
| 20 | CAP217 | BPH | | X | | | | | |
| 21 | CAP589 | BPH | | X | | | | | |
| 22 | CAP304 | N | | | X | | | | |
| 23 | CAP187 | N | | | | | | X | |
| 24 | CAP211 | N | | | | | | X | |

| | | | | | | | | | |
|---|---|---|---|---|---|---|---|---|---|
| 25 | CAP291 | N | | | | | X | | |
| 26 | CAP549 | N | | | | | X | | |
| 27 | CAP267 | N | | X | | | | | |
| 28 | CAP572 | N | | X | | | | | |
| 29 | CAP373 | N | | | X | | | | |
| 30 | CAP62 | N | | | | | | X | |
| 31 | CAP615 | N | | | | | X | | |
| 32 | CAP334 | N | | | | | X | | |
| 33 | CAP760 | N | | X | | | | | |
| 34 | CAP749 | N | | | X | | | | |
| 35 | CAP772 | BPH | | | X | | | | |
| 36 | CAP946 | BPH | | | | | X | | |
| 37 | CAP686 | BPH | | | | | X | | |
| 38 | CAP606 | BPH | | | | | | | X |
| 39 | CAP628 | N | | | X | | | | |
| 40 | CAP763 | BPH | | X | | | | | |
| 41 | CAP731 | BPH | | | X | | | | |
| 42 | CAP633 | BPH | | X | | | | | |
| 43 | CAP627 | BPH | | X | | | | | |
| 44 | CAP914 | BPH | | | | | | X | |
| 45 | CAP661 | BPH | | X | | | | | |
| 46 | CAP988 | BPH | | X | | | | | |
| 47 | CAP821 | BPH | | X | | | | | |
| 48 | CAP724 | BPH | | X | | | | | |
| 49 | CAP604 | BPH | | X | | | | | |
| 50 | CAP798 | BPH | | X | | | | | |
| 51 | CAP939 | BPH | | X | | | | | |
| 52 | CAP944 | BPH | | | | | X | | |
| 53 | CAP791 | BPH | | | X | | | | |
| 54 | CAP897 | BPH | | X | | | | | |
| 55 | CAP736 | BPH | | | X | | | | |
| 56 | CAP621 | BPH | | X | | | | | |
| 57 | CAP844 | BPH | | | | | X | | |
| 58 | CAP625 | BPH | | | | | X | | |
| 59 | CAP673 | BPH | | | | | | X | |
| 60 | CAP497 | RP | | | | | | X | |
| 61 | CAP538 | RP | | | X | | | | |
| 62 | CAP476 | RP | | | | | | X | |
| 63 | CAP247 | RP | | X | | | | | |
| 64 | CAP320 | RP | | | | | | X | |
| 65 | CAP316 | RP | | | | | X | | |
| 66 | CAP418 | RP | | X | | | | | |
| 67 | CAP160 | RP | | X | | | | | |
| 68 | CAP485 | RP | | X | | | | | |

| | | | | | | | | | |
|---|---|---|---|---|---|---|---|---|---|
| 69 | CAP 295 | RP | | X | | | | | |
| 70 | CAP981 | RP | | | X | | | | |
| 71 | CAP338B | RP | | | X | | | | |
| 72 | CAP916 | RP | | X | | | | | |
| 73 | CAP1000 | RP | | | | | X | | |
| 74 | CAP104 | RP | | X | | | | | |
| 75 | CAP158 | RP | | | | | | X | |
| 76 | CAP648 | RP | | | | | X | | |
| 77 | CAP766 | RP | | | | | X | | |
| 78 | CAP331 | RP | | X | | | | | |
| 79 | CAP677 | RP | | | | | X | | |
| 80 | CAP954 | RP | | | | | X | | |
| 81 | CAP964 | RP | | X | | | | | |
| 82 | CAP730 | RP | | | X | | | | |
| 83 | CAP624 | RP | | | X | | | | |
| 84 | CAP654 | RP | | X | | | | | |
| 85 | CAP702 | RP | | X | | | | | |
| 86 | CAP422 | RP | | X | | | | | |
| 87 | CAP824 | RP | | X | | | | | |
| 88 | CAP399 | RP | | X | | | | | |
| 89 | CAP649 | RP | | X | | | | | |
| 90 | CAP851 | RP | | X | | | | | |
| 91 | CAP993 | RP | | | X | | | | |
| 92 | CAP704 | RP | | X | | | | | |
| 93 | CAP644 | RP | | | X | | | | |
| 94 | CAP944 | RP | | | | | X | | |
| 95 | CAP716 | RP | | X | | | | | |
| 96 | CAP756 | RP | | X | | | | | |
| 97 | CAP887 | RP | | X | | | | | |
| 98 | CAP201 | CaP | | | | | | X | |
| 99 | CAP472 | CaP | | | | | | X | |
| 100 | CAP310 | CaP | | | | | | X | |
| 101 | CAP177 | CaP | | | | | | X | |
| 102 | CAP207 | CaP | | | | | | X | |
| 103 | CAP520 | CaP | | | | | | X | |
| 104 | CAP353 | CaP | X | | | | | | |
| 105 | CAP276 | CaP | | | | | X | | |
| 106 | CAP220 | CaP | | | | | | X | |
| 107 | CAP336 | CaP | | | | | X | | |
| 108 | CAP132 | CaP | X | | | | | | |
| 109 | CAP167 | CaP | X | | | | | | |
| 110 | CAP177-2 | CaP | | | | | | X | |
| 111 | CAP501 | CaP | | | | | | | X |
| 112 | CAP369 | CaP | | | | X | | | |

| | | | | | | | | | |
|---|---|---|---|---|---|---|---|---|---|
| 113 | CAP829 | CaP | | | | X | | | |
| 114 | CAP696 | CaP | | | | | | | X |
| 115 | CAP848 | CaP | | | | X | | | |
| 116 | CAP678 | CaP | X | | | | | | |
| 117 | CAP435 | CaP | X | | | | | | |
| 118 | CAP339 | CaP | | | | | | | X |
| 119 | CAP770 | CaP | | | | X | | | |
| 120 | CAP336 | CaP | | | | | | X | |
| 121 | CAP737 | CaP | | | | | | X | |
| 122 | CAP806 | CaP | | | | | X | | |

## A-3. PUBLICATION

The following publication was done in collaboration with Dr. Nima Sayyadi, *et al*. I participated in the optimisation of the antibody labelling and in the standardisation of the immunoluminescence assay, using the probe synthesised, purified and characterised by Dr. Sayyadi.

analytical chemistry

Article

pubs.acs.org/ac

# Sensitive Time-Gated Immunoluminescence Detection of Prostate Cancer Cells Using a TEGylated Europium Ligand

Nima Sayyadi,*[,†,‡] Irene Justiniano,[†,⊥] Russell E. Connally,[§] Run Zhang,[†] Bingyang Shi,[†] Liisa Kautto,[†] Arun V. Everest-Dass,[†,‡] Jingli Yuan,[∥] Bradley J. Walsh,[⊥] Dayong Jin,[‡,#] Robert D. Willows,[†] James A. Piper,[§,‡] and Nicolle H. Packer*[,†,‡]

[†]Department of Chemistry and Biomolecular Sciences, Macquarie University, Sydney, New South Wales 2109, Australia

[‡]ARC Centre of Excellence for Nanoscale Biophotonics (CNBP), Macquarie University, Sydney, New South Wales 2109, Australia

[§]Department of Physics and Astronomy, Macquarie University, Sydney, New South Wales 2109, Australia

[∥]State Key Laboratory of Fine Chemicals, School of Chemistry, Dalian University of Technology, Dalian, Liaoning Province 116024, China

[⊥]Minomic International Ltd., Macquarie Park, Sydney, New South Wales 2113, Australia

[#]School of Mathematical and Physical Sciences, Faculty of Science, University of Technology, Sydney, New South Wales 2007, Australia

Supporting Information

**ABSTRACT:** We describe the application of a synthetically developed tetradentate $\beta$-diketonate-europium chelate with high quantum yield (39%), for sensitive immunodetection of prostate cancer cells (DU145). MIL38 antibody, a mouse monoclonal antibody against Glypican 1, conjugated directly to the chelate via lysine residues, resulted in soluble (hydrophilic) and stable immunoconjugates. Indirect labeling of the antibody by a europium chelated secondary polyclonal antibody and a streptavidin/biotin pair was also performed. All of these bright luminescent conjugates were used to stain DU145 cells, a prostate cancer cell line, using time gated luminescence microscopy for imaging, and their performances were compared to conventional FITC labeling. For all prepared conjugates, the europium chelate in conjunction with a gated autosynchronous luminescence detector (GALD) completely suppressed the cellular autofluorescence background to allow capture of vivid, high contrast images of immune-stained cancer cells.

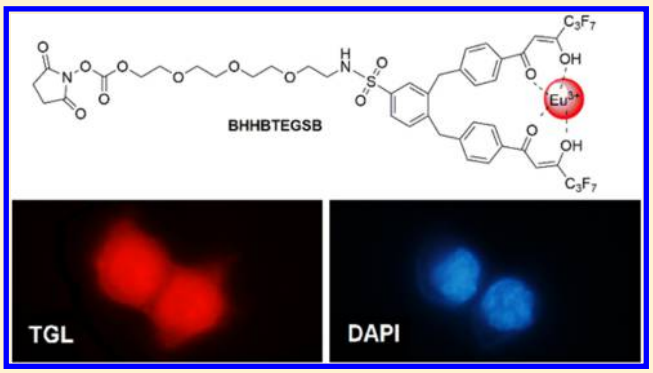


Rapid, sensitive, and noninvasive diagnostic tests for cancer have the potential to lead to better treatment outcomes and lower healthcare costs.[1−4] Prostate cancer screening relies on a set of tests including prostate specific antigen (PSA) levels in blood, clinical evaluation, such as digital rectal examination (DRE), and needle biopsy of the prostate. PSA screening is sensitive, but its specificity is poor, and its use remains controversial.[5,6] Needle biopsy is an invasive procedure that has inherent risks and puts patients under great discomfort, so it is not performed routinely.[7,8] Prostate cancer-screening tests are thus required to be more robust and conclusive to avoid unnecessary biopsies. Urinary cytology can be used as a noninvasive method to detect cancer cells in urine sediments with high specificity, but with low sensitivity, particularly in early stages.[9,10] Often prostate cancer cells are misidentified, as they are less abundant in comparison with other urinary tract cells, and their differentiation can be tricky.[11] Several studies have suggested the use of biomarker panels for immunodetection of prostate cancer cells in urine as a complement for traditional urine cytology analysis.[12−15] A fundamental problem in the detection of nonabundant malignant cells in biological fluids is the weak signal-to-noise ratio (SNR) obtained when using common fluorescence probes, such as fluorescein isothiocyanate (FITC), because of the overlapping of signal with commonly encountered autofluorescent molecules within biofluid matrices; these factors combine to greatly reduce detection efficacy.

Lanthanide ions have unique emission characteristics, including long excited-state lifetimes, sharply spiked emission spectra and large Stokes shifts. These characteristics, when using pulsed excitation in combination with time-gated detection techniques, are advantageous for discriminating against autofluorescence.[16] A detection limit of $10^{-15}$ M can be achieved with lanthanides, exceeding sensitivity achievable

**Received:** June 4, 2016
**Accepted:** September 5, 2016
**Published:** September 5, 2016





DOI: 10.1021/acs.analchem.6b02191
*Anal. Chem.* 2016, 88, 9564−9571

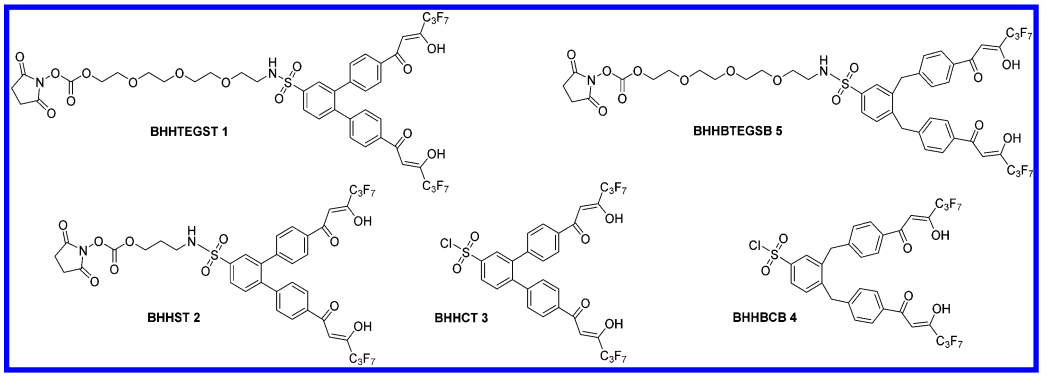


**Figure 1.** BHHCT derivatives: **1**, BHHTEGST; **2**, BHHST; **3**, BHHCT and BHHBCB derivatives; **4**, BHHBCB; and **5**, BHHBTEGSB. See Supporting Information for the IUPAC name of the compounds.

with conventional fluorophores and making luminescent probes an attractive alternative to radioisotopes.[17]

To increase the luminescent output and consequently the detection sensitivity of luminescent probes it is a common strategy to attach multiple luminophores onto a carrier molecule such as an antibody (Ab), which is then used to label the target biomolecule, for instance surface antigens on cancer cells. With conventional fluorophores this approach often results in self-quenching, which is exacerbated by fluorescence resonance energy transfer (FRET) from an excited to a nearby nonexcited dye molecule that efficiently absorbs the energy.[18] In contrast, the excited-state of the lanthanide ion in the chelate constructs is not subject to self-quenching with an adjacent chelate because of the absence of a receiver of the luminescence emission at the atomic level.[16] However, multiple conjugation of lanthanide chelates onto a carrier molecule such as an antibody is problematic since it often results in precipitation of the labeled material. This effect is partially due to the hydrophobic features of the aromatic antenna (organic chromophore) present in lanthanide chelates.[19]

To avoid the difficulty in direct conjugation of luminophores to primary antibodies (Ab) and also to provide a higher labeling degree of luminophores per target molecule, indirect labeling using secondary reagents such as streptavidin (SA, for a biotinylated antibody),[20−24] secondary antibodies,[25] bovine serum albumin (BSA),[26−29] or thyroglobulin (TG)[21,30] have been widely developed. Nevertheless, conjugation of multiple luminophores to the secondary reagent remains susceptible to precipitation and aggregation of bioconjugates.[19]

We have recently developed a novel europium ligand BHHTEGST **1** with enhanced aqueous solubility by insertion of a hydrophilic tetraethylene glycol (TEG) spacer arm between *o*-terphenyl and a *N*-hydroxysuccinimide ester (NHS) moiety. It was previously shown that the direct conjugation of BHHTEGST **1** to an antibody resulted in an improved hydrophilic immunoconjugate that retained selectivity and stability in aqueous solutions.[31,32] BHHTEGST **1** is the next generation of an earlier developed *β*-diketone europium ligand BHHST **2**[25] synthesized from its parent BHHCT **3** molecule as shown in Figure 1. We have also reported a new class of tetradentate *β*-diketone europium ligand BHHBCB **4**[28] with significantly improved quantum yield (40%) over BHHCT **3**[29] (25%) and increased stability of europium(III) chelation.

We describe here the modification of BHHBCB **4** with a tetraethylene glycol (TEG) spacer arm and a NHS ester as an activated attachment point, resulting in an enhanced aqueous soluble europium chelate with high quantum yield. Using this synthetic strategy, we have successfully synthesized and fully characterized BHHBTEGSB **5** and determined that luminescence emission from this compound is significantly more intense (2.5 times) in comparison with our previously reported ligand BHHTEGST **1**. TGL staining of cancer cells using antibody conjugated BHHBTESGB **5** probe resulted in higher signal-to-noise ratio (SNR) (1.7 times) compare with BHHTEGST **1** probe (see Figures S14 and S30). Consequently, we proceeded to investigate its application for immunodetection of prostate cancer cells (DU145) using MIL38 antibody (kindly provided by Minomic International Ltd.). This antibody has been shown to bind to a cell surface glycoprotein (GPC1) in prostate cancer cell lines (i.e., DU145 and PC3) and on prostate cancer cells isolated from patients urine.[33]

To investigate the time gated luminescence (TGL) immunodetection of DU145 cells in the form of a homogeneous platform, direct conjugation of BHHBTEGSB to the MIL38 antibody was performed as cell primary staining reagent. In addition, indirect immunoassays were developed by conjugating streptavidin (SA, for binding to MIL38-biotin) and an antimouse IgG antibody (for binding to MIL38) with the europium ligand. Gated Autosynchronous Luminescence Detector (GALD, www.gator4d.com.au)[34] was used to obtain high contrast luminescence images with short exposure time; the antibody-labeled cells were easily visible through the eyepiece with the naked eye, while autofluorescence was completely suppressed.

## EXPERIMENTAL SECTION

**General Information.** Synthetic procedures and chemical characterization of the europium chelate are provided in the Supporting Information. Unless otherwise noted, materials obtained from commercial suppliers were used without further purification. The reactions were carried out under an inert atmosphere of nitrogen with dry solvents under anhydrous conditions.

**Materials.** 4′,6-Diamidino-2-phenylindole dihydrochloride hydrate (DAPI) (D9642), europium(III) chloride hexahydrate (203254), deuterium oxide ($D_2O$) (151882), FITC (46951), antimouse IgG (produced in rabbit) (M7023), and paraformaldehyde (P6148) were purchased from Sigma-Aldrich Australia. NHS-PEG4-Biotin (21330), streptavidin (43-4301) were purchased from Thermo Fisher Scientific Australia. Sephadex column (PD MiniTrap G-25) (28-9180-07) was purchased from GE healthcare life sciences, Australia. Human prostate cancer cell line DU145 and human bladder cancer cell line C3 were provided by Minomic International Ltd. Recombinant monoclonal IgG (MIL38) specific to a surface antigen present on DU145 cells was provided by Minomic International Ltd.


DOI: 10.1021/acs.analchem.6b02191
*Anal. Chem.* 2016, 88, 9564−9571

**Characterization of Chelates.** The progress of the reactions was monitored by analytical HPLC. High-resolution mass spectra were taken using a mass spectrometer (Agilent 6538 Q-TOF with dual-ESI source). $^{1}H$ and $^{13}C$ NMR spectra were recorded with Bruker Avance Spectrometer [400 MHz ($^{1}H$) and 100 MHz ($^{13}C$)] in $CDCl_3$ at 298 K. Analytical reversed phase (RP) HPLC, using a Gemini-NY C18 column (5 $\mu$m, 4.6 mm ID, 250 mm) with a flow rate of 1.0 mL/min, was performed on a Shimadzu LC consisting of a DGV-12A degasser, SIL-10AD auto injector, SPD-M10A tunable absorbance detector. Preparative HPLC was carried out using an Econosil C18 column (10 $\mu$m, 22 mm ID, 250 mm) with a flow rate of 9.0 mL/min with 0.01% (v/v) TFA and acetonitrile gradient solvent system. UV−visible light absorption spectra on protein and conjugated protein concentration was collected on a NanoDrop 2000 UV (Thermo Scientific) spectrometer. Luminescence data was captured on an Agilent Cary Eclipse Fluorescence Spectrophotometer. A Sephadex column [PD MiniTrap G-25; GE healthcare life sciences (28-9180-07)] was used for buffer exchange of antibody ($NaHCO_3$, 100 mM and pH 8.5) and purification of conjugated antibody/streptavidin (100−200 $\mu$g, 1 $\mu$g/$\mu$L).

**Conjugation of BHHBTEGSB with Primary Antibody MIL38/Streptavidin/Secondary Antibody.** BHHBTEGSB contains an *N*-hydroxysuccinimide ester that enables its attachment to a protein via the amino group of lysine residues and N-termini. In the conjugation reaction, 100 $\mu$g antibody or streptavidin was exchanged into 100 mM $NaHCO_3$, pH 8.5, and then mixed with different molar excess of the BHHBTEGSB ligand (see Table 1). After incubation for 1 h at 37 °C the reaction mixtures were passed through a Sephadex column (PD MiniTrap) using 0.1× PBS as eluent to purify the conjugated protein from excess of BHHBTEGSB ligand. The fractions corresponding to labeled conjugates were collected according to absorbance detection using an Eppendorf BioPhotometer (280 and 320 nm).

**Table 1. Calculation of the Number of Ligands (BHHBTEGSB) Attached to 1°Ab (MIL38-BHHBTEGSB$_x$) after Conjugation Reactions Were Performed with Five Different Molar Ratios of Ligand to 1°Ab of 10:1, 20:1, 30:1, 40:1, and 60:1[a]**

| | number of ligands per protein (calculated ratio after purification) | | |
|---|---|---|---|
| conjugation molar ratio (experimental conditions) BHHBTEGSB: °1Ab/SA/°2Ab | MIL38-BHHBTEGSB$_x$ | SA-BHHBTEGSB$_x$ | 2°Ab-BHHBTEGSB$_x$ |
| 10:1 | $x$ = 7 | $x$ = 7 | |
| 20:1 | $x$ = 16 | $x$ = 14 | $x$ = 16 |
| 30:1 | $x$ = 27 | $x$ = 18 | $x$ = 28 |
| 40:1 | $x$ = 34 | | $x$ = 36 |
| 60:1 | $x$ = 40 | | |

[a]The number of ligands attached to SA (SA-BHHBTEGSB$_x$) after conjugation reactions were performed with three different molar ratios of ligand to SA of 10, 20, and 30. The number of ligands attached to 2°Ab (2°Ab-BHHBTEGSB$_X$) after conjugation reactions were performed with three different molar ratios to 2°Ab of 20, 30 and 40.

**Cell Culturing and Labeling.** The prostate cancer (DU145, ATCC HTB-81) and bladder cancer cell line (C3) were maintained in RPMI 1640 medium supplemented with fetal bovine serum (FBS) [10% w/v for DU145 and 20% w/v for C3) with 1 mM glutamine, in small culture flasks (T25, Sigma-Aldrich, Australia) at 37 °C in a humidified 5% $CO_2$ atmosphere. Cells were grown to 80% confluence, washed three times in PBS pH 7 to remove excess medium. Cell monolayers were detached from the culture flask by adding 0.25% w/v trypsin and 0.02% w/v EDTA in PBS and incubating at 37 °C for 1−5 min. Cell count and viability were calculated with TC20TM Automated Cell Counter (Bio-Rad, Australia) using 10 $\mu$L of cells mixed with 0.4% w/v Trypan blue (1:1).

Cells were then seeded into RPMI 1640 medium in six well culture plates each containing sterilized coverslips at approximately 1 × $10^5$ cells/well. Cells were grown at 37 °C for 12 h. After reaching 80% confluency the cell monolayers were fixed by adding 4% v/v paraformaldehyde (PFA) in PBS and incubated at RT for 30 min and fixed cells were then washed 3 x PBS (2 mL) and blocked with 1% (w/v) BSA in PBS.

For direct TGL labeling (Figure 3A) cells were stained by addition of 20 $\mu$L of MIL38-BHHBTEGSB (0.5 mg/mL) in 1 mL PBS per well and incubated for 30 min. Followed by 3 times wash with PBS (2 mL-each 5 min incubation). For indirect TGL labeling (Figure 3B); 20 $\mu$L of MIL38-Biotin (0.5 mg/mL) were added in 1 mL PBS per well and incubated for 30 min followed by 3 times wash with PBS. Then SA-BHHBTEGSB 40 $\mu$L (0.5 mg/mL) was added in 1 mL PBS, incubated for 30 min, and washed 3 times with PBS. For the secondary antibody indirect TGL labeling (Figure 3C) 20 $\mu$L of MIL38 (0.5 mg/mL) was added in 1 mL PBS per well and incubated for 30 min followed by 3 times wash with PBS. Then 2°Ab-BHHBTEGSB 40 $\mu$L (0.5 mg/mL) was added in 1 mL PBS and incubated for 30 min and washed 3 times with PBS.

**Cell Imaging.** Coverslips were placed upside down on microscopy slides on 5 $\mu$L of europium chloride [$EuCl_3$, 20 mM in fluorescence enhancing buffer (FEB)[35]] and 2 $\mu$L of DAPI (2 $\mu$g/mL in PBS). Addition of the $EuCl_3$ solution was performed at the end of immunolabeling procedure to reduce nonspecific binding and aggregation of the antibody conjugates. Finally, antibody-labeled cells were examined using bright field, DAPI and FITC filter on an Olympus CKX41 inverted microscope. All bright-field, fluorescence and time-gated luminescence imaging was performed on an Olympus BX51 upright fluorescence microscope. Time-gated luminescence imaging was performed using the Gated Autosynchronous Luminescence Detector (GALD),[34] which was inserted into the DIC slot of the microscope. TGL images were captured without a fluorescence filter using a DP72 color camera set for ASA speed of 200 and exposure period of 1.0 s; all images were stored as TIFF files as captured. FITC fluorescence imaging was carried out using a 100 W mercury arc lamp and a FITC filter set with 300 ms exposure times. DAPI staining images were captured with the same source of UV lamp and DAPI filter with 10 ms exposure time. Original images are as captured; no postprocessing image enhancement or false coloring has been performed.

**Quantification of BHHBTEGSB Ligands Attached to Primary Antibody MIL38/Streptavidin/Secondary Antibody.** UV−visible absorption analysis of BHHBTEGSB (NanoDrop UV spectrometer) indicated a maximum UV absorbance at 335 nm and a shoulder at 280 nm, which overlaps with that of the antibody MIL38. To evaluate the conjugation efficiency of BHHBTEGSB moiety to the antibody, molar extinction coefficients of the ligand at 335 and 280 nm were separately obtained from UV−visible analysis of solution of HPLC pure lyophilized ligand at 335 and 280 nm, respectively [$\varepsilon_{335}$ = 3.10 × $10^4$ $M^{-1}.cm^{-1}$, $\varepsilon_{280}$ = 1.64 × $10^4$ $M^{-1}.cm^{-1}$] (Table S1). The concentration of ligand was then obtained by reading the absorbance of conjugates at 335 nm and using the known molar extinction coefficient of the ligand at 335 nm (on the assumption that the extinction coefficient of BHHBTEGSB **5** does not change on the labeled antibody). The conjugation efficiency was evaluated by subtracting the measured absorbance at 280 nm of the conjugate from the expected absorbance of the free ligand at 280 nm based on the ligand absorbance at 335 nm. This enabled calculation of the protein to ligand ratio depending on the extinction coefficients of the primary antibody, streptavidin, or secondary antibody used in the conjugation. The extinction coefficient of primary and secondary antibody was obtained from a known amount of pure protein and for streptavidin the extinction coefficient used according to literature.[36] The number of BHHBTEGSB molecules per antibody was then obtained by dividing the molar ratio of ligand to antibody.

**Preparation of Fluorescence Enhancing Buffer Solution 10× (FEB).** According to N. Arnaud et al.,[35] a 44 mL solution of 0.1 M sodium hydroxide solution was prepared and the pH was adjusted to 4.7 with glacial acetic acid, then 1% by volume of Triton X-100 was


DOI: 10.1021/acs.analchem.6b02191
Anal. Chem. 2016, 88, 9564−9571

added. Trioctylphosphine oxide (38 mg) was dissolved in ethanol (5 mL) and added to the sodium acetate solution (1.25 mL), and then 1× FEB was used for the experiments.

**Quantification of Signal-to-Noise Ratio (SNR).** Original images of stained cells were analyzed to determine the signal-to-noise ratio (SNR) using ImageJ software (version 1.46r). The signal is represented by the brightest region of the target signal ($S$) and noise is the mean nontarget signal ($N$). ImageJ is used to measure peak signal intensity ($S$) of an area in the target cell and noise is the mean intensity of pixels defined by an area in a noncell containing area.

## RESULTS AND DISCUSSION

**Synthesis of Europium Chelate and Solubility Analysis of Immunoconjugate.** The synthetic strategy of tetraethylene glycol linker with amine functionality **6** was previously described[31] and was used for the synthesis of BHHBTEGSB **5**. The maximum yield of compound **7**, was achieved by addition of BHHBCB **4** in a dropwise fashion to a solution of **6**, 4-dimethylaminopyridine (DMAP) and *N*,*N*-diisopropylethylamine (DIPEA) in dry acetonitrile at room temperature, resulting in 80% yield of **7** (Scheme 1). The final

**Scheme 1. Synthesis of BHHBTEGSB 5**[a]

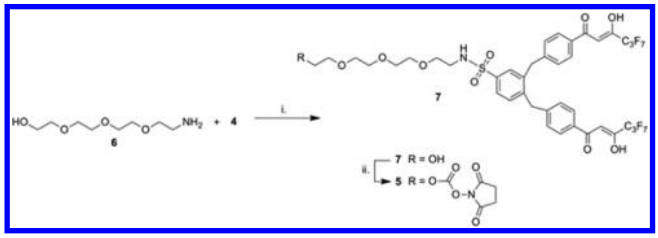


[a]Reaction conditions: (i) DMAP, DIPEA, MeCN, 80%; (ii) DSC, DMAP, DIPEA, MeCN, 55%.

stage of BHHBTEGSB **5** synthesis was performed by using *N*,*N*-disuccinimidyl carbonate (DSC), DMAP, DIPEA in dry acetonitrile, and the crude reaction mixture was purified via preparative C18 HPLC and lyophilized to give a yellow powder of BHHBTEGSB **5** in 55% yield.

To examine the effect of the tetraethylene glycol linker of BHHBTEGSB **5** on solubility and stability of the conjugated antibody [MIL38-BHHBTEGSB] in comparison with BHHBCB **4**, a series of experiments was performed by increasing the molar ratio of BHHBTEGSB **5** and BHHBCB **4** to a constant amount of antibody MIL38 in the conjugation reaction.

It was observed that by addition of 50 mol equiv of BHHBCB **4** to MIL38 (100 $\mu$L, 0.5 $\mu$g/$\mu$L) the conjugated antibody precipitated while conjugation to MIL38 with the same molar ratio of BHHBTEGSB **5** resulted in a clear solution as shown in Figure 2. This visual observation was confirmed through turbidity analysis of the suspension at OD600 nm; MIL38-BHHBCB conjugate had an optical density of 0.598 whereas MIL38-BHHBTEGSB returned a value of zero. These results indicate that BHHBTEGSB **5** conjugate (MIL38-BHHBTEGSB) possesses higher aqueous solubility when compared to BHHBCB **4** conjugate (MIL38-BHHBCB).

**Physical and Photophysical Properties of BHHBTEGSB 5 and Immunoconjugates.** Physical and photophysical properties of BHHBTEGSB **5** including extinction coefficient, chelation capacity of $Eu^{3+}$, luminescence emission (in MQ water, $D_2O$ and FEB), stability of $Eu^{3+}$ chelation by the diketone moiety, lifetime and quantum yield were investigated

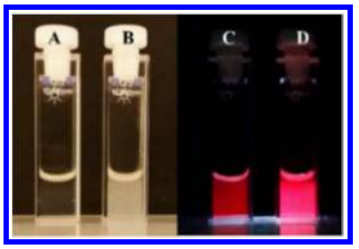


**Figure 2.** Visualization of clear solution of MIL38-BHHBTEGSB (A) and cloudy suspended colloids of MIL38-BHHBCB (B), luminescence of MIL38-BHHBTEGSB-Eu (C), and MIL38-BHHBCB-Eu (D) after addition of $Eu^{3+}$ to A and B and irradiation with 365 nm UV light.

and compared with the non-TEGylated BHHBCB **4** ligand, see Supporting Information for details (Figure S10–S18).

To determine quantum yield (QY) we compared BHHBTEGSB **5** with BHHBCB **4** (QY of 40%).[28] Using experimentally determined parameters (see Supporting Information), according to Latva et al.[37] the QY of BHHBTEGSB-Eu was determined to be 39% as summarized in Table S2 (for details, see Figures S19–S21).

As described in the following conjugation section, a series of conjugations of ligand to primary antibody (MIL38) were carried out by increasing the molar ratio of ligand to antibody. The conjugated antibodies were purified and the number of ligand molecules per antibody were determined (MIL38-BHHBTEGSB$_x$, $x$ = 7, 16, 27, 34, and 40 (Table 1). The luminescence intensity of MIL38 conjugates (1–2 $\mu$M) was measured with a gate delay of 100 $\mu$s on an Agilent Cary Eclipse Fluorescent Spectrophotometer and a strong positive correlation with intensity was observed (Figure S22). Luminescence intensity was plotted as a function of fluorescence to protein ratio (FPR) with the results shown in Figure S23 and the luminescence intensity of the bioconjugates showed a linear correlation ($R^2$ = 0.9958) to the number of ligands attached, confirming that luminophore moieties are not self-quenching in this configuration.

**Conjugation and Optimization of Luminophore to Primary MIL38 Ab, SA, and 2° Ab.** Figure 3 schematically depicts the different approaches of immuno-staining of prostate cancer DU145 cells used in this study; (A) has luminophore directly bound to the primary antibody (MIL38), while (B) and (C) utilize indirect TGL approaches via biotin–streptavidin coupling and secondary (antimouse IgG) antibodies, respectively.

While the tetraethylene glycol linker also facilitates the attachment of a high number of ligands to the lysine residues in the antibodies and streptavidin, it is essential to find the best ratio of ligand to protein (or fluorescence to protein ratio, FPR) that maintains the functionality of the conjugated protein. A series of conjugations of ligand to MIL38 were carried out by increasing the molar ratio of ligand to antibody from 10 to 60 mol equiv. The conjugated antibodies were purified and the number of ligand molecules per antibody were determined by UV–visible spectroscopy analysis using the molar extinction coefficient at 280 and 335 nm for each component (Table S1 and Figure S24). Table 1 illustrates the number of ligand molecules per antibody (MIL38-BHHBTEGSB$_x$, $x$ = 7, 16, 27, 34, and 40) where the molar ratio of ligand to antibody in each case was 10:1, 20:1, 30:1, 40:1, and 60:1, respectively.

In a similar fashion, the optimal FPR for SA was determined; 10, 20, and 30 molar excess of BHHBTEGSB to SA were used in the conjugation reaction. The conjugated SA with ligand was



DOI: 10.1021/acs.analchem.6b02191
Anal. Chem. 2016, 88, 9564–9571

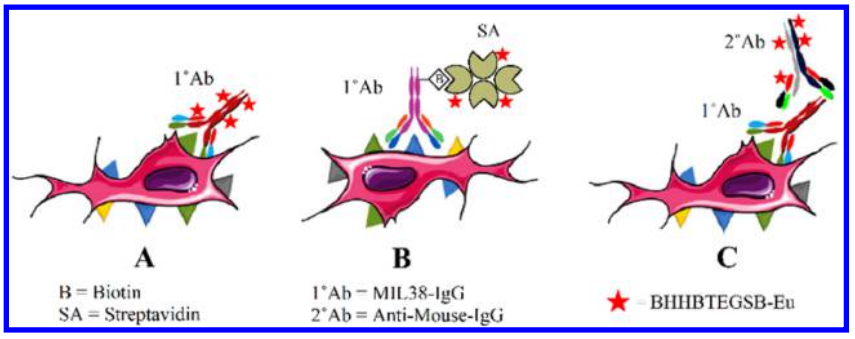


**Figure 3.** Direct and indirect TGL labeling of prostate cancer cells, (A): Direct conjugation of luminophore to primary antibody (1°Ab, MIL38) [MIL38-BHHBTEGSB-Eu]. Indirect TGL reagents; (B) Streptavidin (SA) conjugated with europium ligand for binding to biotinyl-ated primary antibody (MIL38-biotin) [SA-BHHBTEGSB-Eu-MIL38-Biotin], (C) Secondary antibody (2°Ab-Anti-Mouse-IgG) conjugated with europium ligand for binding to primary antibody (MIL38) [2°Ab-BHHBTEGSB-Eu-MIL38]. Scheme adapted with permission from Bünzli et al. *Analyst*, **2009**, *134* (10), 1991. Copyright 2009 The Royal Society of Chemistry.

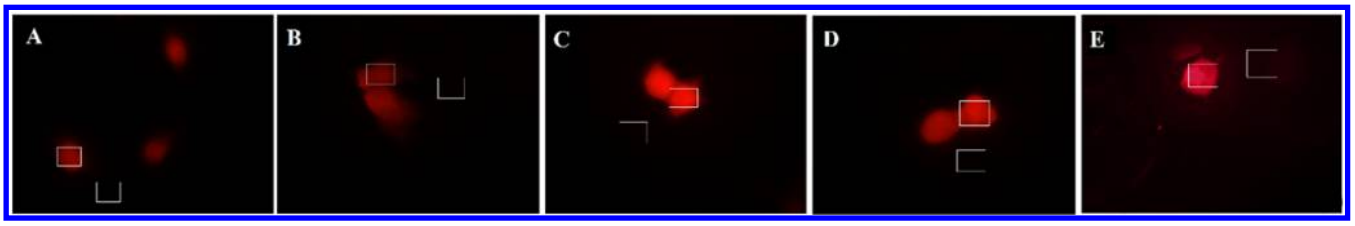


**Figure 4.** Direct europium luminescent staining of DU145 cells using MIL38-BHHBTEGSB$_x$ ($x$ = 7, 16, 27, 34, and 40 for A–E, respectively; lower to higher ligand to MIL38 conjugation ratio). Images were captured in TGL mode by DP72 color camera with identical exposure times (1.0 s). Image analysis with ImageJ software, with boxes showing the regions used for the peak signal intensity of desired target cell ($S$) and noise ($N$) is the mean intensity of non-cell-containing area.

then purified and the number of ligands per SA was determined by UV–visible spectroscopy analysis. Table 1 illustrates the obtained number of ligand molecules per streptavidin for each condition tested (SA-BHHBTEGSB$_x$, $x$ = 7, 14, and 18) where the molar ratio of ligand to streptavidin in each case was 10:1, 20:1, and 30:1, respectively (Figure S25).

Following the conjugation of BHHBTEGSB ligand to streptavidin, we observed a tendency for the immunoconjugate to precipitate when a molar excess above 30 was used. To avoid this, we selected the midrange conjugation (SA-BHHBTEGSB$_{14}$) to proceed for immuno-staining of prostate cancer cells DU145.

A similar approach was carried out to identify an optimized conjugated secondary antibody (antimouse IgG, 2°Ab) with BHHBTEGSB ligand. The molar excess of 20, 30, and 40 of ligand BHHBTEGSB to 2°Ab in conjugation reaction resulted in 16, 28, and 36 ligands per antibody respectively (Table 1). We have observed that higher luminophore to antibody ratios result in precipitation of the conjugated antibody. The conjugate 2°Ab-BHHBTEGSB$_{28}$ was the optimal conjugate used for the prostate cancer cell Immuno-staining. (Figure S26).

The five different immunoconjugates of primary antibody (MIL38-BHHBTEGSB$_x$, $x$ = 7, 16, 27, 34, 40) were tested in immuno-staining of cancer cell lines, using DU145 cells as positive control (GPC1+) and C3 bladder cancer cell line that does not express MIL38 antigen (GPC1-),[38,39] as negative control. The stained cells were inspected under TGL and conventional epifluorescence mode using a DAPI filter set.

Representative images for five samples were taken and analyzed to determine the signal-to-noise ratio (SNR) as shown in Figure 4. A linear response in luminescence signal was observed as the ligand to antibody ratio (FPR) was increased from 7 to 16–27 to deliver signal intensities of 89 and 127–255 (saturation level) respectively. However, as FPR was increased further to 34 and 40, the background signal escalated, but the signal was already at saturation level, therefore causing a reduction of SNR (Figure 5).

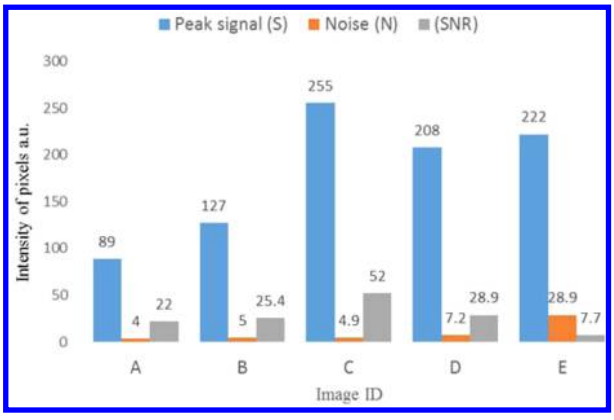


**Figure 5.** Calculated SNRs for prostate cancer cells (DU145) labeled with MIL38-BHHBTEGSB$_x$ ($x$ = 7, 16, 27, 34, and 40) extracted from Figure 4.

Care was taken to perform the bioconjugation reaction by maintaining temperature, time and concentration constant for each reaction. Nevertheless, subtle differences are still present and it is difficult to draw a narrow line between the FPR and resultant SNR. After many replicate experiments it is concluded that the FPR in the range of 20 to 30 is the optimal molar ratio of BHHBTEGSB to antibody to produce a conjugated antibody that maintains its native selectivity function with highest signal-to-noise ratio (SNR). The optimized conjugate MIL38-


DOI: 10.1021/acs.analchem.6b02191
*Anal. Chem.* 2016, 88, 9564–9571

BHHBTEGSB$_x$ ($20 < x < 30$) was used for further staining of prostate cancer cells.

SDS-PAGE analysis of the reduced conjugated antibody (MIL38-BHHBTEGSB) confirmed the attachment of europium ligand to both heavy and light chains as shown in Figure S27.

Immuno-staining of cancer cells (DU145 and C3) with MIL38-BHHBTEGSB$_{20-30}$ conjugate under TGL microscopy (GALD), shows that the specificity of the antibody is preserved after conjugation with europium ligand (Figures 6 and S28).

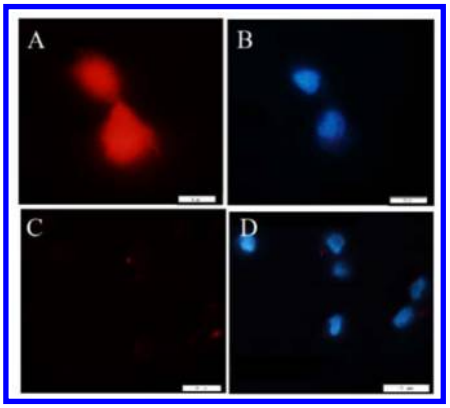


**Figure 6.** Staining of prostate cancer cells DU145 (A, B), and bladder cancer cells C3 (C, D) with MIL38-BHHBTEGSB$_{20-30}$, (A,C) time gated luminescence (TGL); (B,D) DAPI nuclear staining. Scale bar 10 $\mu$m.

As a validation of the specificity of the conjugated antibody, the corresponding FITC antibody conjugate (MIL38-FITC) was prepared and used for immuno-staining of DU145 and C3 cells. The conjugation was performed using the same strategy as employed for the europium ligand by targeting the amino groups of lysine residues of the antibody for covalent attachment of the fluorophore (FITC), and purifying the conjugate by gel filtration as described above. The cell staining protocol was then optimized to maximize fluorescence yield with the lowest background. MIL38-FITC specifically labeled DU145 cells and showed no binding to C3 cell line with identical FITC channel exposure times (300 ms) (Figure S29).

To demonstrate the detection sensitivity of the europium chelate in comparison with FITC probe, ImageJ software was used to quantify the intensity of pixels in the original images of stained cells by both probes. As shown in Figure 7, the average SNR achieved for europium staining of DU145 cells was at least 7 fold higher than FITC.

**Comparative Study of Direct TGL Immuno-Staining of Primary Ab (MIL38) with Indirect Staining Reagents (SA and 2°Ab).** As an alternative to the direct immuno-staining assay, secondary reagents for immunoassays were prepared. Streptavidin (SA) is a 52 kDa protein which contains 32 lysine residues, and forms a tetramer with four biotin binding sites. Conjugation of europium ligands to SA was reported using a modified SA with covalent attachment to BSA[5,10] for better solubility and potentially a better carrier of the lanthanide ligand. We thus investigated the use of SA as a scaffold for europium ligand conjugation. Experimentally it was observed that SA is very sensitive to the amount of bound ligand and that conjugations performed using higher than 30 molar excess of BHHBTEGSB resulted in precipitation of the conjugate. A 20 molar excess of BHHBTEGSB to SA was used, and after

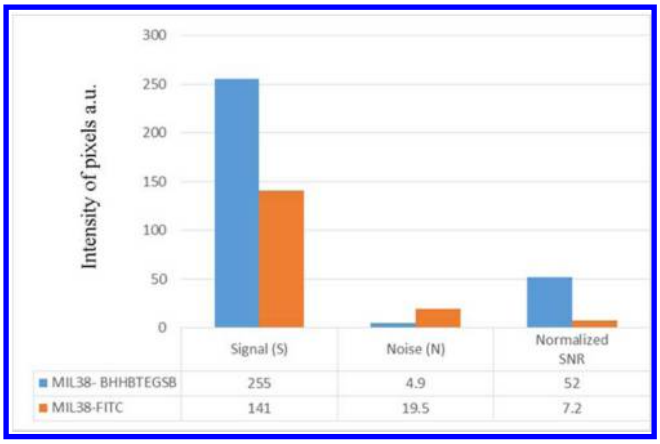


**Figure 7.** Representation of signal-to-noise ratios (SNRs) for prostate cancer cells (DU145) labeled with MIL38-BHHBTEGSB$_{20-30}$ and MIL38-FITC. (For details, see Figures S33 and S34.)

purification, the product was identified as a soluble conjugate with an average of 14 ligands per SA (SA-BHHBTEGSB$_{14}$). SA conjugated protein has the tendency to bind nonspecifically to endogenous biotin sites[40] which has required optimization,[41,42] however, we did not observe nonspecific staining of the cancer cells in our experiments (Figure 8C). For the streptavidin conjugate (SA-BHHBTEG), biotinylated primary antibody (MIL38-Biotin) was prepared. Briefly, NHS-PEG$_4$-Biotin was added in 3−5 molar excess and the biotinylated antibody was purified by gel filtration.

Conjugation of BHHBTEGSB ligand to secondary antibody (antimouse-IgG-2°Ab) was performed in a similar manner as for the direct conjugation to MIL38. It was found that the 30 molar excess of BHHBTEGSB ligand to 2°Ab resulted in a soluble and stable conjugate which contains 28 ligands on average per Ab (2°Ab-BHHBTEGSB$_{28}$). Higher molar excess (~40) of ligand to 2°Ab tends to result in aggregated conjugates which were not suitable for immunolabeling.

Parallel staining was carried out using the three immunoconjugate complexes (A) MIL38-BHHBTEGSB$_{20-30}$, (B) SA-BHHBTEGSB$_{14}$-MIL38-Biotin, and (C) 2°Ab-BHHBTEGSB$_{28}$-MIL38 for immuno-staining of prostate cancer cells (DU145) (as per Figure 3 diagram). The fixed cells were incubated with (A) MIL38-BHHBTEGSB$_{20-30}$, (B) MIL38-Biotin, and (C) MIL38 with the same concentration (10 $\mu$g/mL) for 30 min. For indirect TGL reagents (SA and 2°Ab) a further step was carried out by addition of SA-BHHBTEGSB$_{14}$ and 2°Ab-BHHBTEGSB$_{28}$ (10 $\mu$g/mL) for 30 min, respectively. Finally, the excess and unbound reagents were removed and slides prepared with europium chloride and visualized using bright-field, DAPI filter and TGL mode microscopy. Representative images of corresponding immunostained cell lines (direct and indirect TGL immunoassay) are shown in Figure 8.

For the direct TGL immunoassay, MIL38-BHHBTEGSB$_{20-30}$ probe was used to selectively immunostain DU145 cells (Figure 8A). C3 cell line was exposed to the same probe under identical conditions as a negative control (Figure 8G). For the indirect immunoassay approach, SA-BHHBTEGSB$_{14}$-MIL38-Biotin complex was employed to selectively immunostain DU145 cells as shown in Figure 8C. In parallel, two negative controls were prepared under identical conditions. First, nonbiotinylated MIL38 was used for staining of DU145 which resulted in nil staining (Figure S32D) and also


DOI: 10.1021/acs.analchem.6b02191
Anal. Chem. 2016, 88, 9564−9571

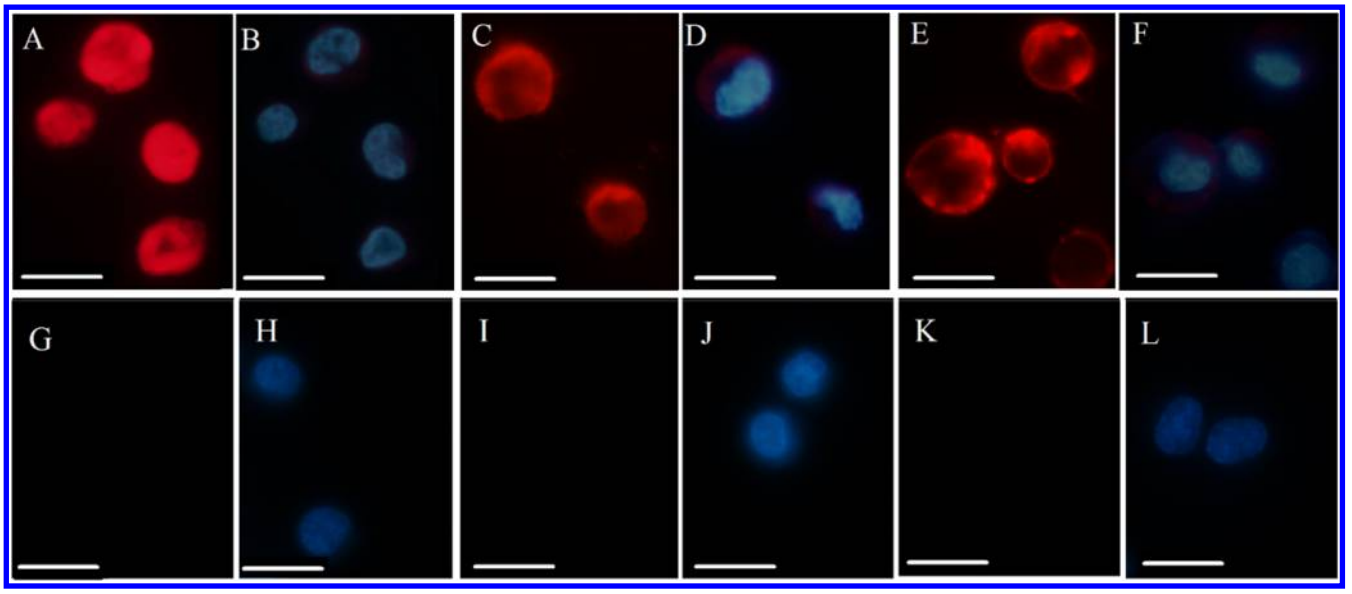


**Figure 8.** Immuno-staining of prostate cancer cells (DU145) using MIL38-BHHBTEGSB$_{20-30}$ [A], SA-BHHBTEGSB$_{14}$-MIL38-Biotin [C], and antimouse 2°Ab-BHHBTEGSB$_{28}$-MIL38 [E] with detection using TGL. Panels B, D, and F show DAPI nuclear staining of panels A, C, and E, respectively. C3 cell line used using as a negative control using MIL38-BHHBTEGSB$_{20-30}$ [G], SA-BHHBTEGSB$_{14}$-MIL38-Biotin [I], and antimouse 2°Ab-BHHBTEGSB$_{28}$-MIL38 [K] under TGL condition. Panels H, J, and L show DAPI nuclear staining of panels G, I, and K, respectively. Oil immersion 100× objective used, TGL exposure times (1.0 s). Scale bar: 10 $\mu$m. (For details, see Figures S28–S30.)

the SA-BHHBTEGSB$_{14}$-MIL38-Biotin complex was used for staining of C3 cell line - again no TGL luminescence was observed (Figure 8I).

As a second indirect immunoassay approach, 2°Ab-BHHBTEGSB$_{28}$-MIL38 complex selectively also immunostained DU145 cells (Figure 8E). Two parallel negative controls were run under identical conditions; the lack of primary antibody MIL38 (Figure S33D) did not result in staining of the DU145 cells and a mixture of 2°Ab-BHHBTEGSB$_{28}$-MIL38 did not stain the C3 cells (Figure 8K), confirming the selectivity of this approach.

To compare the sensitivity of immunoluminescence staining of prostate cancer cells between directly and indirectly labeled antibody binding assays, corresponding images were analyzed by using ImageJ software. Averaged results of replicated experiments show MIL38-BHHBTEGSB delivered the highest signal intensity ($S$ = 202) compared to SA-BHHBTEGSB$_{14}$-MIL38-Biotin ($S$ = 160) and 2°Ab-BHHBTEGSB$_{28}$-MIL38 ($S$ = 165) while background TGL levels ($N$) were very similar. The calculated SNR ratio obtained for each labeling method is shown in Figure 9.

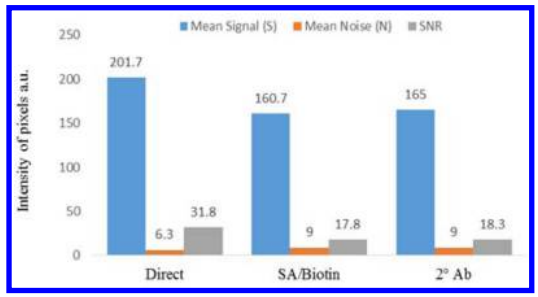


**Figure 9.** Average SNR for images corresponding to direct and indirect antibody binding MIL38 staining of DU145 cells. Direct staining using MIL38-BHHBTEGSB$_{20-30}$, indirect using SA-BHHBTEGSB$_{14}$-MIL38-Biotin and 2°Ab-BHHBTEGSB$_{28}$-MIL38. (For details, see Figures S34–S36.)

## CONCLUSION

In summary, a tetraethylene glycol linker provides a hydrophilic arm between the ligand BHHBTEGSB **5** and lysine residues in the IgG antibody MIL38. This direct modification of the antibody permits the attachment of a higher multiplicity of ligands per antibody while retaining solubility and specificity of the immunoconjugate. The optimized antibody-ligands conjugate (MIL38-BHHBTEGSB$_{20-30}$) in conjunction with the time-gated luminescence detection provides high SNR with superior contrast and high definition microscopic images. This approach was also successfully developed as an indirect detection platforms using streptavidin/biotin and labeled secondary antibody which showed less sensitive but still highly selective TGL luminescent staining of the DU145 prostate cancer cells. The sensitivity of staining of prostate cancer cells DU145 was quantified by analysis of corresponding TGL images, and determined that SNR was superior in the direct antibody labeling approach. The synthesis of ligand is straightforward and the modified Eu chelate is a very bright, effective label for antibody mediated rare cell detection and has immediate potential for the preparation of stable, aqueous soluble conjugates of a wide range of proteins.

## ASSOCIATED CONTENT

### Supporting Information

The Supporting Information is available free of charge on the ACS Publications website at DOI: 10.1021/acs.analchem.6b02191.

Synthesis of BHHBCB **4** and BHHBTEGSB **5**; data supporting synthesis of titled compound; photophysics and solubility data; calculation of quantum yield (PDF)

## AUTHOR INFORMATION

### Corresponding Authors

*E-mail: Nima.Sayyadi@mq.edu.au.



DOI: 10.1021/acs.analchem.6b02191
*Anal. Chem.* 2016, 88, 9564–9571

*E-mail: Nicki.Packer@mq.edu.au. Fax: 612 (9850 8313).

### Notes

The authors declare no competing financial interest.

## ■ ACKNOWLEDGMENTS

We gratefully acknowledge Minomic International Ltd, Macquarie University and the Australian Research Council (ARC) Linkage Grant LP130100517 and ARC Centre of Excellence for Nanoscale Biophotonics (CNBP) CE140100003 for the financial and technical support given to this research.

## ■ REFERENCES

(1) Budd, G. T.; Cristofanilli, M.; Ellis, M. J.; Stopeck, A.; Borden, E.; Miller, M. C.; Matera, J.; Repollet, M.; Doyle, G. V.; Terstappen, L. W.; Hayes, D. F. *Clin. Cancer Res.* **2006**, *12*, 6403−6409.
(2) Ferrari, M. *Nat. Rev. Cancer* **2005**, *5*, 161−171.
(3) Racila, E.; Euhus, D.; Weiss, A. J.; Rao, C.; McConnell, J.; Terstappen, L. W. M. M.; Uhr, J. W. *Proc. Natl. Acad. Sci. U. S. A.* **1998**, *95*, 4589−4594.
(4) Kapoor, P.; Greipp, P. T.; Morice, W. G.; Rajkumar, S. V.; Witzig, T. E.; Greipp, P. R. *Br. J. Haematol.* **2008**, *141*, 135−148.
(5) Duffy, M. J. In *Advances in Cancer Biomarkers*; Springer, 2015; pp 27−39.
(6) McDonald, M. L.; Parsons, J. K. *Urol. Clin. North Am.* **2016**, *43*, 39−46.
(7) Sanders, A.; Buchan, N. *ANZ. J. Surg* **2013**, *83*, 246−248.
(8) Ehdaie, B.; Vertosick, E.; Spaliviero, M.; Giallo-Uvino, A.; Taur, Y.; O'Sullivan, M.; Livingston, J.; Sogani, P.; Eastham, J.; Scardino, P.; et al. *J. Urol.* **2014**, *191*, 660−664.
(9) Rosario, D. J.; Lane, J. A.; Metcalfe, C.; Donovan, J. L.; Doble, A.; Goodwin, L.; Davis, M.; Catto, J. W.; Avery, K.; Neal, D. E.; et al. *BMJ* **2012**, *344*, d7894.
(10) McCroskey, Z.; Pambuccian, S. E.; Kleitherms, S.; Antic, T.; Cohen, M. B.; Barkan, G. A.; Wojcik, E. M. *Am. J. Clin. Pathol.* **2015**, *144*, 902−908.
(11) Kim, L.; Song, J. Y.; Choi, S. J.; Park, I. S.; Han, J. Y.; Kim, J. M.; Chu, Y. C. *Korean J. Pathol.* **2011**, *45*, 79−86.
(12) Schröder, F. H.; Hugosson, J.; Roobol, M. J.; Tammela, T. L.; Ciatto, S.; Nelen, V.; Kwiatkowski, M.; Lujan, M.; Lilja, H.; Zappa, M.; et al. *N. Engl. J. Med.* **2009**, *360*, 1320−1328.
(13) Pal, R. P.; Kockelbergh, R. C.; Pringle, J. H.; Cresswell, L.; Hew, R.; Dormer, J. P.; Cooper, C.; Mellon, J. K.; Barwell, J. G.; Hollox, E. J. *BJU Int.* **2016**, *117*, 686.
(14) Nickens, K. P.; Ali, A.; Scoggin, T.; Tan, S. H.; Ravindranath, L.; McLeod, D. G.; Dobi, A.; Tacha, D.; Sesterhenn, I. A.; Srivastava, S.; et al. *Prostate* **2015**, *75*, 969−975.
(15) Fujita, K.; Pavlovich, C. P.; Netto, G. J.; Konishi, Y.; Isaacs, W. B.; Ali, S.; De Marzo, A.; Meeker, A. K. *Hum. Pathol.* **2009**, *40*, 924−933.
(16) Lakowicz, J. R. *Principles of Fluorescence Spectroscopy*, 2nd ed.; Plenum Press: New York, 1999; p 496.
(17) Selvin, P. R. *Annu. Rev. Biophys. Biomol. Struct.* **2002**, *31*, 275.
(18) Chen, R. F.; Knutson, J. R. *Anal. Biochem.* **1988**, *172*, 61−77.
(19) Hagan, A. K.; Zuchner, T. *Anal. Bioanal. Chem.* **2011**, *400*, 2847−2864.
(20) Chan, M. A.; Bellem, A.; Diamandis, E. *Clin. Chem.* **1987**, *33*, 2000−2003.
(21) Morton, R. C.; Diamandis, E. P. *Anal. Chem.* **1990**, *62*, 1841−1845.
(22) Scorilas, A.; Diamandis, E. P. *Clin. Biochem.* **2000**, *33*, 345−350.
(23) Diamandis, E. P. *Clin. Biochem.* **1988**, *21*, 139−150.
(24) Suonpää, M.; Markela, E.; Ståhlberg, T.; Hemmilä, I. *J. Immunol. Methods* **1992**, *149*, 247−253.
(25) Connally, R.; Veal, D.; Piper, J. *Microsc. Res. Tech.* **2004**, *64*, 312−322.
(26) Evangelista, R. A.; Pollak, A.; Allore, B.; Templeton, A. F.; Morton, R. C.; Diamandis, E. P. *Clin. Biochem.* **1988**, *21*, 173−178.
(27) Wu, F. B.; Zhang, C. *Anal. Biochem.* **2002**, *311*, 57−67.
(28) Zhang, L.; Wang, Y. J.; Ye, Z. Q.; Jin, D. Y.; Yuan, J. L. *Bioconjugate Chem.* **2012**, *23*, 1244−1251.
(29) Yuan, J.; Matsumoto, K.; Kimura, H. *Anal. Chem.* **1998**, *70*, 596−601.
(30) Shankaran, P.; Reichstein, E.; Khosravi, M. J.; Diamandis, E. P. *J. Clin. Microbiol.* **1990**, *28*, 573−579.
(31) Sayyadi, N.; Connally, R. E.; Try, A. *Chem. Commun.* **2016**, *52*, 1154−1157.
(32) Sayyadi, N.; Care, A.; Connally, R. E.; Try, A. C.; Bergquist, P. L.; Sunna, A. *Sci. Rep.* **2016**, *6*, 27564.
(33) Truong, Q.; Justiniano, I. O.; Nocon, A. L.; Soon, J. T.; Wissmueller, S.; Campbell, D. H.; Walsh, B. J. *J. Cancer* **2016**, *7*, 1002−1009.
(34) Connally, R. *Anal. Chem.* **2011**, *83*, 4782−4787.
(35) Arnaud, N.; Georges, J. *Analyst* **1997**, *122*, 143−146.
(36) Gill, S. C.; Von Hippel, P. H. *Anal. Biochem.* **1989**, *182*, 319−326.
(37) Latva, M.; Takalo, H.; Mukkala, V.-M.; Matachescu, C.; Rodríguez-Ubis, J. C.; Kankare, J. *J. Lumin.* **1997**, *75*, 149−169.
(38) Nguyen-Khuong, T.; White, M. Y.; Hung, T. T.; Seeto, S.; Thomas, M. L.; Fitzgerald, A. M.; Martucci, C. E.; Luk, S.; Pang, S. F.; Russell, P. J.; et al. *Proteomics* **2009**, *9*, 1883−1892.
(39) Brown, J.; Russell, P.; Philips, J.; Wotherspoon, J.; Raghavan, D. *Br. J. Cancer* **1990**, *61*, 369.
(40) Hollinshead, M.; Sanderson, J.; Vaux, D. J. *J. Histochem. Cytochem.* **1997**, *45*, 1053−1057.
(41) Wood, G. S.; Warnke, R. *J. Histochem. Cytochem.* **1981**, *29*, 1196−1204.
(42) Matsumoto, V. *Histochemistry* **1985**, *83*, 325−330.



DOI: 10.1021/acs.analchem.6b02191
*Anal. Chem.* 2016, 88, 9564−9571

# Supporting Information:

## Sensitive time-gated immunoluminescence detection of prostate cancer cells using a TEGylated europium ligand.

Nima Sayyadi,[a,b *] Irene Justiniano,[a,e] Russell E. Connally,[c] Run Zhang,[a] Bingyang Shi,[a] Liisa Kautto,[a] Arun V. Everest-Dass,[a,b] Jingli Yuan,[d] Bradley J. Walsh,[e] Dayong Jin,[b,f] Robert D. Willows,[a] James A. Piper[c,b] and Nicolle H. Packer [a,b *]

[a] Department of Chemistry and Biomolecular Sciences, Macquarie University, Sydney.

[b] ARC Centre of Excellence for Nanoscale Biophotonics (CNBP), Macquarie University, , Sydney.

[c] Department of Physics and Astronomy, Macquarie University, Sydney.

[d] State Key Laboratory of Fine Chemicals, School of Chemistry, Dalian University of Technology, Dalian, China,

[e] Minomic International Ltd, Macquarie Park, Sydney.

[f] School of Mathematical and Physical Sciences, Faculty of Science, University of Technology, Sydney.

*Corresponding authors: Nima.Sayyadi@mq.edu.au and Nicki.Packer@mq.edu.au

Contents Page

## Organic synthesis and characterization:

The IUPAC name of the compounds: BHHTEGST **1**: (4,4'–bis(1",1",1",2",2",3", 3"-heptafluoro-4",6"-hexanedion-6"-yl)sulfonylamino-tetraethyleneglycol-succinimidyl carbonate-*o*-terphenyl)]. BHHST **2**: (4,4'–bis(1",1",1",2",2",3", 3"-heptafluoro-4",6"-hexanedion-6"-yl)sulfonylaminopropyl-ester-*N*-succinimide-ester-*o*-terphenyl)], BHHCT **3**: (4,4'–bis(1",1",1",2",2",3", 3"-heptafluoro-4",6"-hexanedion-6"-yl)chlorosulfo-*o*-terphenyl)], BHHBCB **4**: 1,2-bis[4′-(1″,1″,1″,2″,2″,3″,3″-heptafluoro-4″,6″-hexanedion-6″-yl)-benzyl]-4-chlorosulfobenzene. BHHBTEGSB **5**: 1,2-bis[4′-(1″,1″,1″,2″,2″,3″,3″-heptafluoro-4″,6″-hexanedion-6″-yl)-benzyl]-4- sulfonylamino-tetraethyleneglycol-succinimidyl carbonate-benzene.

### 1. BHHBCB 4

The purity of BHHBCB was confirmed by $^{1}H$ and $^{13}C$ NMR analysis; and the spectra are in accordance with the report by Zhang, L. *et al*.,[1] as shown in Figure S1 and S2.

$^{1}H$ NMR (400 MHz, $CDCl_3$) δ 4.09 (s, 2H), 4.13 (s, 2H), 6.57 (s, 2H), 7.17 (t, $J$ = 8.0 Hz, 4H), 7.38 (d, $J$ = 8.0 Hz, 1H), 8.84−7.95 (m, 6H); $^{13}C$ NMR (100 MHz, $CDCl_3$) δ 39.13, 39.16, 93.7, 125.9, 128.2, 128.3, 128.8, 129.2, 129.3, 131.5, 132.0, 140.1, 143.3, 144.6, 144.7, 146.2, 184.7.

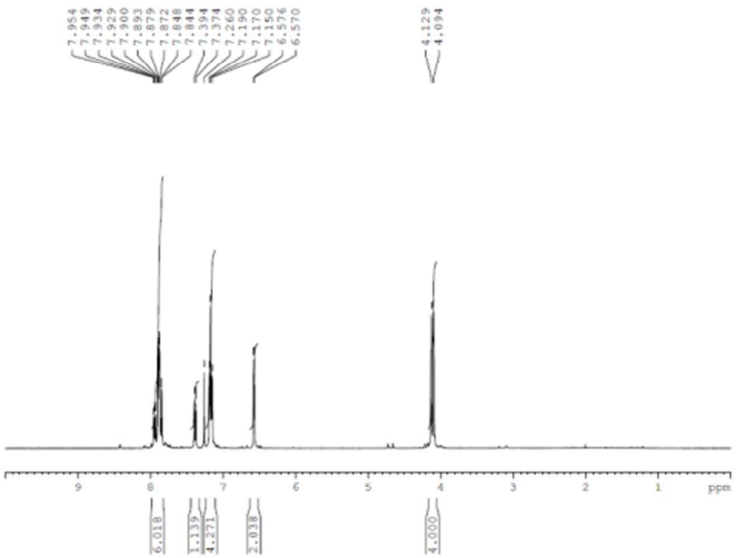


**Figure S1:** 400 MHz $^{1}H$ NMR spectrum of BHHBCB.

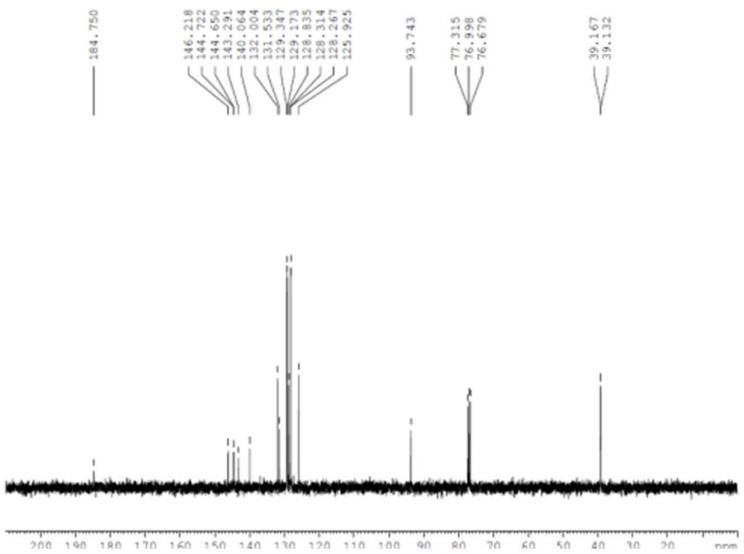


**Figure S2:** 100 MHz $^{13}$C NMR spectrum of BHHBCB.

## 2. BHHBCB-TEG-OH

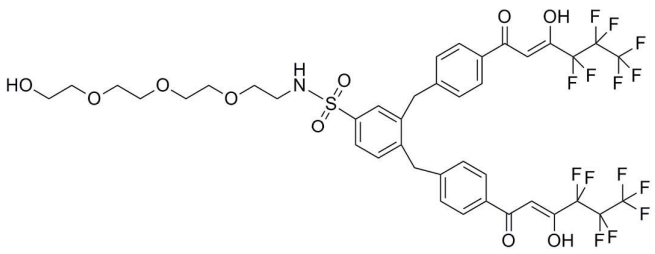


A stirred solution of 2-[2-[2-(2-aminoethoxy)ethoxy]ethoxy]ethanol (20 mg, 0.1 mmol), *N*,*N*-4-dimethylaminopyridine (2 mg, 0.01 mmol) and triethylamine (18 μL, 0.12 mmol) in dry acetonitrile (5 mL) were combined under anhydrous conditions. Then a solution of BHHBCB **4** (50 mg, 0.06 mmol) in dry acetonitrile (1 mL) was added in drop wise *via* a syringe over a 10 minutes period. The progress of the reaction was monitored by analytical HPLC which indicated the completion of reaction after one hour. Acetonitrile was removed under reduced pressure at 45 °C and the residue was purified by preparative HPLC to give BHHBCB-TEG-OH (50 mg, >80%) as a yellow oil. $^{1}$H NMR (400 MHz, $CDCl_3$) δ 3.12 (m, 2H), 3.36 (m, 14H), 4.03 (d, $J$ = 16 Hz, 4H), 6.56 (s, 2H), 7.14 (m, 4H), 7.27 (m, 1H), 7.85 (m, 2H), 7.84 (m, 4H); $^{13}$C NMR (100 MHz, $CDCl_3$) δ 39.0, 37.1,42.9, 61.4, 69.7, 69.8, 70.0, 70.3, 70.4, 72.1, 93.7, 125.9, 128.1, 129.1, 129.2, 131.1, 131.2, 131.5, 138.9, 139.1, 142.8, 145.7, 145.9, 185.0. ESI-MS (positive mode): *m/z* = 990 [$M^+$−H], 40%), 1012 ([M+Na]$^+$, 100%).

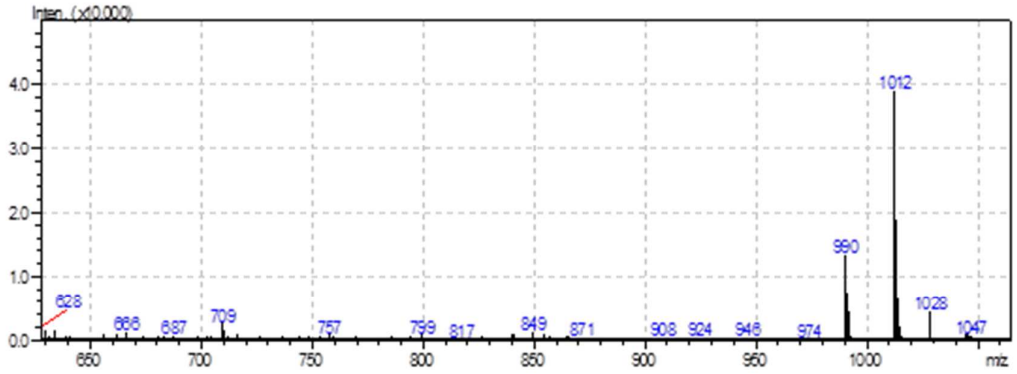


**Figure S3:** ESI-MS of BHHBCB-TEG-OH (positive mode): m/z = 990 [$M^+$−H], 40%), 1012 ([MNa]$^+$, 100%).

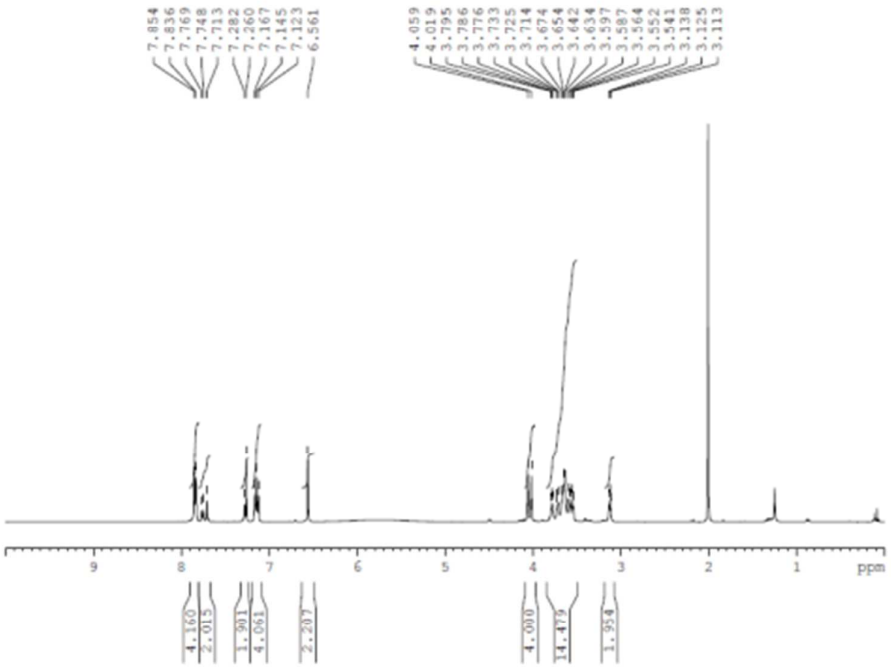


**Figure S4:** 400 MHz $^1$H NMR spectrum of BHHBSB-TEG-OH.

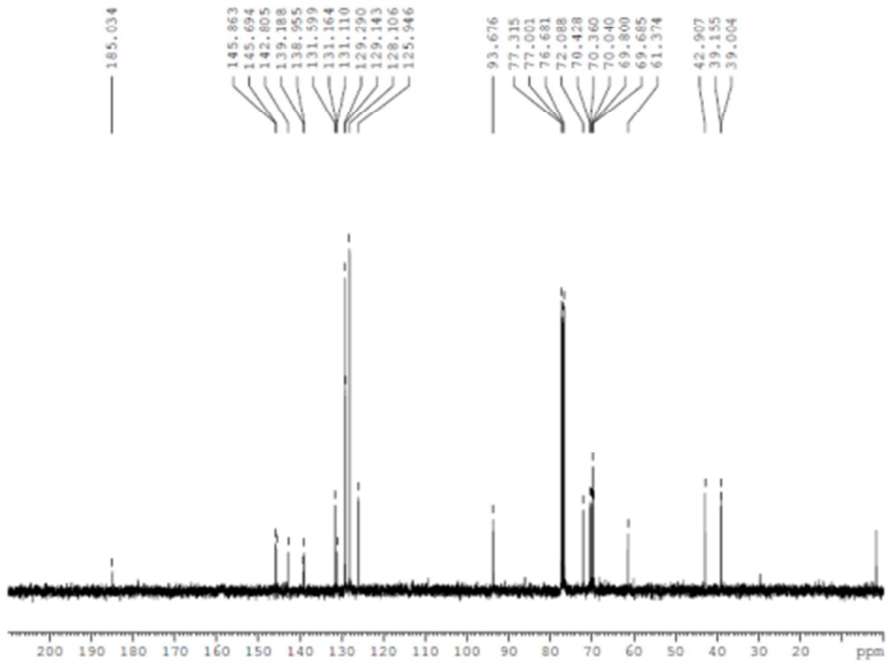


**Figure S5:** 100 MHz $^{13}$C NMR spectrum of BHHBSB-TEG-OH **7**.

3. **BHHBTEGSB 5**: 1,2-bis[4′ -(1″ ,1″ ,1″ ,2″ ,2″ ,3″ ,3″ -heptafluoro-4″ ,6″ -hexanedion-6″ -yl)-benzyl]-4- sulfonylamino-tetraethyleneglycol-succinimidyl carbonate-benzene

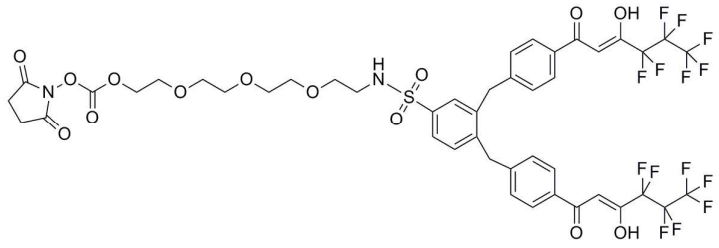

To a stirred solution of BHHBCB-TEG-OH **7** (50 mg, 0.05 mmol), 4-dimethylaminopyridine (DMAP) (6 mg, 0.05 mmol) and triethylamine (22µL, 0.15 mmol) in dry acetonitrile (3 mL) under anhydrous conditions was added *N*,*N*-disuccinimidyl carbonate (40 mg, 0.15 mol). The mixture was then stirred for 3 h at room temperature, after which time analytical HPLC analysis of the reaction mixture indicated the completion of reaction. Then solvent (acetonitrile) was removed under reduced pressure at 45 °C and the residue was purified by preparative HPLC to give BHHBTEGSB **5** as light yellow oil (31 mg, 55%). $^{1}$H NMR (400 MHz, $CDCl_3$) δ 2.81 (m, 4H), 3.11 (m, 4H), 3.61 (m, 12H), 4.02 (d, *J* = 16 Hz, 4H), 6.54 (s,

2H), 7.12 (m, 4H), 7.27 (m, 1H), 7.72 (m, 2H), 7.80 (m, 4H); $^{13}$C NMR (100 MHz, $CDCl_3$) δ 25.4, 39.0, 39.1, 43.0, 45.9, 62.2, 68.3, 69.3, 70.1, 70.2, 70.4, 70.5, 70.8, 76.7, 77.0, 77.3, 93.7, 126.0, 128.1, 129.1, 129.3, 131.6, 142.1, 145.6, 145.8, 185.2. ESI-MS (positive mode): *m/z* = 1153 ([MNa]$^+$, 100%); HRMS (ESI): *m/z* = 1131.2049 calculated for $C_{45}H_{41}F_{14}N_2O_{14}S$ [M$^+$−H]; *m/z* = 1153.1869 calculated for $C_{45}H_4F_{14}N_2O_{14}SNa$ ([M+Na]$^+$); Found =*m/z* 1131.2014 ([M$^+$−H], 92%); 1153.1825 ([M+Na]$^+$, 8%).

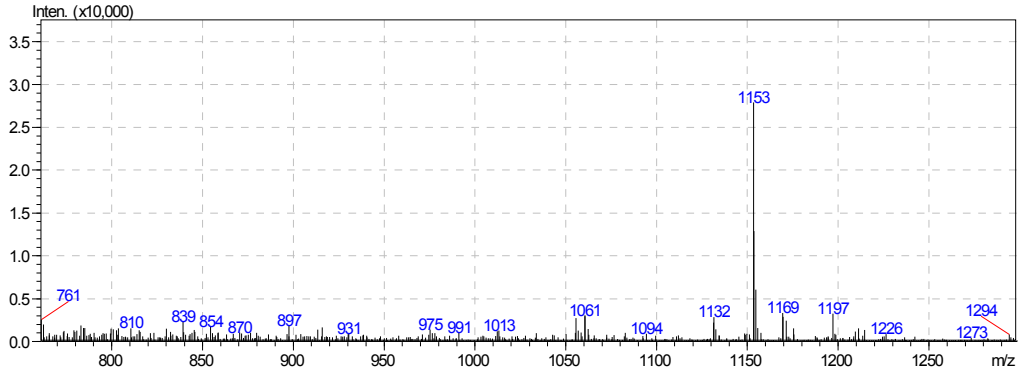


**Figure S6:** ESI-MS spectrum of BHHBTEGSB **5** (positive mode): m/z = 1153 ([M+Na]$^+$, 100%)

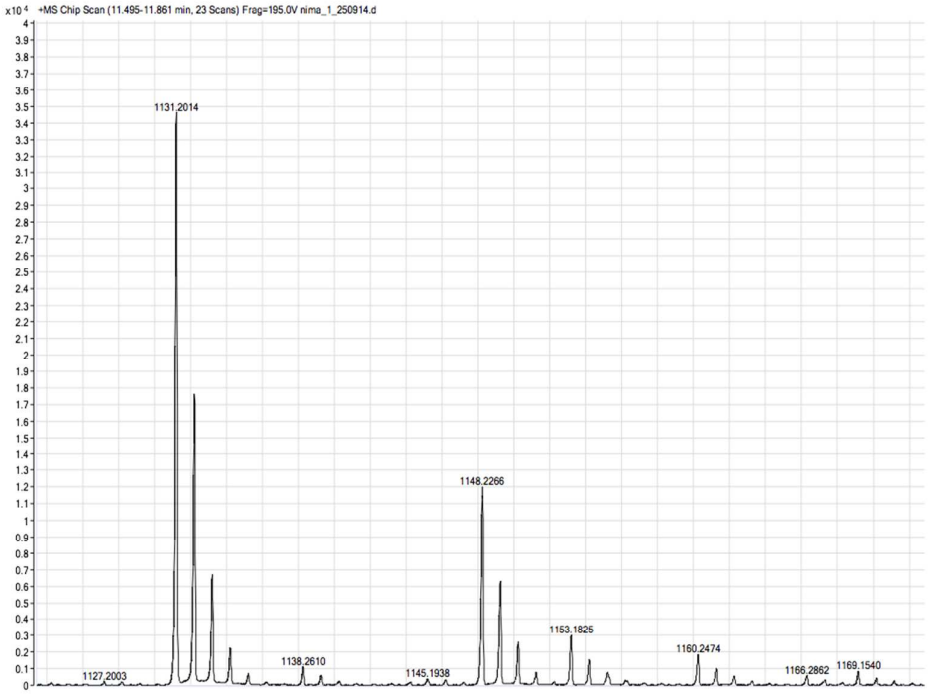


**Figure S7:** High resolution mass spectrometry (HRMS) [positive mode] of BHHBTEGSB **5**.

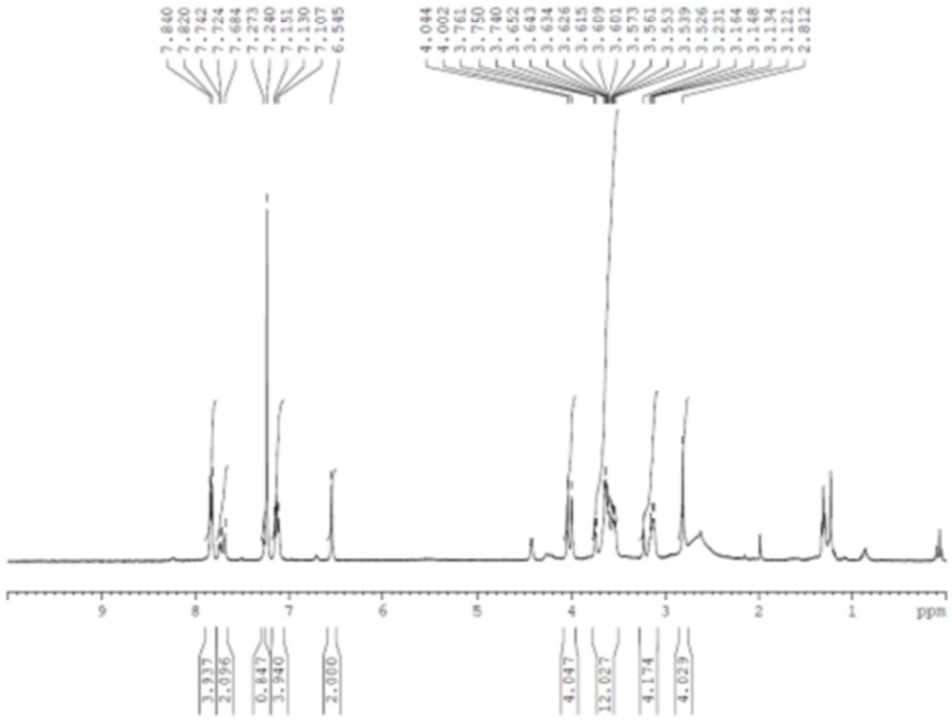


**Figure S8:** 400 MHz $^{1}$H NMR spectrum of BHHBTEGSB **5**.

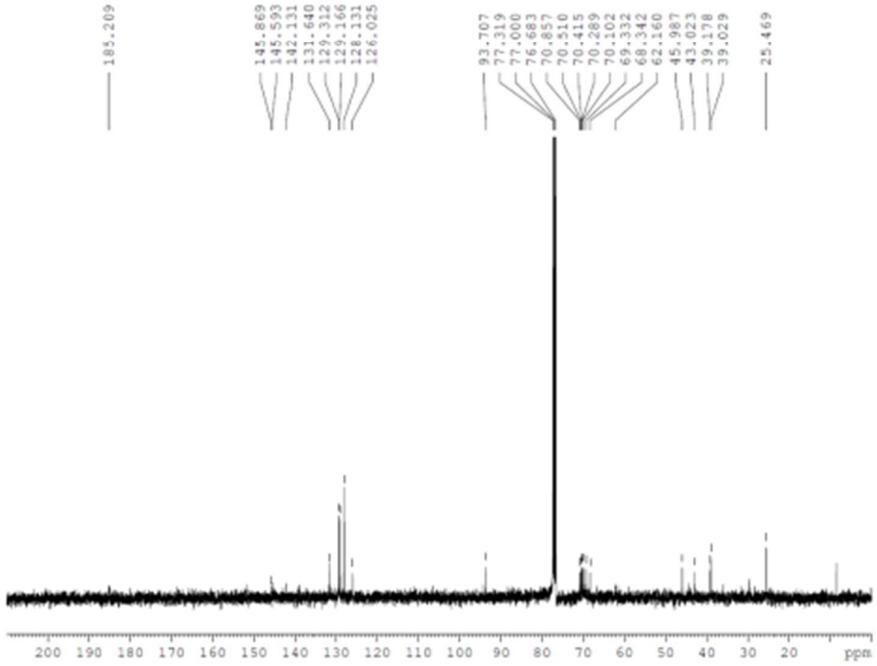


**Figure S9:** 100 MHz $^{13}$C NMR spectrum of BHHBTEGSB **5**.

**HPLC purification details:**

Analytical HPLC was performed using a DENALI C18 column (5 µm, 4.6 mm ID, 250 mm) with a flow rate of 0.8 mL/min. HPLC solvent A (water with 0.01% TFA), solvent B (Acetonitrile) using the following gradient: (1) 0-5 min 10% ACN; (2) 5-25 min 10 to 100% ACN (3) 25-45 min 100% ACN. HPLC profile of BHHBCB **4** [retention time of 36 minutes], BHHBCB-TEG-OH **7** [retention time of 33.7 minutes], BHHBTEGSB 5 [retention time of 33.2 minutes]. Preparative HPLC was carried out using an Econosil C18 column (10 µm, 22 mm ID, 250 mm) with a flow rate of 9.0 mL/min. HPLC solvent A (water with 0.01% TFA), solvent B (acetonitrile) using the following gradient: (1) 0-5 min 10% ACN; (2) 5-20 min 10 to 100% ACN (3) 22-45 min 100% ACN. BHHBCB-TEG-OH **7** [retention time of 29.5 minutes, BHHBTEGSB **5** [retention time of 28 minutes].

**UV-visible absorption profile of BHHBCB and BHHBTEGSB:**

UV-visible absorption spectra of the BHHBTEGSB and BHHBCB were investigated using a NanoDrop 2000 UV (Thermo Scientific) spectrometer. All ligands have the same maximum peak absorption at 335 nm as shown in Figure S10. Three replicates of each ligand were prepared and the average UV-visible absorption was used to calculate extinction coefficient of ligands at 335 nm as shown in Table S1.

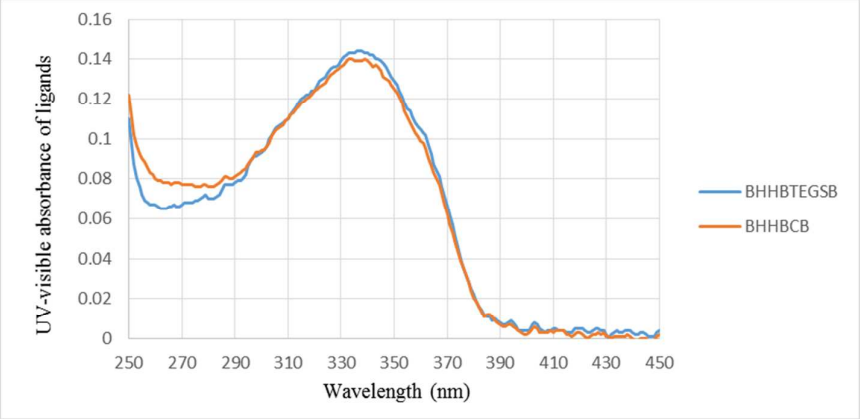


**Figure S10:** UV-visible profile of BHHBTEGSB and BHHBCB ligands (~45 µM) ($\lambda_{ex.max}$ =335 nm).

***Experimental:***

From a stock solution of 1.5/2.1 mg of chelates BHHBCB/BHHBTEGSB in 100 µl DMF, 5.0 µl were taken and added to 95 µl of DMF. From this solution, 5.0 µl were added to 95 µl of FEB and analysed on the NanoDrop 2000 UV (Thermo Scientific) spectrometer. Three replicates for each ligand were performed and the average reading was used for calculation of extinction coefficient of ligands at 335 nm.

| Ligand | UV-visible Absorption (average of 3 replicates) | M (mmol/mL) | $\varepsilon_{335}$ $M^{-1}cm^{-1}$ (average of 3 replicates) | Cell length (cm) |
|---|---|---|---|---|
| BHHBCB | 0.139 | ~ 4.50 x$10^{-05}$ | 30876 | 0.1 |
| BHHBTEGSB | 0.144 | ~ 4.60 x$10^{-05}$ | 31017 | 0.1 |

**Table S1:** Extinction coefficient of ligands at 335 nm.

## Titration of BHHBCB and BHHBTEGST with $Eu^{+3}$

The capacity of both BHHBTEGSB **5** and BHHBCB **4** ligands for chelation of $Eu^{3+}$ was determined by titration of ligands with $Eu^{3+}$. The luminescence intensity for both chelates was increased by addition of $Eu^{+3}$ ions until the molar ratio of $Eu^{3+}$ to ligand reached equivalency as shown in Figure S11. The luminescence intensity of either chelate did not increase on further addition of $Eu^{3+}$ ions (up to 10 eq. of ligands), implying the chelates form a stable complex at 1:1 ratio with $Eu^{3+}$ (BHHBTEGSB-Eu & BHHBCB-Eu). The formation of stable 1:1 complex of $Eu^{3+}$ ions to ligands is in accordance with previous studies on similar diketone chelates.[2,3]

Dilute solutions of BHHBTEGSB and BHHBCB (2.5 µM) were prepared in $NaHCO_3$ buffer (100 mM; pH=8). Luminescence emission at 613 nm was monitored for each chelate as fractional equivalents of europium chloride solution were carefully added over a period of 3 hours and twenty minutes. Luminescence emission was measured (Agilent Cary Eclipse Fluorescence Spectrophotometer) 20 min after each addition and titration curves were obtained by plotting the luminescence intensity against the Eu/BHHBCB and Eu/ BHHBTEGSB molar ratios respectively.

## Experimental:

1.40 mg purified and lyophilized powder of BHHBTEGSB and ~1.04 mg of BHHBCB were accurately weighed (0.01 mg accuracy scale) and dissolved in 50 µL of DMF. 5 µL of dissolved ligands were diluted to 500 µL with $NaHCO_3$ buffer (100 mM; pH=8) for each ligand respectively. From this solution 10 µL were added to 1 mL $NaHCO_3$ buffer in a quartz cuvette containing europium chloride [from 0.1 up to 10 equivalent of ligand (2.5 µM)]. A stock solution of $Eu^{+3}$ was prepared in a 10 mL volumetric flask by dissolving (0.916 mg, 0.25 mM) europium chloride hexahydrate in 100 mM $NaHCO_3$ buffer. Each experiment was incubated for 20 min at room temperature Luminescence intensity was measured using a Cary fluorescence spectrophotometer.
Also the structure of chelation of europium III ion with both chelates are shown in figure S12.

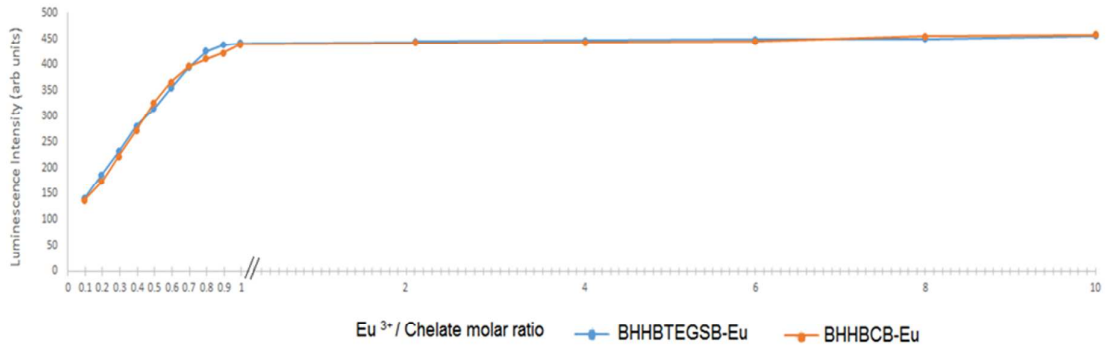


**Figure S11:** Binding isotherm of luminescence emission intensity ($\lambda_{em}$-max = 613 nm) of BHHBTEGSB-Eu & BHHBCB-Eu chelates (2.5 µM) at different molar ratio of $Eu^{3+}$ to ligand (0.1-10 eq.). Emission was seen to peak around 1:1 equivalency of $Eu^{3+}$ ion to ligand. Excited at 335 nm and luminescence emission recorded at 613 nm. (//: After 1:1 ratio of Eu to ligand the units of x-axis was changed from 0.1 to 1.0).

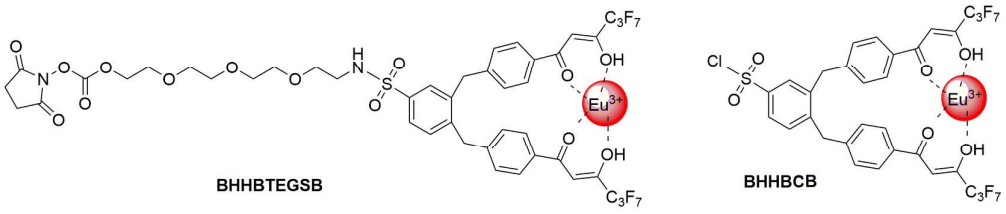


**Figure S12:** The europium chelation structure of BHHBTEGSB-Eu and BHHBCB-Eu.

## Luminescence spectra of Eu chelates

The luminescence spectral profiles of both chelates BHHBTEGSB-Eu and BHHBCB-Eu were also examined. As shown in Figure S13 both chelates (at 5.0 µM) present the identical luminescence emission spectra (excitation at 335 nm and maximum emission at 613 nm). This suggests that the TEG linker NHS group in BHHBTEGSB **5** has negligible interaction with the diketone-$Eu^{3+}$ complex and its photophysical activity remains largely comparable to BHHBCB **4**.

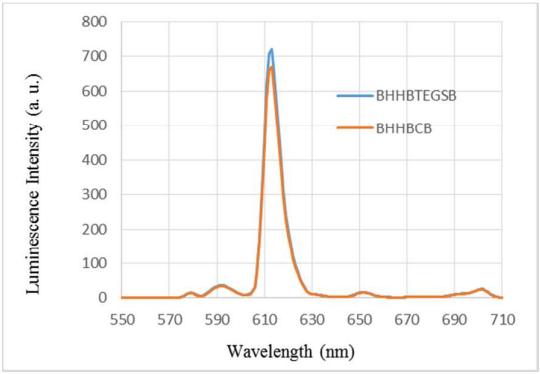


**Figure S13:** Luminescence emission of BHHBCB-Eu and BHHBTEGSB-Eu (5.0 µM) in FEB solutions. Excited at 335 nm and maximum luminescence emission observed at 613 nm.

Also the luminescence spectral profiles of BHHBTEGSB-Eu and our previously reported ligand BHHTEGST **1** were compared and it was confirmed that BHHBTEGSB **5** possesses higher luminescence emission intensity than BHHTEGST **1** (Figure S14).

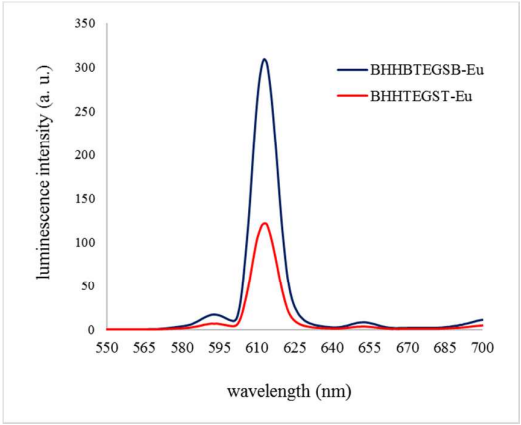


**Figure S14:** Luminescence emission of BHHBTEGSB-Eu and BHHTEGST-Eu (2.5 µM) in FEB solutions. Excited at 335 nm and maximum luminescence emission observed at 613 nm.

**Conjugation of BHHBCB and BHHBTEGSB to BSA for stability testing:**

The stability of $Eu^{3+}$ chelation by the diketone moiety present in both BHHBTEGSB **5** and BHHBCB **4** was also investigated. Each ligand was conjugated to bovine serum albumin (BSA) and the conjugated BSA was titrated with EDTA whilst monitoring luminescence emission intensity. Both BSA-$BHHBTEGSB_{22}$-Eu ($10^{-6}$M) and BSA-$BHHBCB_{16}$-Eu ($10^{-6}$M) displayed similar stability in the presence of EDTA ($10^{-7}$ to $10^{-1}$ M). The europium chelation of both ligand was stable up to $1.0 \times 10^{-2}$ M EDTA where EDTA is at a $10^4$ times molar excess of BSA-ligand-Eu. A slight reduction of luminescence was observed when the concentration of EDTA increased from $10^{-3}$ to $10^{-2}$ M. Further addition of EDTA resulted in loss of luminescence; indicating that 0.1 M EDTA competitively coordinates with the $Eu^{3+}$ and makes it unavailable to the ligands (figure S16). Both BHHBCB **4** and BHHBTEGSB **5** displayed higher chelation stability compared to data previously reported on BHHTEGST **1** and BHHCT **3** chelates.[3] The results of the EDTA titration are in accordance with a previous study.[1]

**Experimental:**

10mg/ml of Bovine Serum Albumin Fraction V (10735078001) were dissolved in $NaHCO_3$ buffer (100 mM; pH=8). 10 µL of this solution (100 µg) were added to 200 µL of $NaHCO_3$ buffer (100 mM; pH=8) followed by addition of 5 µL of ligand (10 mg/ml in DMF). The reaction mixture was incubated for 1 hr at 37 °C and conjugated BSA was purified on Sephadex G-25 (4.5 cm length, 0.9 cm ID) using 0.05 M Tris buffer pH=7.8 as eluent. The conjugated fractions were collected and analyzed by using a NanoDrop spectrophotometer (280 nm and 335 nm). [BSA molecular weight 66.5 kDa contains 59 lysine residues with extinction coefficient of 43,824 $M^{-1}cm^{-1}$ at 280 nm].[4]

The ultraviolet absorbance spectrum of conjugated BSA was obtained using a NanoDrop 2000 UV spectrometer as shown in Figure S15. The number of conjugated ligand per BSA was determined to be BSA-$BHHBTEGSB_{22}$ and BSA-$BHHBCB_{16}$.

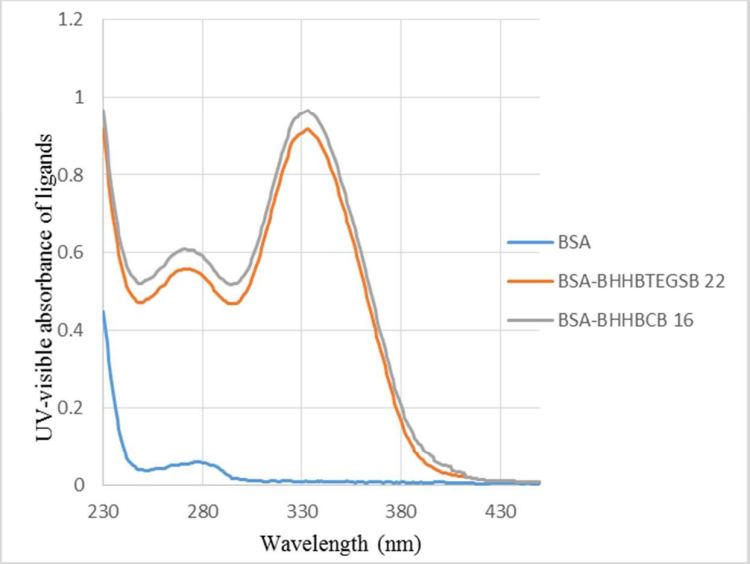


**Figure S15:** UV-visible profile of BSA and BSA conjugated to BHHBTEGSB & BHHBCB ligands

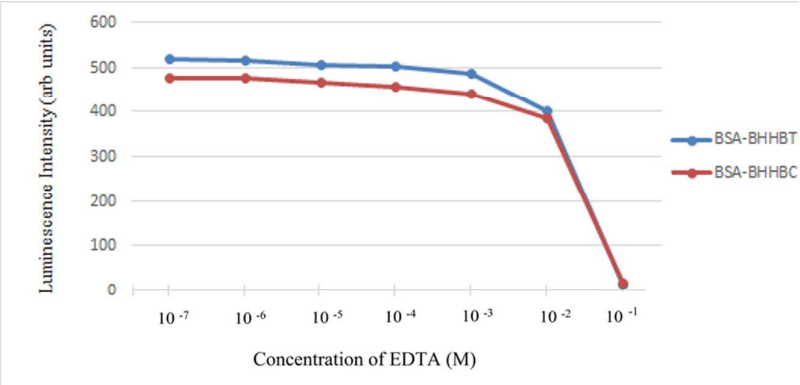


**Figure S16:** Luminescence intensities of BSA-BHHBTEGST$_{22}$-Eu and BSA-BHHBCB$_{16}$-Eu chelates at different concentration of EDTA ($10^{-7}$- $10^{-1}$ M).

## Luminescence of chelates in water, deuterium oxide and fluorescence enhancing buffer (FEB) solutions

For each chelate (5.0 µM), luminescence intensity (excitation at 335 nm and maximum luminescence emission 613 nm) in water, $D_2O$ and fluorescence enhancing buffer (FEB) was measured with a gate delay of 100 µs on an Agilent Cary Eclipse Fluorescent Spectrophotometer. For each compound, luminescence intensity was lowest in water, slightly higher in $D_2O$ and significantly enhanced in FEB (3.6 fold for BHHBCB **4** and 3.4 fold for BHHBTEGSB **5** relative to water, SI, Figure S17-18).

**Experimental:**
1.40 mg of purified and lyophilized powder of BHHBTEGSB and 1.00 mg of BHHBCB were accurately weighed (0.01 mg accuracy scale) and dissolved in 500 µL of DMF. 10 µL of this solution were diluted in 500 µL of MQ water, deuterium oxide or FEB and 10 µL of each mixture were added to 1 mL (a) MQ water (b) deuterium oxide (c) FEB, each containing europium chloride 10 µM, in a quartz cuvette for each ligand respectively. The final ligand concentration in this mixture was 5.0 µM Luminescence intensity was measured using a Cary fluorescence spectrophotometer as shown in Figure S17 and S18, with excitation at 335 nm and maximum luminescence emission observed at 613 nm.

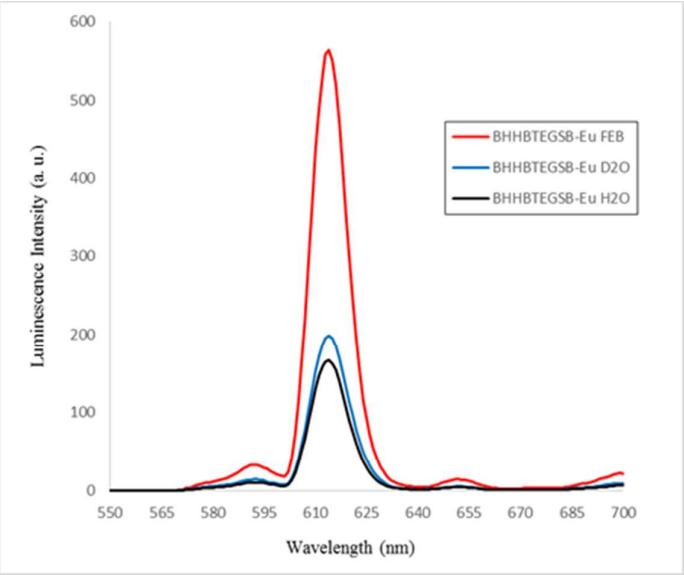


**Figure S17:** Luminescence emission of BHHBTEGSB-Eu (5.0 µM) in water, deuterium oxide and FEB solutions.

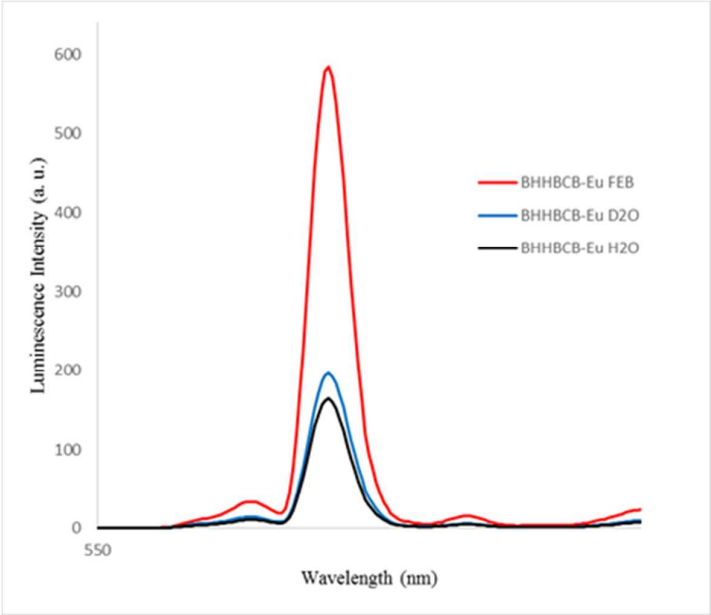


**Figure S18:** Luminescence emission of BHHBCB-Eu (5.0 µM) in water, deuterium oxide and FEB solutions.

## Lifetime of chelates and quantum yield:

As described above 5.0 µM solution of chelates were prepared in a 1 mL quartz cuvette containing Fluorescence Enhancing Buffer (FEB) and europium chloride (10 µM). Luminescence intensity was measured using a Cary fluorescence spectrophotometer. The delay time was set from 100 µs to 1000 µs (10 readings, 100 µs increment) while the other parameters were kept constant including gate time (5.0 ms, excitation slit (5 nm) and emission slit (5 nm). Then the Ln of luminescent intensity (at 613 nm) for chelates was plotted against the delay time (µs) and the negative reciprocal of the slope is used to calculate the luminescence lifetime (τ) shown in Figure S19 and 20 and Table S2. (Excitation at 335 nm and maximum luminescence emission observed at 613 nm).

| Ligands | $\varepsilon_{335}$ nm | Life time µs (FEB) | Luminescence Emission (FEB) | QY | Brightness $dm^3\ mol^{-1}\ cm^{-1}$ |
|---|---|---|---|---|---|
| BHHBCB | 30876 | 303 | 272.4 | 0.40[1] | 12350 |
| BHHBTEGSB | 31017 | 294 | 283.7 | 0.39 | 12097 |

**Table S2:** molar extinction coefficient, Life time and quantum yield for BHHBCB and BHHBTEGSB.

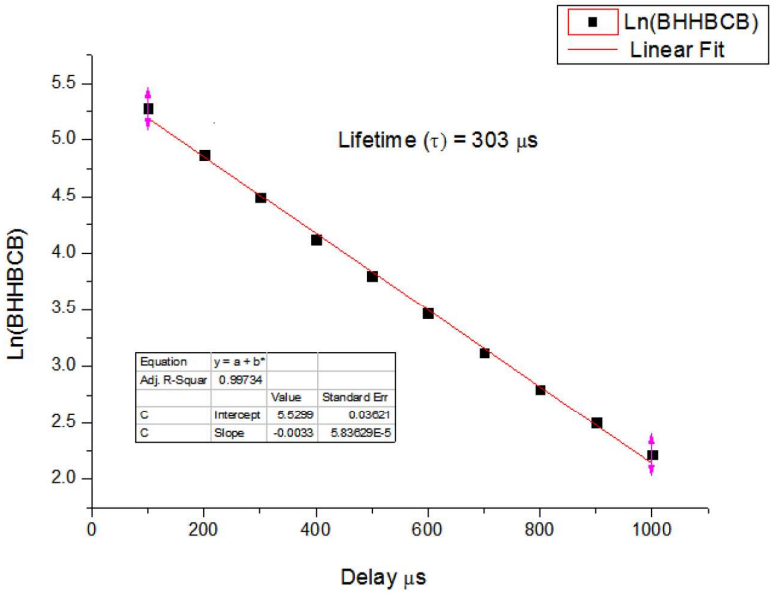


**Figure S19:** Ln plot of intensity over the period 100 to 1000 µs for BHHBCB. Time-gated luminescence spectra were measured on a Agilent Cary Eclipse Fluorescent Spectrophotometer with the conditions of delay time 0.1 to 1.0 ms; gate time, 5.0 ms, excitation slit, 5 nm; and emission slit, 5 nm. Excitation at 335 nm and maximum luminescence emission at 613 nm.

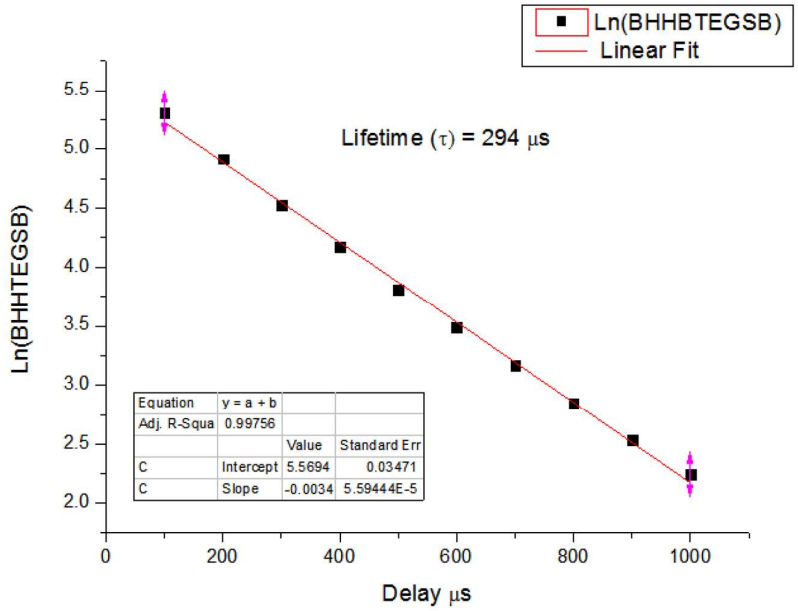


**Figure S20:** Ln plot of intensity over the period 100 to 1000 μs for BHHBTEGSB. Time-gated luminescence spectra were measured on a Agilent Cary Eclipse Fluorescent Spectrophotometer with the conditions of delay time 0.1 to 1.0 ms; gate time, 5.0 ms; excitation slit, 5 nm; and emission slit, 5 nm. Excitation at 335 nm and maximum luminescence emission at 613 nm.

## Quantum Yield Calculations:

As noted in the text, whilst BHHBTEGSB is clearly a derivative of BHHBCB with the same parent molecule, we observe a small difference in molar extinction coefficient, similar intensity of emission and slightly shorter luminescence lifetime.

Using these experimentally determined parameters, we used the method reported by Latva *et al.* to determine QY of BHHBTEGSB.[5]

Where ε represents the molar extinction coefficient at the excitation wavelength, C is the

$$(1)\ \phi_x = \phi_{ref}\frac{I_{Tx}.\varepsilon_{ref}}{I_{Tref}.\varepsilon_x}$$

concentration and IT represents the integrated luminescent emission. The subscripts $_{ref}$ and $_x$ refer to the reference compound with known QY and the unknown compound respectively. The concentrations were the same for each compound enabling us to simplify the equation to:

$$(2)\ \phi_x = 0.4\frac{79504\times30876}{80643\times31017}$$

Which gives us a figure of 0.39 for BHHBTEGSB quantum yield.

Deslandes *et al.* report a method of evaluating actual efficiency of a luminescent label by taking into account the brightness as determined by the product of the extinction coefficient at the excitation wavelength and the luminescence quantum yield.[5] Using this parameter, we arrive at a figure of 12350 $dm^3$ $mol^{-1}$ $cm^{-1}$ for BHHBCB and 12097 for BHHBTEGSB (Figure S21). These values are substantially above the lower limit ~300 $dm^3$ $mol^{-1}$ $cm^{-1}$ reported for the brightness characterizing an efficient luminescent lanthanide complex.[6]

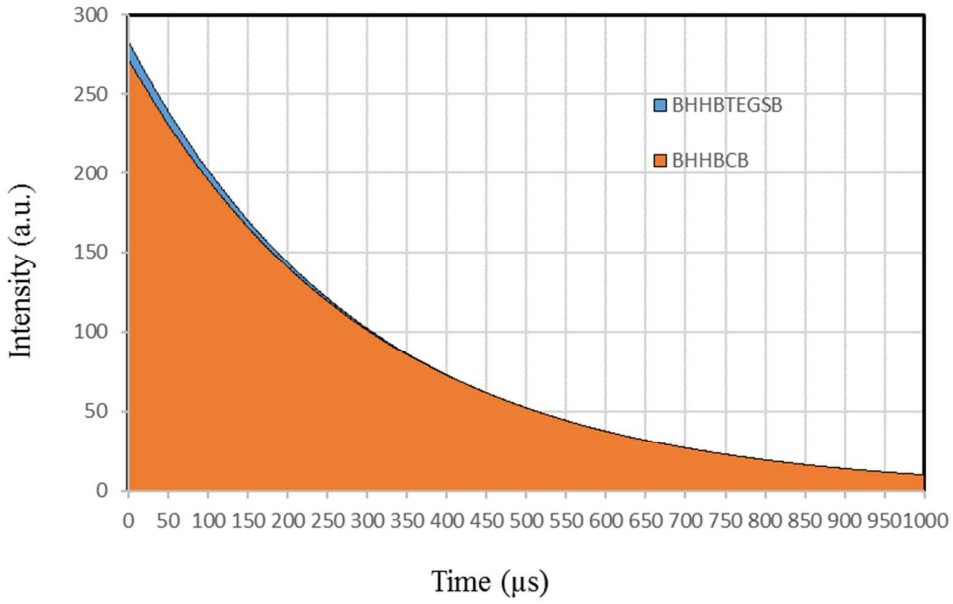


**Figure S21**: The area under the curve was calculated at 1 nm resolution over the interval 0-1000 µs using the exponential function $I_T = 272.4\ e^{-T/303}$ for BHHBCB and $I_T = 281.7\ e^{-T/294}$ for BHHBTEGSB. The integral for each was then used to calculate quantum yield; the integral for BHHBCB was 80,643 and 79,504 for BHHBTEGSB, (Excitation 335 mn, Emission 613 nm).

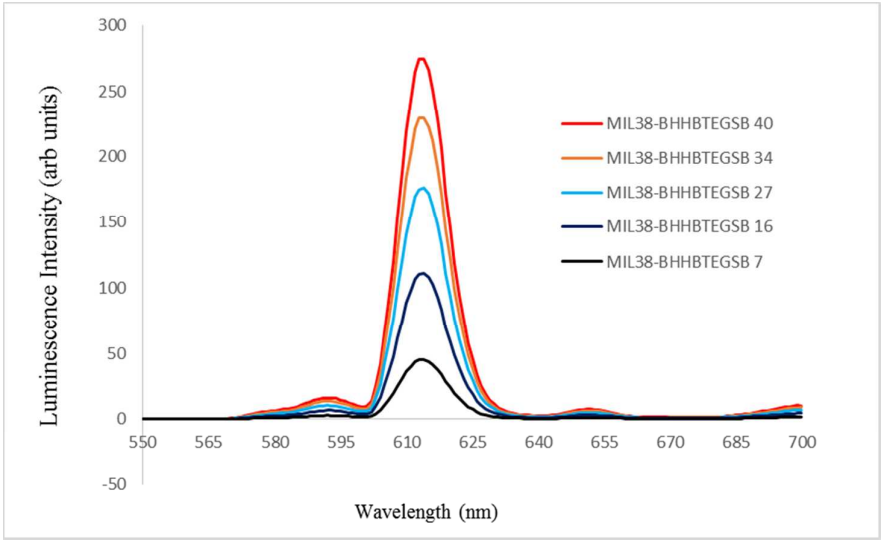


**Figure 22:** Luminescence profile of conjugated antibodies; [MIL38-BHHBTEGSB$_x$-Eu, X= 7, 16, 27, 34 & 40]. (1-2 µM), Excited at 335 nm and maximum luminescence emission observed at 613 nm.

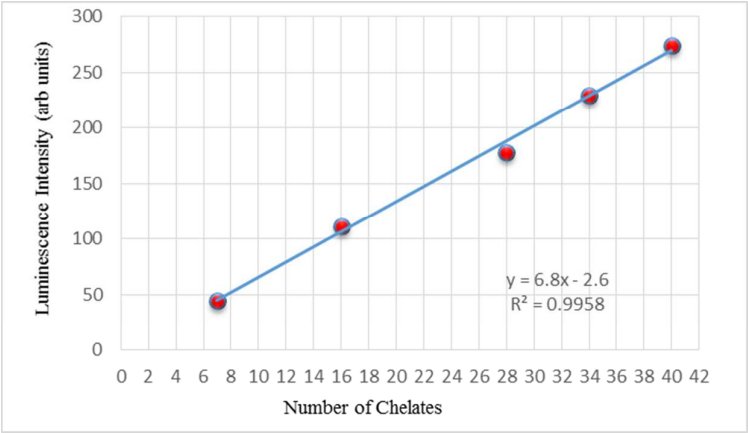


**Figure 23:** Correlation of number of ligands attached to antibody (MIL38-BHHBTEGSB$_x$-Eu, Number of chelate X= 7, 16, 27, 34 & 40) (1-2 µM) to luminescence emission. Excited at 335 nm and maximum luminescence emission observed at 613 nm.

## Quantification of BHHBTEGSB ligands attached to antibody MIL38/ streptavidin & antibody Anti-Mouse IgG

The number of BHHBTEGSB molecules per antibody was obtained by dividing the molar ratio of ligand to antibody. (See table 1, Figure S24)

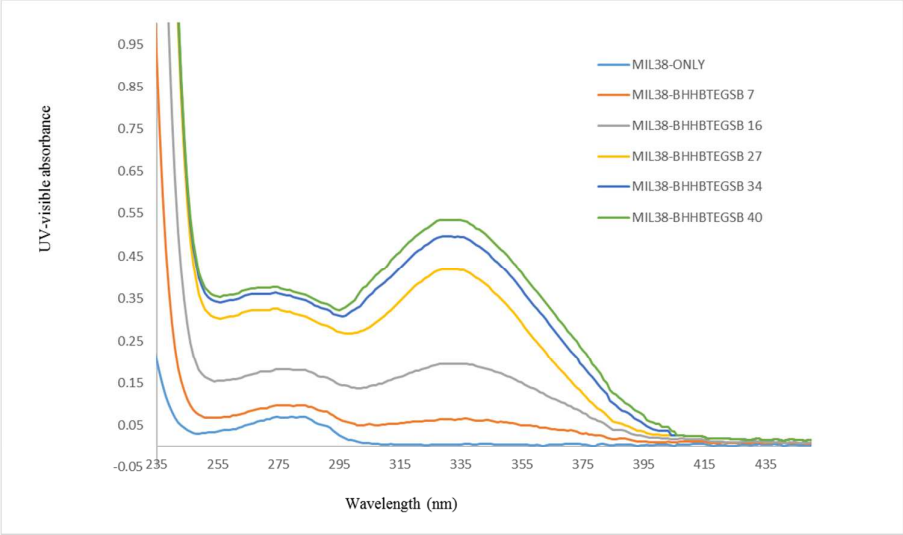


**Figure S24:** UV-visible spectra of unlabelled MIL38 and the five levels of BHHBTEGSB conjugation with MIL38. The band at 335 nm (from BHHBTEGSB component absorbance) intensifies with respect to the band at 280 nm (from protein component absorbance) as a result of the number of attached equivalents of BHHBTEGSB **5** is increased.

The UV-visible absorbance spectrum of conjugated streptavidin was obtained using a NanoDrop 2000 UV (Thermo Scientific) spectrometer as shown in Figure S25. (See Table 1)

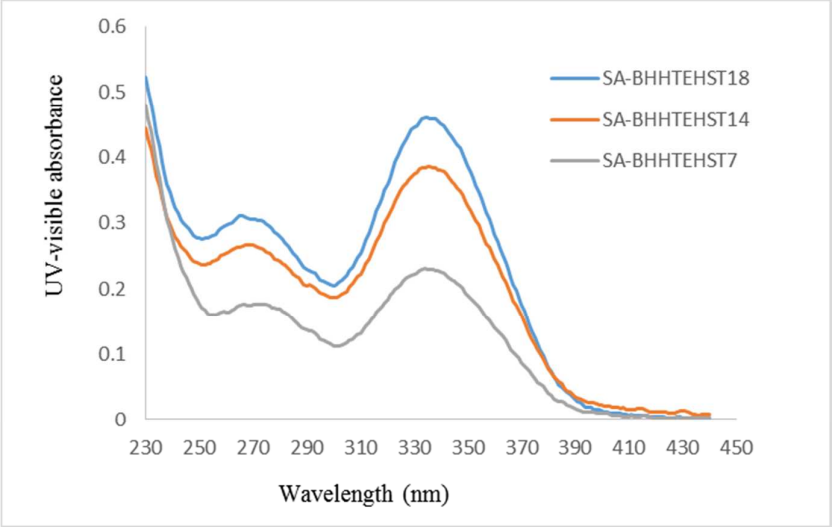


**Figure S25**. UV-visible absorbance spectrum of conjugated streptavidin with BHHBTEGSB

The UV-visible absorbance spectrum of conjugated Anti-Mouse IgG was obtained using a NanoDrop 2000 UV (Thermo Scientific) spectrometer as shown in Figure S26. (See Table 1)

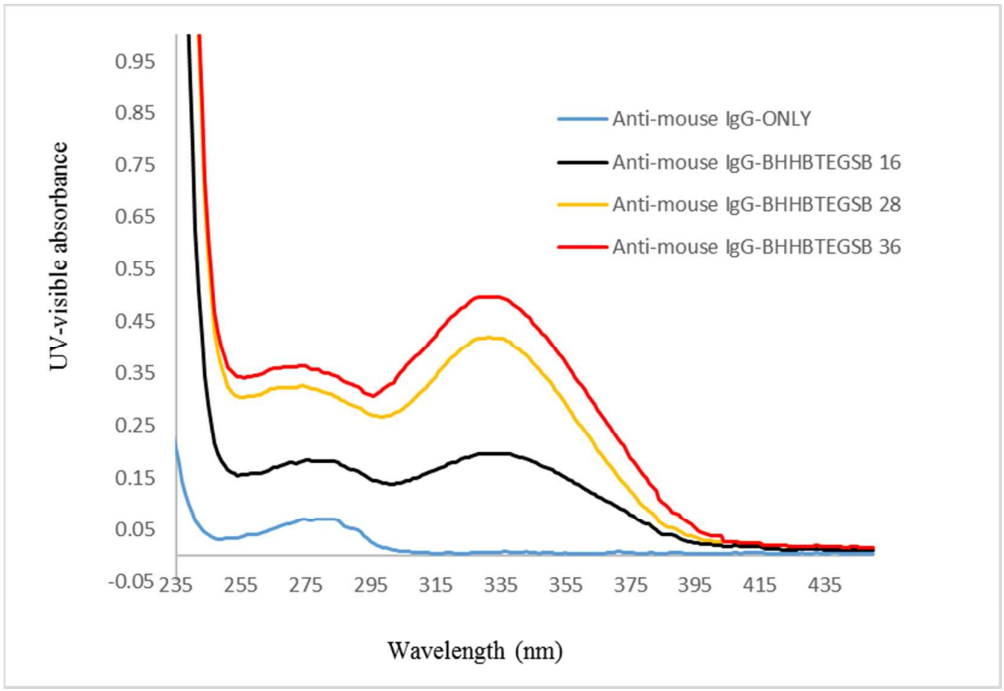


**Figure S26.** UV-visible spectrum of Anti-mouse IgG only and the three levels of BHHBTEGSB conjugation with Anti-mouse IgG. The band at 335 nm (from BHHBTEGSB component absorbance) intensifies with respect to the band at 280 nm (from protein component absorbance) as a result of the number of attached equivalents of BHHBTEGSB **5** is increased.

**Gel electrophoresis analysis of MIL38-BHHBTEGSB**

When the gel was visualized after addition of europium chloride solution under the UV-visible light (365 nm), the red europium luminescence emission was brighter from the heavy chain than the light chain indicating that the heavy chain which contains more lysine residues accommodated a higher number of ligands in comparison with the antibody light chain. Conjugated antibody MIL38 with europium ligand was reduced with DTT and run in SDS-PAGE,as shown below (Figure S27); lanes: **A** Novex standard; **B** and **C** same conjugated antibody MIL38-BHHTEGSB; **D** non-conjugated antibody. Left image, gel stained with Coomassie Brilliant Blue; Right image; same gel after addition of europium III chloride solution and visualized under UV-visible light (355 nm).

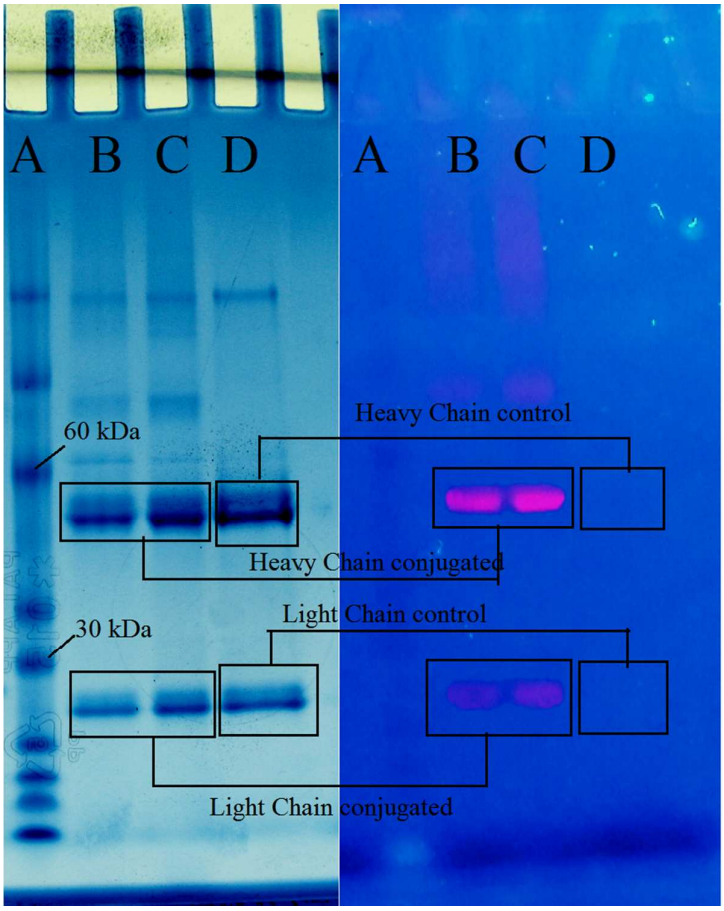


**Figure S27.** Gel electrophoresis analysis of conjugated antibody (MIL38-BHHBTEGSB), Left image: Gel stained with Coomassie Brilliant Blue. Left image: $EuCl_3$ solution was added and visualised under UV-visible light 365 nm [red images enhanced for better visualization] (A) Novex standard, (B & C) conjugated antibody, (D) unconjugated antibody.

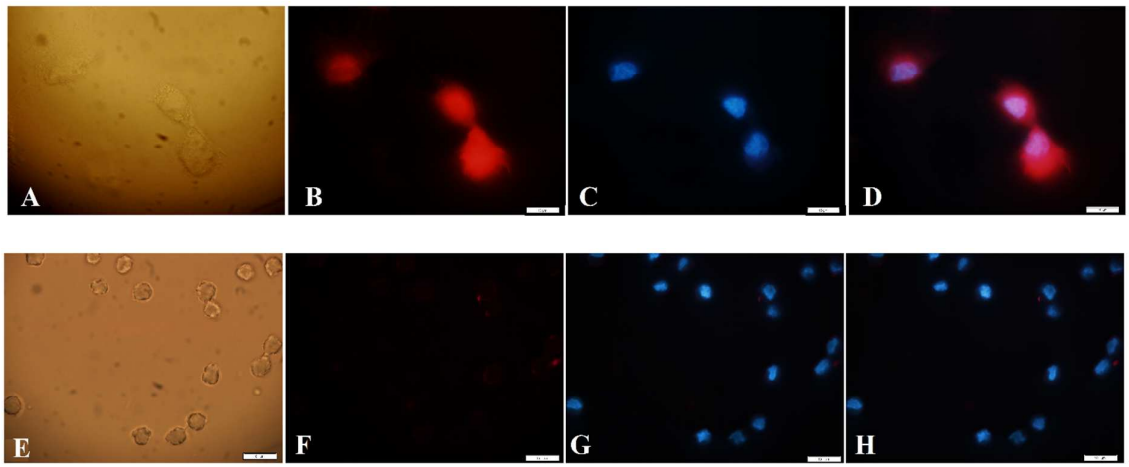


**Figure S28.** Staining of prostate cancer cells DU145 [A, B, C & D], and bladder cancer cells C3 [E, F, G & H] with MIL38-BHHBTEGSB$_{20\text{-}30}$, (A, E) Bright field; (B, F) Time gated luminescence (TGL); (C, G) DAPI nuclear staining; (D, H) Merge TGL & DAPI. Oil immersion 100X objective, TGL exposure times (1.0 Sec.) (B &F); Scale bar 10 µm.

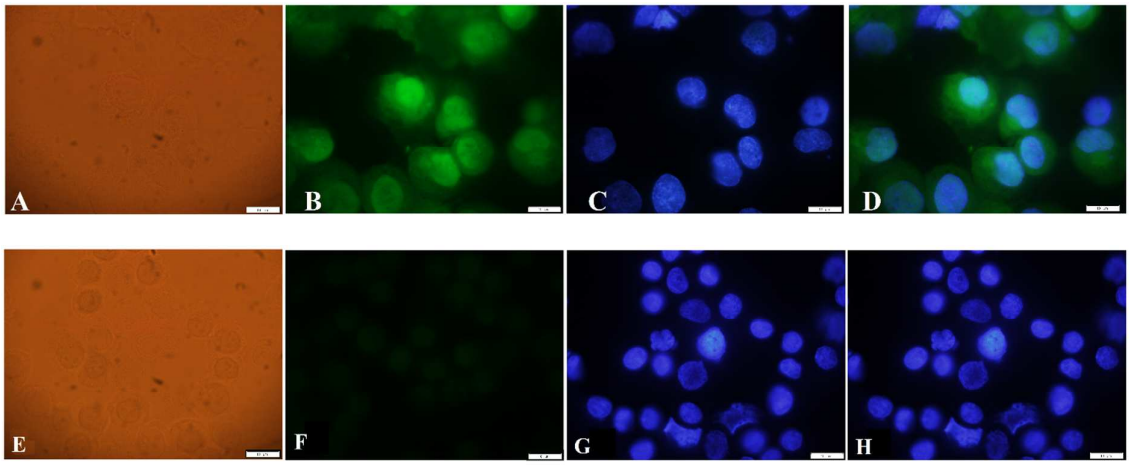


**Figure S29.** Staining of prostate cancer cells DU145 [A, B, C & D] and bladder cancer cells C3 [E, F, G, H] with MIL38-FITC conjugate. (A, E) Bright field, (B, F) FITC filter set, (C,G) DAPI nuclear staining (D, H) Merge of FITC and DAPI, Oil immersion 100X objective, FITC exposure time of 300 ms; Scale bar 10 µm.

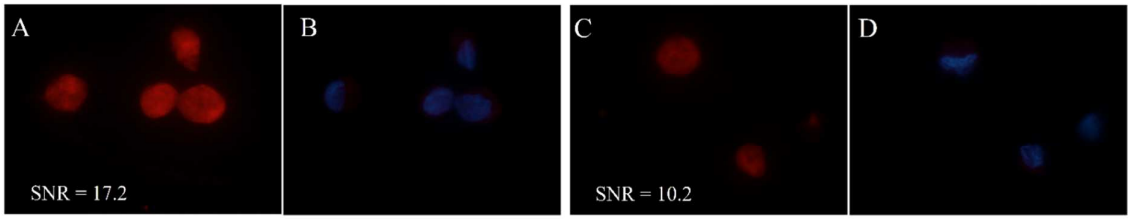


**Figure S30.** Staining of prostate cancer cells DU145 with Cetuximab-BHHBTEGSB (A) and Cetuximab-BHHTEGST (C) Time gated luminescence (TGL); (B, D) DAPI nuclear staining; Representative images with quantified signal to noise ratio (SNR) of stained cells. The SNR of cells using BHHBTEGSB probe quantified to 17.2 whereas for BHHTEGST probe SNR was 10.2 [Cetuximab antibody is targeting epidermal growth factor receptor (EGFR) that expressed by DU145 prostate cancer cells][7].

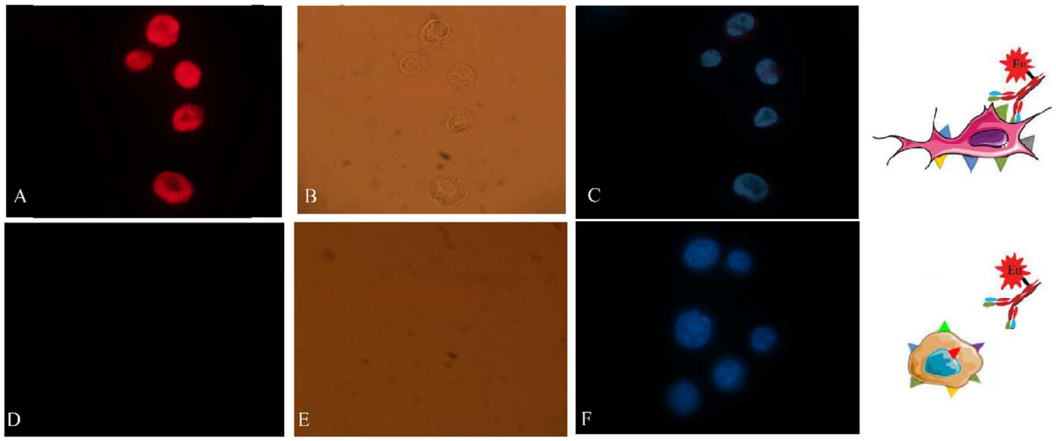


**Figure S31.** IgG (MIL38-BHHBTEGSB$_{20\text{-}30}$) staining of prostate cancer cells (DU145), (A, D) Time gated luminescence (TGL), (B, E) Bright field, (C, F) Nuclear staining (DAPI). [A, B, C = prostate cancer cells (DU145)], [D, E & F negative cell line C3 (bladder cancer)], Oil immersion 100 x objective used, exposure time of 1 s; Scale bar 10 µm

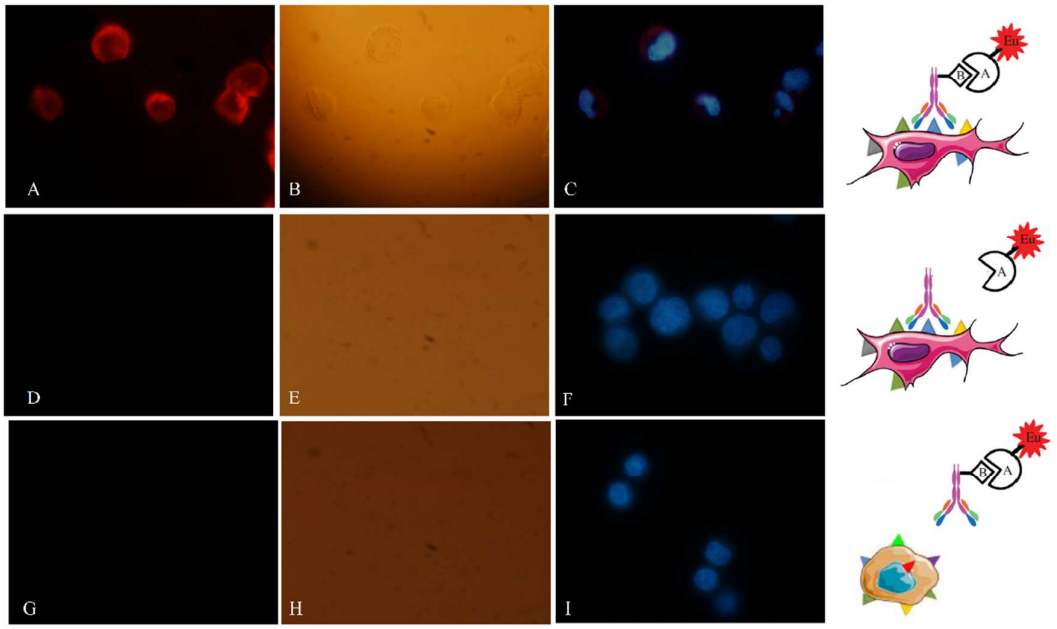


**Figure S32.** SA-BHHBTEGSB$_{14}$-MIL38-Biotin staining of prostate cancer cells (DU145), (A, D, G) Time gated luminescence (TGL), (B, E, H) Bright field, (C, F, I) Nuclear staining (DAPI). [A, B, C = prostate cancer cells (DU145) using MIL38-Biotin], [D, E & F = negative control using MIL38], [G, H, I= negative cell line C3 (bladder cancer) using MIL38-Biotin], Oil immersion 100 x objective used, exposure time of 1 s; Scale bar 10 µm

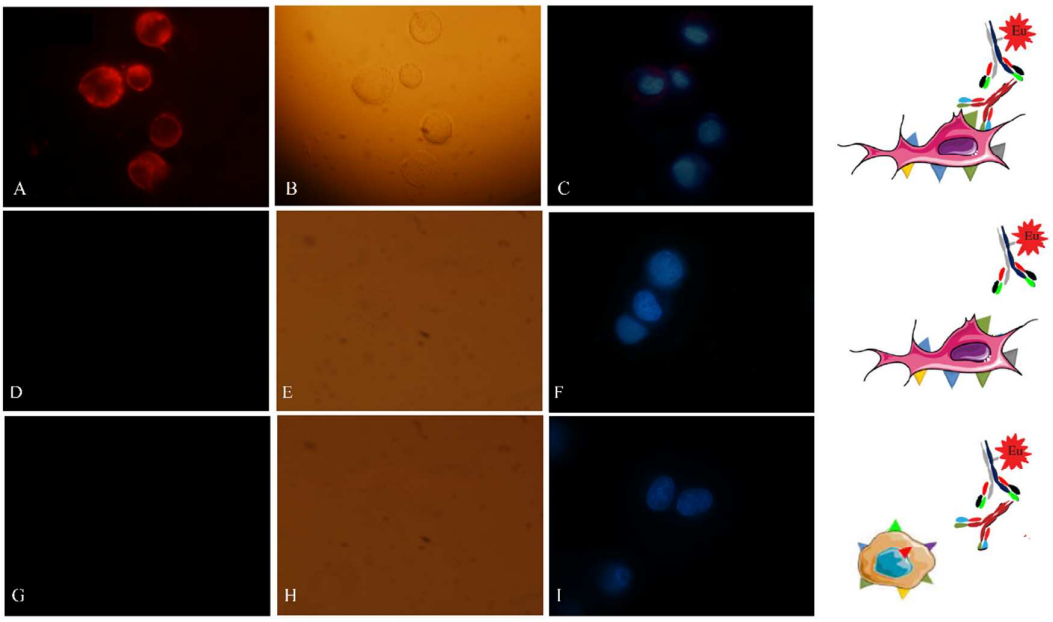


**Figure S33.** 2˚Ab-BHHBTEGSB$_{28}$ staining of prostate cancer cells (DU145), (A, D, G) Time gated luminescence (TGL), (B, E, H) Bright field, (C, F, I) Nuclear staining (DAPI). [A, B, C = prostate cancer cells (DU145) using MIL38], [D, E & F = negative control no MIL38], [G, H, I= negative cell line C3 (bladder cancer) using MIL38], Oil immersion 100 x objective used, exposure time of 1 s; Scale bar 10 µm

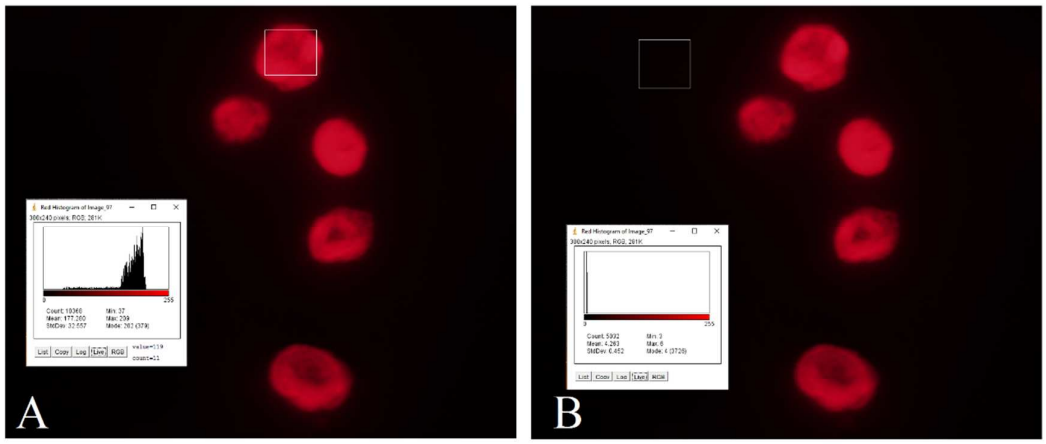


**Figure S34.** Quantification of signal to noise ratio in europium labelled prostate cancer cells (DU145) under time-gated microscopy using MIL38-BHHBTEGSB$_{20\text{-}30}$. (A) Signal 209 [Maximum brightness in cell] (B) Background 6 [mean red channel] Signal to noise ratio (SNR) calculated to be 34.8.

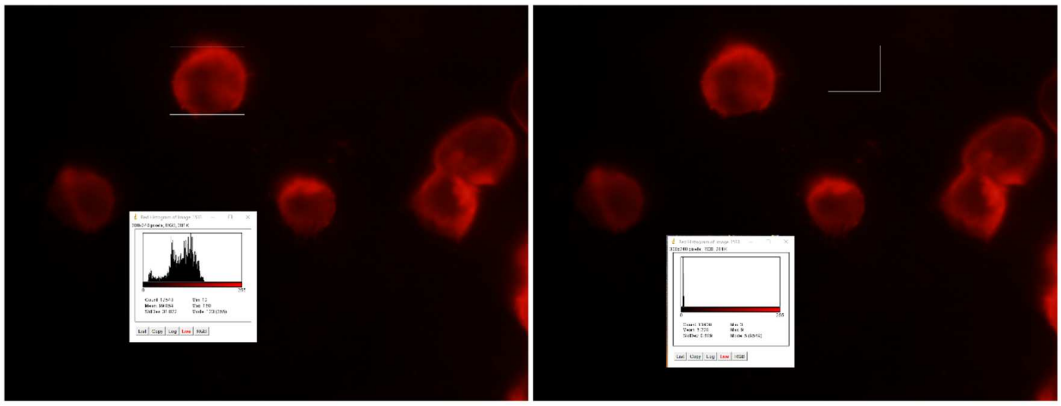

**Figure S35.** Quantification of signal to noise ratio in europium labelled prostate cancer cells (DU145) under time-gated microscopy using SA-BHHBTEGSB$_{14}$-MIL38-Biotin. (A) Signal 160 [Maximum brightness in cell] (B) Background 9 [mean red channel] Signal to noise ratio (SNR) calculated to be 17.8.

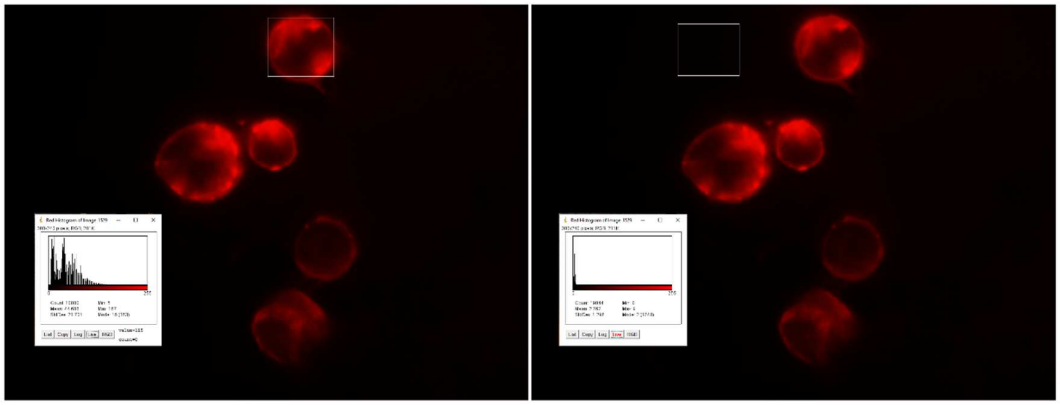

**Figure S36.** Quantification of signal to noise ratio in europium labelled prostate cancer cells (DU145) under time-gated microscopy using 2°Ab-BHHBTEGSB$_{28}$. (A) Signal 167 [Maximum brightness in cell] (B) Background 9 [mean red channel] Signal to noise ratio (SNR) calculated to be 18.5.

## References:


(1) Zhang, L.; Wang, Y. J.; Ye, Z. Q.; Jin, D. Y.; Yuan, J. L. *Bioconjugate Chem.* **2012**, *23*, 1244-1251.
(2) Wu, F.-B.; Zhang, C. *Anal. Biochem.* **2002**, *311*, 57-67.
(3) Sayyadi, N.; Connally, R. E.; Try, A. *Chem. Commun.* **2016**, *52*, 1154-1157.
(4) *The Plasma proteins : structure, function, and genetic control / edited by Frank W. Putnam*; Academic Press: New York, 1975.
(5) Latva, M.; Takalo, H.; Mukkala, V.-M.; Matachescu, C.; Rodríguez-Ubis, J. C.; Kankare, J. *JOL* **1997**, *75*, 149-169.
(6) Deslandes, S.; Galaup, C.; Poole, R.; Mestre-Voegtlé, B.; Soldevila, S.; Leygue, N.; Bazin, H.; Lamarque, L.; Picard, C. *Org. Biomol. Chem.* **2012**, *10*, 8509-8523.
(7) Dhupkar, P.; Dowling, M.; Cengel, K.; Chen, B. *Anticancer Res.* **2010**, *30*, 1905-1910.